Doctoral Dissertation

PROSPECT OF INTEGRALLY ASYMMETRIC CTA-BASED AND THIN FILM COMPOSITE PA-BASED MEMBRANES FOR OSMOTICALLY-DRIVEN SEPARATION PROCESS

Thi Phuong Nga Nguyen

Department of Urban and Environmental Engineering

(Environmental Science and Engineering)

Graduate School of UNIST

2016

PROSPECT OF INTEGRALLY ASYMMETRIC CTA-BASED AND THIN FILM COMPOSITE PA-BASED MEMBRANES FOR OSMOTICALLY-DRIVEN SEPARATION PROCESS

Thi Phuong Nga Nguyen

Department of Urban and Environmental Engineering
(Environmental Science and Engineering)

Graduate School of UNIST

Prospect of integrally asymmetric CTA-based and thin film composite PA-based membranes for osmotically-driven separation process

A dissertation
submitted to the Graduate School of UNIST
in partial fulfillment of the
requirements for the degree of
Doctor of Philosophy

Thi Phuong Nga Nguyen

1. 20. 2016 Month/Day/Year of submission
Approved by

Advisor
Young-Nam Kwon

Prospect of integrally asymmetric CTA-based and thin film composite PA-based membranes for osmotically-driven separation process

Thi Phuong Nga Nguyen

This certifies that the dissertation of Thi Phuong Nga Nguyen is approved.

01. 20. 2016 Month/Day/Year of submission

Advisor: Young-Nam Kwon

Jaewon Cho: Thesis Committee Member #1

Changha Lee: Thesis Committee Member #2

Nowon Kim: Thesis Committee Member #3

In-Chul Kim: Thesis Committee Member #4;

ABSTRACT

Osmotically-driven separation processes have been known as the forward osmosis (FO) and pressure-retarded osmosis (PRO). Among membrane technologies applied to water/wastewater treatment, FO has recently attracted much attention of scientists due to its saving energy, low fouling propensity and high rejection to a wide range of contaminants. Meanwhile, PRO has been considered as a potentially alternative power generation. Major challenges limiting the application of FO are a lack of desirable membranes, lack of proper draw solution and effect of concentration polarization (CP) phenomenon. The first part of this dissertation focuses on studying desirable membrane structures for osmotically-driven separation process, namely fabricating membranes to understand the impact of the polymer composition and preparing condition on the membrane formation and subsequently performance, investigating the effect of structure on performance of diverse membranes, and studying chlorination of the membranes. The later part of the dissertation examined the effect of concentration polarization on performances of various membrane structures for a suggestion of a preferred membrane configuration.

A comparison of the structure and performance between integrally asymmetric and thin film composite (TFC) FO membranes were done in this study to gain a better understanding of the FO transport mechanism, and to suggest appropriate characteristics of FO membranes. The effect of structure parameters (S) on the performance of the membranes was also examined. Under various operating conditions, the TFC membranes yielded superior J_w than the integrally asymmetric CTA-based membranes, especially, with larger J_w leading to higher solute resistance at alkaline feed and draw solutions. However, the integrally asymmetric membranes possessed smoother surfaces, resulting in lower fouling propensity than the polyamide TFC membranes. Besides the structure, chemical composition of the skin layer also affected the performance. TFC membranes from Toray Chemical Korea (TCK) showed lower oxygen atomic content on the active layer (AL), higher negatively charged AL and higher fouling propensity compared to the TFC HTI membrane. The TCK membrane with a woven substrate served as a promising membrane, with 2.25 times higher J_w and 1.48 times less J_s/J_w than the TFC HTI membrane. This study showed that a preparation of FO membranes with both enhanced antifouling resistance and TCK membrane-like open and thin structure are required to develop desirable FO membranes.

Integrally asymmetric cellulose triacetate/cellulose acetate (CTA/CA)-based membranes for FO were prepared via immersion precipitation method. The CTA/CA-based membranes were prepared in this studied using 1,4-dioxane and acetone as a solvent mixture, methanol and maleic acid as additives. The optimization of casting composition - 1,4-dioxane/acetone ratio and CTA/CA ratio - and

preparation conditions - substrate type, casting thickness, evaporation time and annealing temperature - was carried out. Membrane properties and performances were investigated against commercially available integrally asymmetric membranes by using various analytical tools and FO test system. The FO membrane prepared under the optimized composition and preparing conditions had a smooth surface, and showed higher water flux (J_w) and salt resistance (in terms of high salt rejection R and low reverse salt flux (RSF) J_s) than the commercial CTA-based membranes. Annealing improved the membrane performance by removing residual additives and solvents. The computerized image processing of optical microscopy images was shown to be useful for assessing the membrane substrates.

The effect of concentration polarization on performances of integrally asymmetric and TFC FO membranes was systematically investigated in two membrane configurations - active layer facing feed solution (AL-FS) and active layer facing draw solution (AL-DS). J_w of the membranes using pure water as FS in AL-DS were 1.7 to 2.6 times higher than those in AL-FS. However, with increasing FS concentration, the J_w in AL-DS declined rapidly and became lower than that in AL-FS. A modeling study showed that the reversal of J_w in the two configurations were resulted from concentrative ECP, and theoretical FS concentrations at which J_w in both configurations were equal were inversely proportional to the initial J_w of the membranes. The turnover of the J_w in AL-DS and AL-FS was also observed within 8 hours when seawater and river water were used as DS and FS, respectively. Moreover, the AL-DS faced the challenge of high fouling propensity and difficulty in cleaning more than the AL-FS. This study suggests that AL-FS membrane configuration is proper for both PRO and FO processes employing real natural water in terms of high membrane performance and ease of cleaning.

The available integrally asymmetric CTA-based and TFC PA-based FO membranes were also studied chlorination by hypochlorite. Performances and properties of various FO membranes were tested and characterized using ATR-FTIR, XPS, zeta potential, NMR and, particularly, ToF-SIMS. ToF-SIMS data suggested that chlorine first reacted with acetyl/acetate group, and then pyranose ring. Chlorine chemically bound and weakened H-bond of the CTA-based membrane, especially, cleaved the pyranose ring at high chlorine dosage, which resulted in the increase of water flux and reverse salt flux (RSF) of the chlorinated CTA-based membrane upon addition of chlorine exposure time or chlorine concentration. The CTA-based membrane structure after chlorination at high chlorine dosage was eventually fatigued upon filtration time. Besides, oxidation of CTA-based membrane by chlorine maximized at pH 7. The PA-based membrane was more vulnerable to chlorine at the acidic condition, resulting in more selectivity loss compared with the CTA-based membrane. However, alkaline chlorine solution insignificantly affected both FO membrane types. The TFC PA-based membrane yielded high water flux in FO but need improving chlorine tolerance for real application in which

pretreatment or membrane cleaning uses chlorine.

Contents

List of figures

List of tables

Nomenclature and Abbreviation

ρ	Fluid density (kg.m^{-3})
μ	Fluid dynamic viscosity (kg. m^{-1}.s^{-1})
ε	Porosity
τ	Tortuosity (μm)
$\pi_{D,b}$	Osmotic pressure of draw solution in bulk (bar)
$\pi_{F,m}$	Osmotic pressure of feed solution at membrane (bar)
A	Water permeability coefficient (L.m^{-2}.h^{-1}.bar^{-1})
B	Salt permeability coefficient (m.s^{-1})
c_{AP}	Concentration of solution at the AL-porous layer interface
c_b	Concentration of feed solution at in the bulk (mol.L^{-1})
c_m	Concentration of feed solution at the membrane-bulk interface (mol.L^{-1})
c_p	Concentration of solute in the permeate product (mol.L^{-1})
D	Diffusion coefficient of draw solute (m^2.s^{-1})
d_h	Hydraulic diameter (m)
i	Dimensionless van't Hoff factor
J_s	Solute flux (mol.m^{-2}.h^{-1})
J_w	Water flux in forward osmosis mode (L.m^{-2}.h^{-1})
$J_{w(RO)}$	Water flux in reverse osmosis mode (L.m^{-2}.h^{-1})
k	Cross-flow cell mass transfer coefficient (m.s^{-1})
K	Solute resistivity (s.m^{-1})
L	Length of channel in reverse osmosis cell
M	molarity (mol.L^{-1})
R	Solute rejection (%)
R_a	Roughness, nm
Re	Reynolds number
R_g	gas constant and equal to 0.08206 (L.atm.mol^{-1}.K^{-1})
R_{int}	The intrinsic solute retention (%)
S	Membrane structure parameter (m)
Sc	Schmidt number
Sh	Sherwood number
T	thermodynamic temperature in Kelvins (K)

t_s	Membrane thickness (μm)
v	Typical velocity of the flow in channel of reverse osmosis cell ($m.s^{-1}$)

AFM	Atomic force microscopy
ATR-FTIR	Attenuated Total Reflectance - Fourier Transform Infrared spectroscopy
CA	Cellulose acetate
CP	Concentration polarization
CTA	Cellulose triacetate
DS	Draw solution
ECP	External concentration polarization
FO	Forward osmosis
FS	Feed solution
HTI	Hydration Technology Innovation
ICP	Internal concentration polarization
PRO	Pressure-retarded osmosis
RO	Reverse osmosis
RSF	Reverse solute flux
SEM	Scanning Electron Microscope
TCK	Toray Chemical Korea
TFC	Thin film composite
ToF-SIMS	Time-of-Flight Secondary Ion Mass Spectrometry
XPS	X-ray photoelectron Spectroscope

I. INTRODUCTION

Firstly, this introduction section presents problem statements which drive this research to study the prospect of integrally asymmetric cellulose triacetate (CTA)-based and thin film composite (TFC) polyamide (PA)-based membranes for the osmotically-driven separation process. After that, this section presents background related to the osmotically-driven separation process. The motivation of this research arrives from the demand of the osmotically-driven separation process, the seeking of desirable membrane structure for osmotically-driven separation process, one of challenges of osmotically-driven separation process – concentration polarization effect - and the chlorination of the membrane in osmotically-driven separation process

1.1 Problem statement

People are facing the water shortage when world population becomes more and more numerous followed by an increase of human demand, industrial activities and pollution. In addition, the increase of world water consumption outpaces that of world population. According to World Water Organization (WWO), world water consumption increased thrice when world population increased twice from 1950 to 2010, and world water demand is subjected to exceed world water supply by 56% by the year 2025 [1]. People, therefore, require more and more advanced technologies for water/wastewater treatment. Membrane technology, particularly reverse osmosis (RO), is one of the most efficient solutions for water purification and desalination. In spite of very wide application of RO in most desalination plants with high salt rejection, people are finding alternative solution to adapt global trend of saving energy owing to high energy consumption of RO. Recently, membrane scientists have paid much attention to forward osmosis (FO) process due to its saving energy. Osmotic pressure difference between a high concentration solution (draw solution - DS) and a lower one (feed solution - FS) plays a role as a driving force in FO instead of hydraulic pressure in RO mode. This osmotic pressure difference induces a net flow of pure water from the FS passing through a semipermeable membrane to the DS side. For instance, in desalination, the FS is seawater or brackish water and the DS can be a mixture of fructose and glucose [2], fructose [3], ammonia-carbon dioxide [4], or inorganic salt, e.g. Na_2SO_4 [5], $MgCl_2$ [6] and $MgSO_4$ [7], which has a much higher osmotic pressure than the FS. Figure 1.1 presents principles in comparison of a pressure-driven process - RO and an osmotically-driven process – FO, of which details will be described in section 1.2.

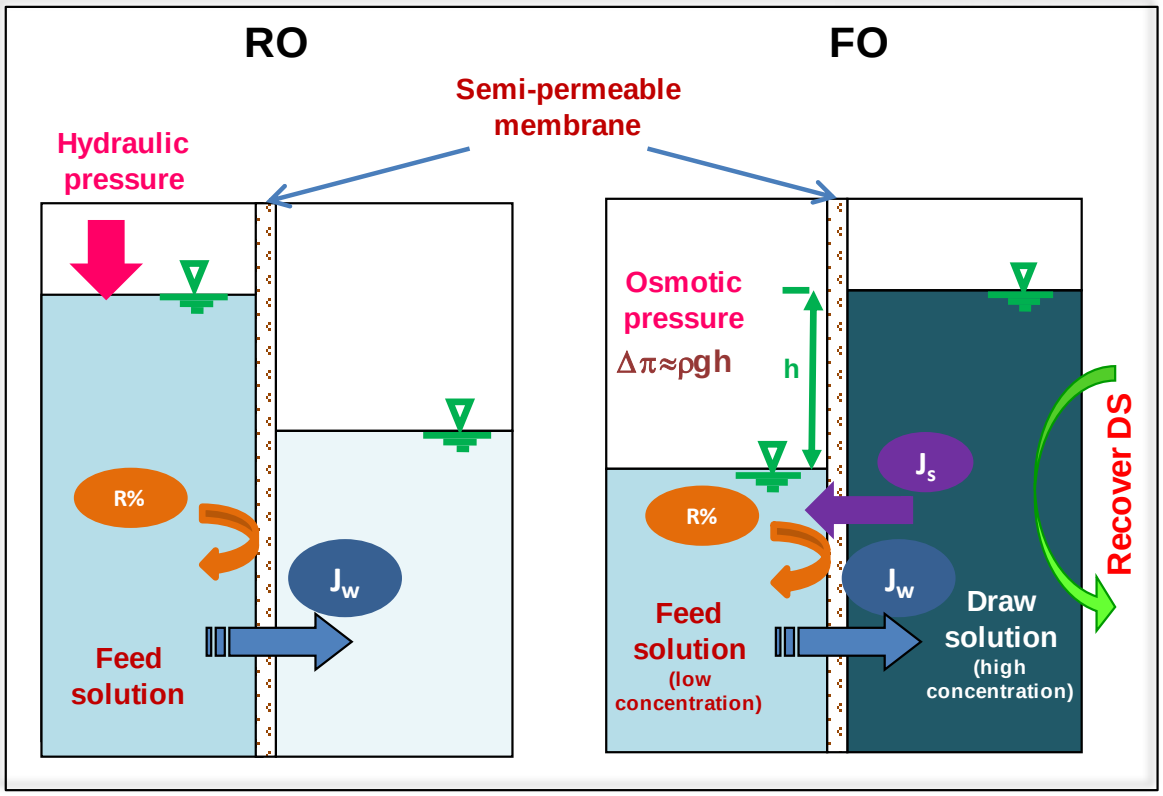

Figure 1. 1 *Principles in comparison of a pressure-driven process (RO) and an osmotically-driven process (FO)*

Because hardly hydraulic pressure is required, FO owns three major advantages, by which FO is considered nowadays not only as an alternative desalination method to conventional and costly methods such as distillation, electrodialysis or RO, but also as a promising method for wastewater treatment, water purification, or food and pharmaceutical processing [8]. First one is more economic benefit among membrane technologies applied to water/wastewater treatment, food process, pharmaceutical industry, and osmotic power due to low energy consumption. Second one is lower fouling and scaling than other pressure-driven processes, such as RO [9]. Third one is easy to be physically cleaned and achieves higher performance recovery compared to membranes used in RO process as a result of less compassion [10, 11].

Beside FO, PRO is also an osmotically-driven process which has been recently considered as an alternative energy production from osmotic pressure. PRO process utilizes osmotic pressure against hydraulic pressure to pressurize the brine solution, turn the hydro-turbine, and generate electricity (Fig. 1.2 [12]). The term PRO was firstly proposed by S. Loeb and R. S. Norman in 1975 [13]. At 2009, the first osmotic power plant producing 2 to 4 kilowatts of power was constructed and operated by Norwegian power company, Statkraft. PRO has been considered and reviewed as a sustainable power

generation process [14]. Widespread application of PRO still needs huge efforts to overcome drawbacks of this process.

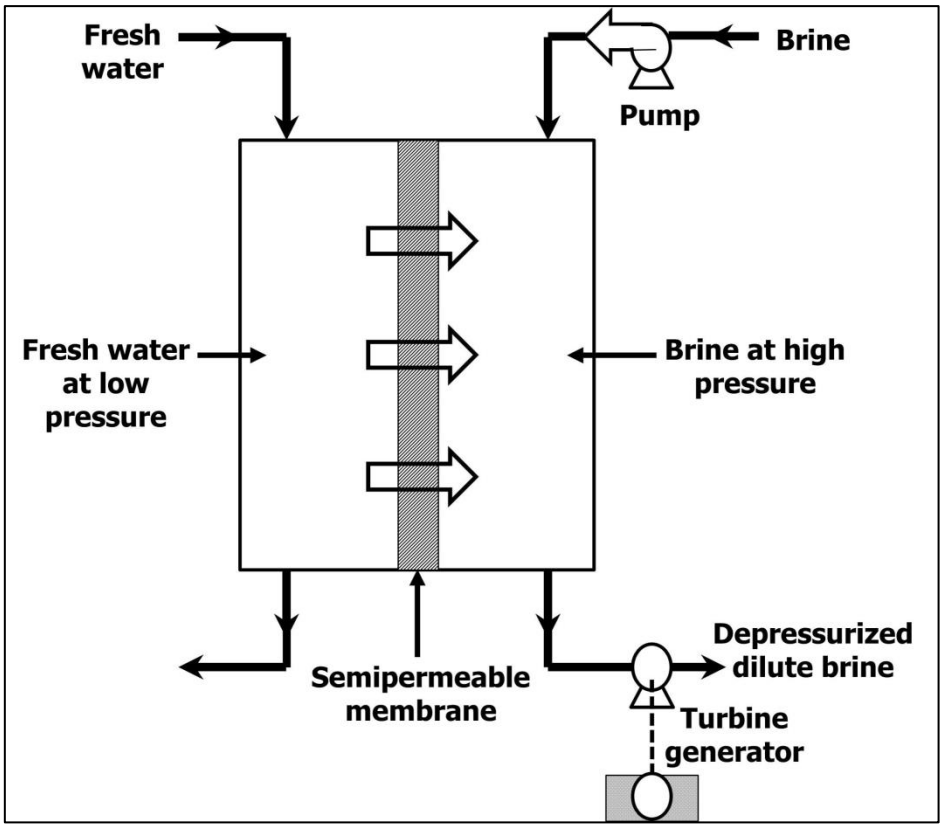

Figure 1. 2 *Conceptual representation of an energy production scheme based on pressure-retarded osmosis (PRO) (adapted from [12])*

Despite above advantages, the propagation of osmotically-drive separation process is limited due to some drawbacks. Its four significant drawbacks are (i) effect of internal concentration polarization (ICP) occurring within the support layer and causing the reduction of osmotic pressure gradient across the active layer, (ii) draw solute diffusion from DS to FS, (iii) lack of useful information of adequate membranes, and (iv) deficiency of proper DSs as well as recovery methods of the DSs. Recently, many membrane researchers have focused on ICP phenomenon [15-17], solute coupled-diffusion [18, 19], draw solutes such as ammonia-carbon dioxide, 2-methylimidazole-based compounds, and fertilizer [4, 20, 21], and effect of DS concentration on FO performance [22]. However, FO membrane researchers are still seeking adequate membranes for osmotically-driven separation process.

The development of FO membranes remains in its primary stage, and the exploration of desirable membranes is an emerging field which has potentially wide applicability in such water and

wastewater treatment. The early study of FO membranes employed reverse osmosis membranes of hydrophilic cellulose acetate (CA) and/or cellulose triacetate (CTA) polymers; which, when applied to FO, show low permeate water flux (J_w) since their porous support layer lead to great ICP. An FO membrane should, therefore, comprise a single thin and dense layer without any support layer [4, 23, 24], though the ensuing mechanical weakness may restrict wide applicability. Flat-sheet CA-based membranes that could eliminate ICP have been made using double-skinned membranes [24-26]; which, however, showed additional resistance to water transport and consequently low J_w. Wei et al. [27] prepared thin film composite (TFC) FO membranes by interfacial polymerization without using nonwoven fabric substrates, and Saren et al. [6] synthesized polyelectrolyte layer membranes using layer-by-layer assembly. However, such attempts have led to higher reverse solute flux (RSF, J_s) than shown by commercial FO membranes. A scaffold-like PES nanofiber with high porosity, low tortuosity and very thin thickness prepared by the electrospinning technique contributed to elimination of the ICP bottleneck of a polysulfone-polyamide TFC membrane in FO [28]. Employing a nanocomposite substrate by incorporating hydrophilic and porous zeolite nanoparticles into polysulfone substrate also helped enhance the water flux while mitigating ICP effect [29]. It was reported through simulation work that monolayer functionalized graphene could be an ideal membrane with zero ICP effect, resulting in 1.7×10^3 times higher water flux than commercial CTA-based membranes [30]. The need to develop membranes with high J_w and excellent salt resistance remains. Study of membrane is one of the prioritized missions for the wide spread application of FO.

Membrane structure is one of the main factors determining the concentration polarization and loss of draw solute during the operation of FO, and consequently, the performance of the membranes. Understating relationship between the membrane brane structure and performance is the core contribution to development of the desirable membranes. Membranes can be categorized into symmetric and asymmetric membranes in term of the structure, which determines the separation mechanism. Owing to high selectivity and permeation, asymmetric membranes, including integrally asymmetric and TFC membranes, have received much attention. Recently, many attempts have been made to synthesize flat-sheet FO membranes from integral type, i.e., double-skin membrane [25], polyethyleneimine-treated amide and imide (PEI treated PAI) copolymer membrane [31] and cellulose triacetate/cellulose acetate-based membranes [32] to the TFC type, i.e., polyamide/polysulfone TFC membranes without nonwoven fabric substrate [27] or with substrate prepared by double-blade casting knife [33], and polyelectrolyte layered membranes prepared via the layer-by-layer assembly method [6]. Approaches for the preparation of TFC FO membranes have also employed new components rather than the typical polysulfone/polyamide, e.g., cellulose acetate/polyamide propionate membrane [34]. Modification of TFC FO membranes has been conducted by incorporating nanoparticles to improve membrane performance [29, 35-37]. Nowadays,

integrally asymmetric CTA-based membranes and TFC membrane samples are commercially available at Hydration Technology Innovations (HTI, USA). However, understanding of the relationship between the structures of integrally asymmetric/TFC membranes and their performances has not yet been clearly revealed.

As listed above, one of major challenges limiting wide application of FO and PRO is the concentration polarization (CP) during the operation. An investigation of CP effect conducted at an early stage of PRO study revealed that ICP caused more than 80% water flux cut off [38]. Later studies have clarified the definitions of CP and proposed formulas for calculating the modulus of CP in asymmetric FO and PRO membranes. Concentration/dilution of solution in the boundary layer on outer surface of the membranes or in the porous support layer of the membranes results in concentrative/dilutive external concentration polarization (ECP) or concentrative/dilutive ICP [15]. Recent modeling study showed that the reduction of J_w by ICP reached 99.9% [39], and a theoretical study on zero-ICP mono-layer graphene oxide membrane (9.4 Å of pore diameter and 10% of porosity) yielded 91.5 $Lcm^{-2}day^{-1}$ (38,125 $Lm^{-2}h^{-1}$), which was 1.7×10^3 times more than J_w of commercial CTA-based FO membrane from Hydration Technology Innovations (HTI, OR, USA) [30].

Many attempts have been conducted to eliminate CP problems in FO and PRO operation, and most of the studies focused on the fabrication of membranes with low ICP problem. Double-skin layered membranes prepared via immersion precipitation method on glass plate showed the reduction of dilutive/concentrative ICP in the porous layer [25, 26]. The TFC membrane prepared on a thin woven fabric (Toray Chemical Korea, Korea) [40] or on a highly porous and thin electrospun nanofiber [28] also contributed to mitigating ICP and yielding high J_w.

Studies on CP in osmotically-drive separation processes showed that J_w in active layer facing feed solution (AL-FS) configuration was lower than that in active layer facing draw solution (AL-DS) configuration [41]. Therefore, AL-DS operation was suggested for the PRO operation, in which more J_w is preferred. However, the AL-DS configuration caused more fouling propensity than AL-FS configuration because foulants in FS could be easily trapped inside the porous layer of the asymmetric membrane and is not easily removed. Even though osmotically-drive separation processes showed low fouling propensity compared with pressure-driven processes such as RO, nanofiltration (NF), ultrafiltration (UF) and microfiltration (MF), the fouling caused by pore clogging inside of membrane is still a challenge to membrane scientists. Therefore, most wastewater treatment using FO process has been suggested AL-FS configuration. Besides, two different types of membrane structure with totally different structures of support layer – integrally asymmetric and TFC – likely show the different behavior of water and solutes transport through the membranes in AL-FS and Al-DS modes. Consequently, the CP effect on the membranes at various structures need systematically investigated

on various membrane structures in osmotically-driven separation process.

Fouling is one of the most challenges of membrane technology in water/wastewater treatment, and augments membrane resistance to water resulting in the decline of the water flux. Therefore, membrane operation requires pretreatment and periodical cleaning to maintain the long lifetime of the membrane. Besides various biocides (ozone, ultraviolet light, chloramine, chlorine dioxide, copper sulfate, iodine, hydrogen peroxide, peracetic acid and dichloroisocyanurate) and cleaning agents (caustic, oxidants, acids, sodium hydroxide, chelating agents and surfactants) associated with many pros and cons for each membrane operation, chlorine is regarded as one of the most convenient and cheap methods to prevent fouling and remove fouling of membranes in water/wastewater treatment [42, 43].

In pretreatment of feed solution, an addition of chlorine and flocculants (aluminum sulfate and polyelectrolytes [44] or poly-aluminum chloride [45]) suppresses microbial growth. However, once membranes are used in real water/wastewater treatment, membrane properties and, subsequently, membrane performance may be affected by the residual chlorine in the water. Although additional treatment of the feed solution prior to the membrane process such as activated carbon filter [42, 44] or dechlorination agents such as sodium bisulfite [42, 46] are used to remove the residual chlorine after the pretreatment, the membrane could be still affected by chlorine arising from the incomplete dechlorination caused by unexpected interferences such as competition of dissolved oxygen with chlorine for sodium bisulfite [46].

For cleaning fouled membranes, free chlorine has been used as a chemical cleaning agent for membranes in pressure-driven processes such as polyethersulfone ultrafiltration membranes [47, 48], polyvinylidene fluoride microfiltration membranes [49-51] or polyamide reverse osmosis (RO) membranes [52]. Compared with pressure-driven processes, the fouling of FO is less severe and more feasible to be cleaned without chemical reagents [53-55] because FO governs osmotic pressure difference instead of hydraulic pressure to induce water from low concentration solution (feed solution – FS) to high concentration one (draw solution – DS). However, the fouling in FO is still a challenge and requires chemical cleaning such as free chlorine if high contaminant FS was used.

Currently, there are two commercial membrane types for FO, namely, integrally asymmetric cellulose triacetate (CTA)-based and thin film composite (TFC) polyamide (PA)-based membranes. The previous study has showed the higher fouling propensity of the TFC FO membrane compared with the integrally asymmetric ones [40]. Cleaning fouled membrane may require using cleaning agents such as free chlorine. Early study has reported that cellulose acetate (CA) RO membrane soaked in 3,600 ppm.h (10 ppm for 15 days) chlorine at pH 5.5 increased about 14% water

permeability coefficient and retained salt rejection, but in 12,000 ~ 15,000 ppm.h (42 ~ 51 ppm for 12 days) chlorine at pH 5.5 increased 34% water permeability coefficient and lost 2.3% salt rejection [56]. The schematic reaction of chlorine and CA/CTA has been proposed in which chlorine sequentially and/or simultaneously oxidized the glucosidic bonds, opened the pyranose ring or oxidized hydroxyl sites to form carbonyl groups; however, there has been insufficient evidence of those proposals [57, 58]. Performance change, hypotheses of mechanism and parameters affecting on the chlorination of the RO membranes, particularly PA-based membranes, have been intensively studied [59-67]. Nevertheless, there is no publication on the chlorination of available FO membranes, neither integrally asymmetric CTA-based nor TFC PA-based membranes. Therefore, it is essential to investigate the property change and performance behavior of the available integrally asymmetric and TFC FO membranes due to the chlorination in FO.

1.2 Background and related researches

This section summarizes the basic knowledge related to the research of this dissertation. All definitions and descriptions about membrane separation, membranes, and specially, osmotically-driven separation process were systematically summarized and presented.

1.2.1 Membrane and membrane separation

The main factor of membrane process is membrane. Membrane is a thin film, plays the role as a barrier between two solutions. Membrane can be categorized based on various criteria. Those membranes can be summarized in Table 1.1 [68, 69]

Table 1. 1 *Categorization of membranes*

<table>
<tr><td rowspan="2">Biological membrane</td><td colspan="3">Living membrane</td></tr>
<tr><td colspan="3">Non-living membrane</td></tr>
<tr><td rowspan="6">Synthetic membrane</td><td rowspan="4">Pore size</td><td colspan="2">MF membrane: 0.05 – 5 µm</td></tr>
<tr><td colspan="2">UF membrane: 1 – 100 nm</td></tr>
<tr><td colspan="2">NF membrane: ~ 1 – 10 nm</td></tr>
<tr><td colspan="2">RO membrane: < 2 nm</td></tr>
<tr><td rowspan="3">Structure</td><td rowspan="3">Symmetric membrane</td><td>cylindrical porous</td></tr>
<tr><td>porous</td></tr>
<tr><td>nonporous membrane</td></tr>
</table>

<table>
<tr><td rowspan="8"></td><td rowspan="2"></td><td colspan="3">Asymmetric membrane: dense toplayer supported by porous sublayer</td><td>(Integral) asymmetric membranes</td></tr>
<tr><td colspan="3"></td><td>Composite membranes</td></tr>
<tr><td rowspan="6">Material</td><td rowspan="4">Organic</td><td colspan="2">Liquid membrane</td><td></td></tr>
<tr><td rowspan="2">Polymeric membrane</td><td>Hydrophilic</td><td>- Cellulose esters
- Polycarbonate (PC)
- Polysulfone/poly(ether sulfone) (PSf/PES)
- Polyimide/poly(ether imide) (PI/PEI)
- (Aliphatic) polyamide (PA)
- Polyetheretherketone (PEEK), etc.</td></tr>
<tr><td>Hydrophobic</td><td>- Polytetrafluoroethylene (PTFE, Teflon)
- Poly(vinylidene fluoride) (PVDF)
- Polypropylene (PP)
- Polyethylene (PE), etc.</td></tr>
<tr><td rowspan="2">Inorganic</td><td colspan="2">Ceramic: alumina (Al_2O_3), zirconia (ZrO_2), titania (TiO_2) silicium carbide (SiC), etc.</td></tr>
<tr><td colspan="2">Metal membrane: stainless steel, palladium, tungsten, silver, etc.</td></tr>
<tr><td rowspan="4">Module</td><td colspan="3">Flat-sheet membrane</td></tr>
<tr><td colspan="3">Spiral wound membrane</td></tr>
<tr><td colspan="3">Tubular</td></tr>
<tr><td colspan="3">Hollow fiber membrane</td></tr>
</table>

There are several methods for membrane fabrication exhibiting various membrane structures as listed below. These processes are reviewed from [68-70]

- Sintering
- Stretching
- Track-etching
- Template leaching
- Phase separation, including Vapour-Induced Phase Separation (VIPS), Liquid-Induced Phase Separation (LIPS), Thermally-Induced Phase Separation (TIPS), Colloidal-Induced Phase Separation (CIPS), Pressure-Induced Phase Separation (PIPS) and Reaction-Induced Phase Separation (RIPS).
- Coating, including Dip-coating, Spray coating, Spin coating, Interfacial polymerization, In-situ polymerization, Plasma polymerization and Grafting.

Selecting fabrication method depends on desirable structure of membrane. For instance, by employing stretching or template leaching, a microporous symmetric membrane can be obtained.

Phase separations methods are commonly used for preparing recently polymeric membranes whereas one of coating method is commonly employed for preparing NF and RO composite membranes.

Each specific characteristic of membrane morphology is characterized by one or several methods. Characteristics of membrane are listed with the utilization of analytical tools in Table 1.2.

Table 1. 2 *Characterization of membranes*

Membrane characteristics	**Analytical tools**
Surface and cross-sectional images	Scanning Electron Microscope (SEM)
Surface conductive and roughness (topography)	Atomic Force Microscope (AFM)
Thickness	Scanning Electron Microscope (SEM) Time-of-Flight Secondary Ion Mass Spectrometry (TOF-SIMS)
Membrane hydrophilicity	Contact angle instrument
Membrane Zeta potential	Zeta potential analyzer
Elemental composition	X-ray photoelectron spectroscopy (XPS) X-ray diffraction Energy-dispersive X-ray spectroscopy (EDS or EDX) Time-of-Flight Secondary Ion Mass Spectrometry (TOF-SIMS)
Transmittance of functional groups	Fourier transform infrared spectroscope (FTIR) Raman spectroscope UV-Vis-NIR (Solid)

The principle of membrane process is employing a semipermeable membrane to allow selective solutes to pass through membrane. Membrane processes can be classified based on driving force, i.e. i) pressure-driven process (Microfiltration – MF, Ultrafiltration – UF, Nanofiltration – NF – and RO), ii) osmosis-driven process (Pressure retarded osmosis – PRO – and FO), iii) electrical potential-driven process (Electrodialysis – ED – and Membrane electrolysis – ME), iv) concentration-driven process (Gas separation – GS, Vapor Permeation – VP, Pervaporation – PV, Carrier mediate transport, Dialysis, Diffusion dialysis – DD – and Membrane contactor – MC), and v) thermal-driven process (Membrane distillation – MD). Detail principles of these membranes are described elsewhere [68, 69, 71].

1.2.2 History of osmotically-driven separation process

Even though the concept of osmosis has been exploited since the early days of mankind, e.g. people desiccated food in salt, or dehydrated and inactivated bacteria and fungi in saline environment, studies on osmotic pressures have recently attracted much attention. Osmotic pressure was firstly termed by Jacobus Henricus Van't Hoff in 1886 when he described a phenomenon of water entry into a permeable vessel full of sugar solution and the subsequent pressure build-up on the permeable wall of the vessel [72]. Then, many studies on osmotic pressure has been done such as theory of osmotic pressure was studied on the nature of solvents and dissolved substances [73], or several direct measuring methods of osmotic pressure were done [74, 75]. And up to now, the calculation of osmotic pressure of Jacobus Henricus van't Hoff is still used as modified for dilute solution by Harmon Northrop Morse in Eq. (1.1), where π is osmotic pressure in atm, i is dimensionless van't Hoff factor, M is molarity in $mol.L^{-1}$, R_g is gas constant and equal to 0.08206 $L.atm.mol^{-1}.K^{-1}$, and T is thermodynamic temperature in Kelvins (K).

$$\pi = iMR_gT \quad (1.1)$$

The term PRO was firstly proposed by S. Loeb and R. S. Norman in 1975 [13]. At 2009, the first osmotic power plant producing 2 to 4 kilowatts of power was constructed and operated by Norwegian power company, Statkraft. PRO has been considered and reviewed as a sustainable power generation process [14]. Currently, HTI is the only company commercializes membranes and products employing principle of osmotically-driven separation process. History of osmotically-driven separation process is briefly reviewed based numbers of published papers and shown in Fig. 1.3.

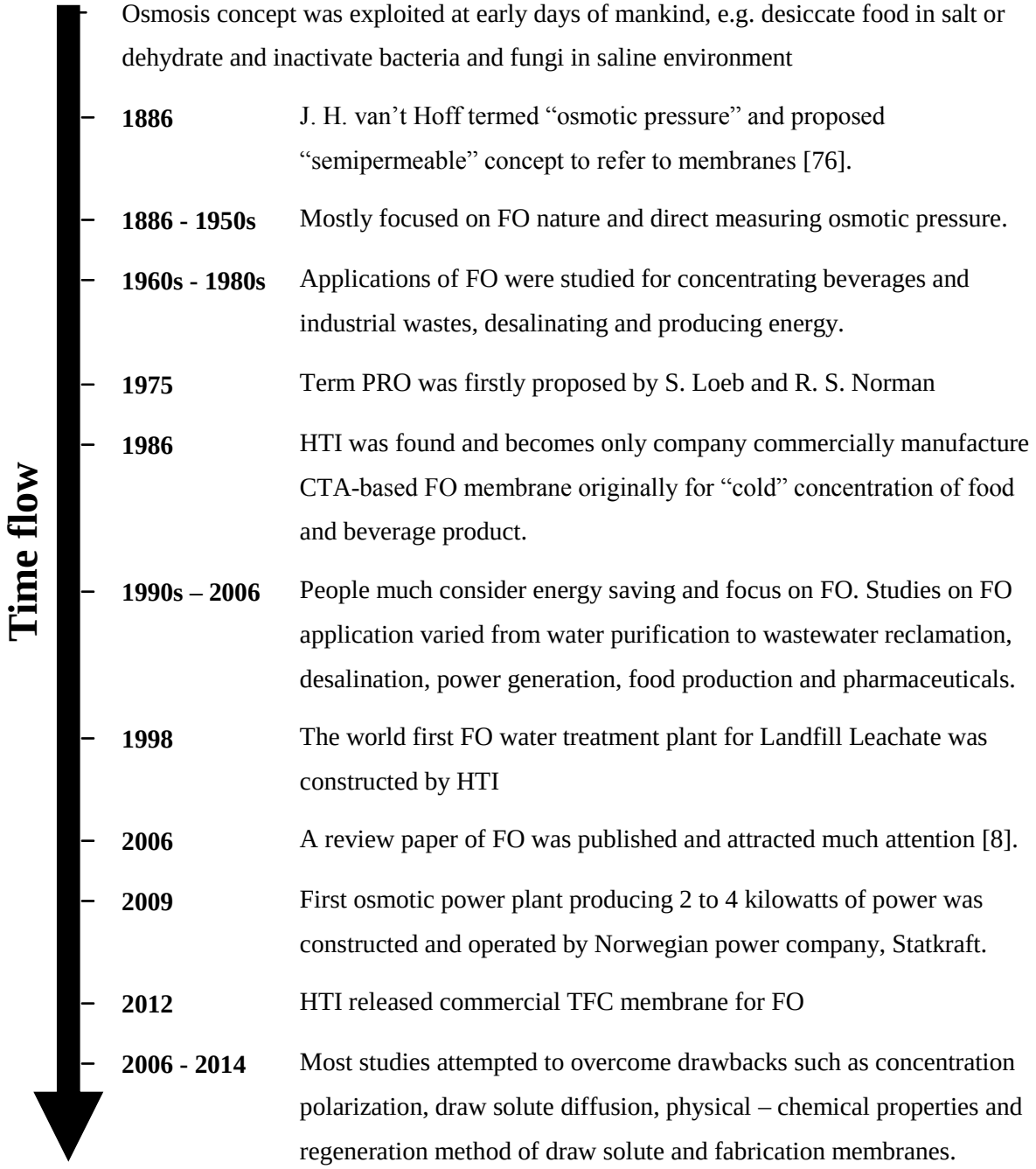

Figure 1. 3 *Development of FO upon time flow*

1.2.3 Effect of concentration polarization on the membrane performance in osmotically-driven separation process

Due to retained solutes and permeate water, the concentration of solutes in boundary layer of the membrane surface can be built-up or diluted. Therefore, this concentration becomes different with the

concentration of solutes in the bulk, which is so-called concentration polarization (CP). CP is classified into external and internal CP (ECP and ICP) based on the position of boundary layer, and into concentrative and dilutive based on the concentration difference.

Concentration polarization occurring outside or inside membrane is named external or internal concentration polarization. Concentration polarization modulus was proposed for ECP in Eq. (1.2) [77]

$$\frac{c_m}{c_b} = \frac{exp^{\left(\frac{J}{k}\right)}}{R_{int}+(1-R_{int})exp^{\left(\frac{J}{k}\right)}} \quad (1.2)$$

Where, R_{int} is the intrinsic solute retention, and $R_{int} = 1 - \frac{c_p}{c_m}$; k is the mass-transfer coefficient; c_m, c_b and c_p are the concentration on the membrane wall, in the bulk and of permeate, respectively. The simple equation is given in Eq. (1.3) is the ECP modulus in the case of all feed solutes are retained by membrane (R_{int} = 1).

$$\frac{c_m}{c_b} = exp^{\left(\frac{J}{k}\right)} \quad (1.3)$$

In order to reduce the ECP, mass-transfer coefficient, mainly determined by diffusion coefficient and flow velocity, should be increased by increasing feed velocity along membrane [77], whereas the ICP is hard to be reduced by increasing the velocity along the membrane.

When the concentration of solutes in the membrane boundary layer is higher than in the bulk, that phenomenon is so-called concentrative concentration polarization, and vice versa is so-called dilutive concentration polarization.

These phenomena are illustrated for asymmetric FO membranes in Fig. 1.4. Concentrative ECP and concentrative ICP occur in the boundary layer of FS – membrane interface and inside the membrane, respectively, whereas dilutive ECP and dilutive ICP occur in the boundary of membrane – DS interface and inside the membrane, respectively. Due to low water flux in FO, the severe effect of concentration polarization arises from accumulation of solutes in support layer. Therefore, the dilutive ICP is predominant in Fig. 1.4a whereas the concentrative ICP is domain in Fig. 1.2b. Comparing two cases in Fig. 1.4 reveals that concentration polarization the most affects decrease of osmotic pressure gradient cross the membrane when active layer faces the FS [15].

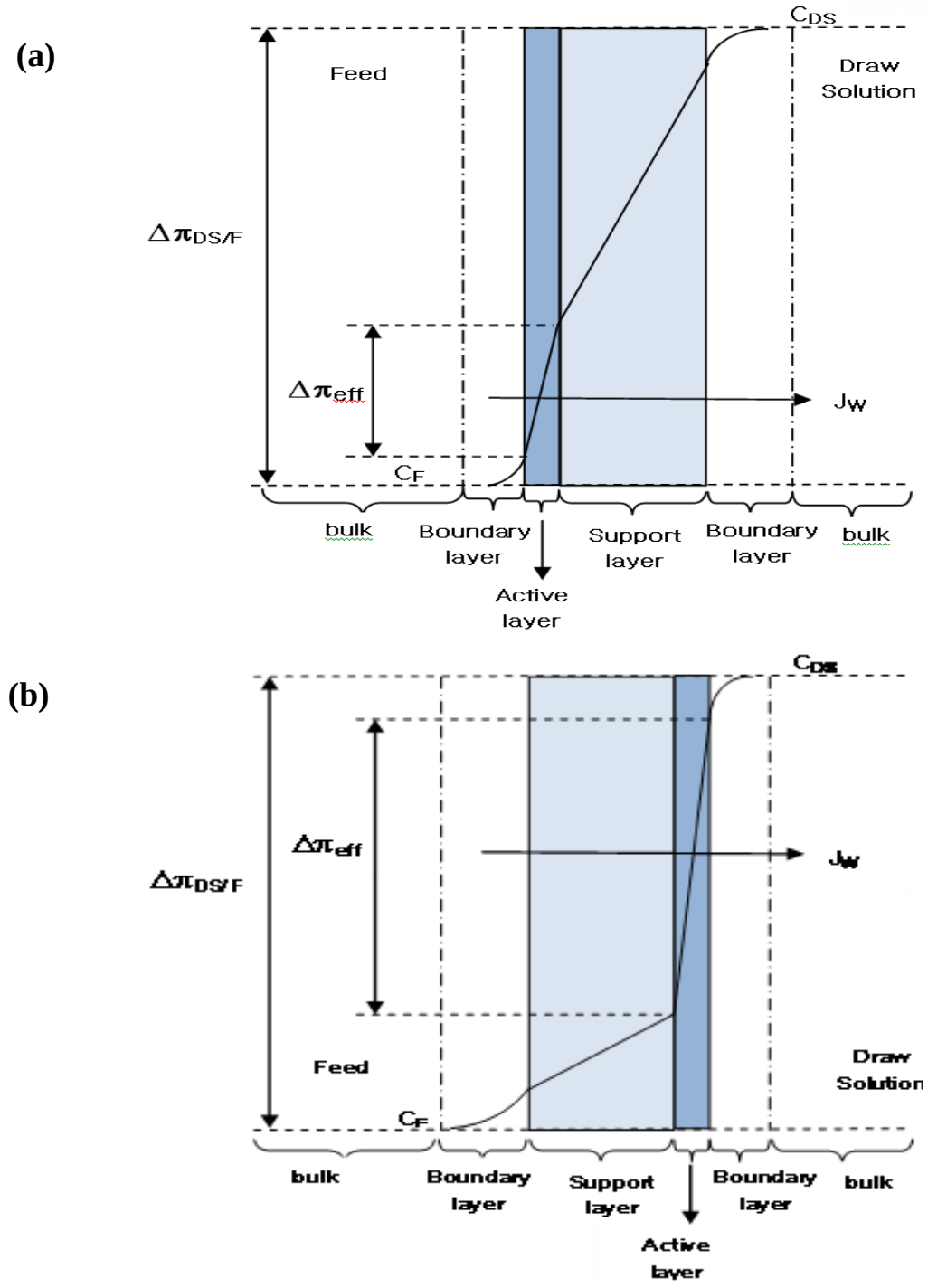

Figure 1. 4 *Concentration profiles of solutes in osmotically-driven separation process with active layer faces to FS (a) and DS (b)*

As listed in section 1.1, one of major challenges limiting wide application of FO and PRO is the concentration polarization (CP) during the operation. An investigation of CP effect conducted at an early stage of PRO study revealed that ICP caused more than 80% water flux cut off [38]. Later

studies have clarified the definitions of CP and proposed formulas for calculating the modulus of CP in asymmetric FO and PRO membranes. Concentration/dilution of solution in the boundary layer on outer surface of the membranes or in the porous support layer of the membranes results in concentrative/dilutive external concentration polarization (ECP) or concentrative/dilutive ICP [15]. Recent modeling study showed that the reduction of J_w by ICP reached 99.9% [39], and a theoretical study on zero-ICP mono-layer graphene oxide membrane (9.4 Å of pore diameter and 10% of porosity) yielded 91.5 $Lcm^{-2}day^{-1}$ (38,125 $Lm^{-2}h^{-1}$), which was 1.7×10^3 times more than J_w of commercial CTA-based FO membrane from Hydration Technology Innovations (HTI, OR, USA) [30].

Many attempts have been conducted to eliminate CP problems in FO and PRO operation, and most of the studies focused on the fabrication of membranes with low ICP problem. Double-skin layered membranes prepared via immersion precipitation method on glass plate showed the reduction of dilutive/concentrative ICP in the porous layer [25, 26]. The TFC membrane prepared on a thin woven fabric (Toray Chemical Korea, Korea) [40] or on a highly porous and thin electrospun nanofiber [28] also contributed to mitigating ICP and yielding high J_w.

Studies on CP in osmotically-drive separation processes showed that J_w in active layer facing feed solution (AL-FS) configuration was lower than that in active layer facing draw solution (AL-DS) configuration [41]. Therefore, AL-DS operation was suggested for the PRO operation, in which more J_w is preferred. However, the AL-DS configuration caused more fouling propensity than AL-FS configuration because foulants in FS could be easily trapped inside the porous layer of the asymmetric membrane and is not easily removed. Even though osmotically-drive separation processes showed low fouling propensity compared with pressure-driven processes such as RO, nanofiltration (NF), ultrafiltration (UF) and microfiltration (MF), the fouling caused by pore clogging inside of membrane is still a challenge to membrane scientists. Therefore, most wastewater treatment using FO process has been suggested AL-FS configuration. Besides, two different types of membrane structure with totally different structures of support layer – integrally asymmetric and TFC – likely show the different behavior of water and solutes transport through the membranes in AL-FS and Al-DS modes. Consequently, the CP effect on the membranes at various structures need systematically investigated on various membrane structures in osmotically-driven separation process.

1.2.4 Membrane fouling and chlorination

Membrane fouling arises from adsorption of solution on/into membrane, cake layer formation of retained solutes, or pore blocking of big particulates, of which depositions are irreversible and increase total resistance of the membrane resulting in the decline of water flux [77]. Different from

concentration polarization, which immediately occurs and reversible due to back diffusion of solutes from the boundary layer of the membrane to the bulk, fouling is a long-term phenomenon and irreversible, which is only reduced by cleaning. Fouling may be categorized into three types, i.e. organic fouling, biological fouling and inorganic fouling (scaling) relating to dissolved organic matters, microorganism and dissolved inorganic matters, respectively.

In order to control fouling, there are two approaches which are pretreatment of feed solution and cleaning membrane. Chlorine, flocculants, pH adjustment, $NaHCO_3$, UV treatment, heat treatment, activated carbon and filters are typical method for pretreatment. For cleaning, hydraulic, mechanic, chemical, or electrical cleaning may be employed. All these methods relates to physical and chemical properties of foulants. Chlorine has been considered as the cheapest and the most convenient way to inactivate microorganism for controlling biogical fouling [42, 43].

1.3 Objective and scopes of the research

Objective of this dissertation is study the effect of membrane structure on the membrane performance in the osmotically-driven separation process in order to contribute understating to the development of desirable membranes and application of the membrane in desalination and energy production. The first part of this dissertation focuses on studying desirable membrane structures for osmotically-driven separation process, namely investigating the effect of structure on performance of diverse membranes and fabricating membranes to understand the impact of the polymer composition and preparing condition on the membrane formation and subsequently performanceThe later part of the dissertation examined the effect of concentration polarization on performances of various membrane structures for a suggestion of a preferred membrane configuration in osmotically-driven separation process. Finally, studying chlorination of the available integrally asymmetric and TFC membranes have been done.

Immersion precipitation (nonsolvent-induced phase separation - NIPS), one of phase inversion methods was employed in this study for preparation of the integrally asymmetric labmade membranes with CTA/CA mixture as polymers. Several composition factors - 1,4-dioxane/acetone ratio and CTA/CA ratio - and preparing conditions – substrate types, casting thickness, evaporation time and annealing temperature - were optimized.

The optimized lab-made membrane for FO is studied the chlorine resistance to contribute understating of the chlorine mechanism and performance change of CTA-based FO membrane in comparison with other polyamide TFC FO and RO membranes in FO mode. The membrane

performance in terms of J_w and J_s of the membrane after being soaked in a hypochlorite solution was tested in FO mode, and compared with the virgin one.

The systematical comparison of membrane performance and properties between the integrally asymmetric and TFC membranes have done with two commercial integrally asymmetric and three TFC membranes. Structural properties of the membranes were analyzed using various analytical tools, and membrane performance was tested under various conditions. Furthermore, the fouling propensity of the membranes was also investigated through organic fouling tests.

Several integrally asymmetric and TFC membranes were tested in both AL-FS and AL-DS configurations. Theoretical J_w were calculated based on a model adopting both ICP and ECP. Furthermore, the effects of CP on the application of PRO using real river water and real seawater as FS and DS, respectively, or in desalination using real seawater as FS were systematically studied. Cleaning efficiency of the membranes was investigated to support the suggestion of proper membrane configuration for osmotic processes.

A lab-scale FO test cell was employed for testing performance of all membranes. Various DS and FS were used according to each experiment set. The membranes were characterized properties by utilizing various analytical tools such as Scanning Electron Microscope (SEM), Zeta potential analyzer, Attenuated total reflectance - Fourier Transform Infrared spectroscopy (ATR-FT-IR), Atomic force microscopy (AFM), Optical microscope and Time-of-Flight Secondary Ion Mass Spectrometry (ToF-SIMS). The membrane performance and surface properties were compared with those of commercial integrally asymmetric FO membranes - HTI1 and HTI2 – and TFC FO – HTI3 - from Hydration Innovation Technology (HTI, Albany, OR, USA). Besides, two TFC FO membranes were supplied from Toray Chemical Korea (TCK, South Korea). Other commercial NF and RO membranes NF270, NF90 and BW30 (DOW FILM-TEC^{TM}, MI, USA) were tested and characterized properties as references in this dissertation.

II. COMPARISON OF INTEGRALLY ASYMMETRIC AND TFC MEMBRANES

The section presents systematical investigation of the structure and subsequent performance of integrally asymmetric and TFC FO membranes to gain a better understanding of the working mechanism of FO membrane, and, to subsequently suggest an appropriate structure for FO membranes. Structural properties of the membranes were analyzed using various analytical tools, and membrane performance was tested under various conditions. Furthermore, the fouling propensity of the membranes was also investigated through organic fouling tests.

2.1 Experimental materials and methodology

2.1.1 Materials

Three commercial membranes from Hydration Technology Innovation (USA) and two membranes from Toray Chemical Korea (Korea) were used as representative FO membranes. The membranes were denoted as HTI1, HTI2, HTI3, TCK-N and TCK-W, respectively. According to the suppliers, HTI1 and HTI2 are integrally asymmetric membranes, while HTI3, TCK-N and TCK-W are TFC membranes. HTI1 was a cellulose triacetate (CTA)-based membrane, of which the polymer layer was embedded on a polyester mesh, while the CTA layer of HTI2 was cast on a polyester nonwoven fabric [32]. TCK-N was prepared on a polyester nonwoven fabric, while TCK-W was prepared on a polyester woven fabric. Commercial polyamide RO membranes (DOW FILMTEC™ BW30 and NF90, Dow, MI, USA) were used as TFC membrane references for chemical analysis. For most experiments, sodium chloride (NaCl, 99% purity, Bioshop, Canada) was used as the DS, while milli-Q water (18 MΩ resistivity, Millipore®, USA) was used as the FS. Isopropanol (99.5% purity, Samchun, Korea) was used as a nonionic solute to evaluate the pore size of the membranes in RO mode. Bovine Serum Albumin (BSA, assay > 96%, A2153-Sigma, USA) was used as a typical organic foulant in the fouling test.

2.1.2 Characterization of membrane properties

2.1.2.1 Measurement of membrane morphologies and surface characteristics

- **Field Emission Scanning Electron Microscope (FE-SEM):** Surface and cross-sectional images of the membranes were obtained using a FE-SEM (Cold FE-SEM SU8000, Hitachi, USA). The dried membranes were rigidly mounted on a sample holder using a conductive adhesive carbon tape. A Pt coating layer was then applied on the membranes using a Turbo Pumped High-Resolution Chromium Sputter Coater (K575X, EMITECH, Germany) at 20 mA and $2x10^{-3}$ mbar for 60 seconds to reduce the electrostatic charge of the membranes. For cross-sectional images, the membranes were carefully cut in liquid nitrogen and mounted on the sample holder afterwards.

- **Attenuated Total Reflectance-Fourier Transform Infrared (ATR-FTIR):** ATR-FTIR spectra of the membranes were measured using a Nicolet 6700 spectrometer (Thermo Scientific, USA) equipped with a flat plate germanium ATR crystal and OMNIC 8.1 software.

- **Atomic Force Microscopy (AFM):** Surface morphologies of the membranes were observed via atomic force microscopy using a Multimode V (Veeco, USA) in tapping mode.

- **Zeta potential:** The zeta potential of the membrane surfaces were measured using a Surpass analyzer (Anton Paar, Austria) equipped with an adjustable gap cell.

- **X-ray photoelectron Spectroscope (XPS):** Atomic percentages of the elements on the membrane active layer were measured using an XPS (K Alpha, Thermo Scientific, USA). The X-ray beam penetrates 5 ~ 10 nm from membrane active layer for analysis of the atomic percentages of the membrane skin. Membranes used for ATR-FTIR, AFM and XPS were freeze dried for at least 40 hours in a vacuum freeze dryer (Biocryos, Korea), while wet membranes were used for zeta potential measurements.

- **Microscope:** Microscopic images of the membrane substrates were taken using an optical microscope at 5x magnification (Axio scope, Carl Zeiss Micro Imaging GmbH, Germany). The images were then analyzed using Igor Pro software (Igor Pro 4.01, WaveMetrics, Inc., USA) for determination of the open space ratio of each substrate. The employment of microscopy and the processing image method to calculate the open space ratio of the substrates was described in a previous study [32]. In this study, the membranes were soaked in excess amount of N-methyl-2-pyrrolidinone (NMP) for at least 48 hours to get bare nonwoven and woven fabrics for microscopic measurement. The bare substrates then were dried in the oven at 30^{o}C before taking the microscopic images.

2.1.2.2 Rejection of ionic and nonionic solutes by membranes

Rejection of ionic and nonionic solutes by the membranes was measured in RO mode in order to illustrate the effects of membrane surface charge and pore size on membrane rejection. The RO set-up

was described in a previous study [32]. Membranes were tested at 25°C and the flowrate of 1 liter per minute (LPM) under 225 psi (15.5 bar) of applied pressure. Membranes were first compacted with deionized water (DI) for 1 hr, then, a 50 L solution of 2000 ppm NaCl and 2000 ppm isopropanol was used as the FS to check membrane rejection of these ionic and nonionic solutes. Water flux was determined after a 1 hour conditioning step by mass change of the collected permeate sample in a Falcon tube per unit of effective membrane area and per unit time as Eq. (2.1).

$$J_{w(RO)} = \frac{\Delta weigth}{\text{water density} \times \text{effective membrane area} \times \Delta time} (Lm^{-2}h^{-1} \text{ or LMH}) \quad (2.1)$$

Rejection of ionic NaCl was determined based on the conductivity of the collected permeate and feed solution, while rejection of nonionic isopropanol was determined based on the total organic carbon (TOC) concentration of the permeate and feed solution. Conductivity was measured by a calibrated conductivity meter (Ultrameter II™, Myron L Company, USA), and TOC was measured using a TOC analyzer (TOC-V, Shimadzu, Japan). Rejection was calculated using Eq. (2.2).

$$R = \left(1 - \frac{\text{Concentration of permeate}}{\text{Concentration of feed}}\right) \times 100\% \quad (2.2)$$

2.1.2.3 Determination of membrane structure parameter S

Herein, the derivation and calculation of structure parameter S were exhibited in detail. Since Yip et al. [78] defined the membrane structure parameter S as a function of solute resistivity K and diffusion coefficient of the draw solute D, S = KD, many attempts have been made to minimize the value of S, indicating the effect of concentration polarization on the FO membranes. The solute resistivity K was calculated by Loeb at al. [79] for the osmotic process with the active layer facing low concentration as

$$K = \frac{1}{J_w} ln \frac{B + A\pi_{D,b}}{B + J_w + A\pi_{F,m}} \quad (2.3)$$

and with the active layer facing high concentration as

$$K = \frac{1}{J_w} ln \frac{B + A\pi_{D,b} - J_w}{B + A\pi_{F,m}} \quad (2.4)$$

In the present study, the value of S was calculated in FO mode where the active layer faces the feed solution (AL-FS), as shown below.

$$S = \frac{D}{J_w} ln \frac{B + A\pi_{D,b}}{B + J_w + A\pi_{F,m}} \quad (2.5)$$

Where D is the salt diffusion coefficient (D of 1 M NaCl at 25°C is 1.48×10^{-9} $m^2 s^{-1}$ [80]). J_w is the water flux in the FO test. The J_w of the membranes was obtained herein using 1 M NaCl as the DS and

milli-Q as the FS at 25°C, with the flowrate of 1 LPM using AL-FS membrane orientation. $\pi_{D,b}$ and $\pi_{F,m}$ are osmotic pressure of the draw solution in bulk and osmotic pressure of the feed solution at the membrane, respectively, as determined by the OLI data (OLI system, Inc., NJ, USA). When 1 M NaCl was used as the DS and milli-Q was used as the FS, $\pi_{D,b}$ = 47.39 bar and $\pi_{F,m}$ = 0 bar. A is the water permeability coefficient, determined from the flux of the membrane in RO mode ($J_{w(RO)}$) using milli-Q water as the FS at each 2.5 bar increment of pressure from 5.5 bar to 15.5 bar after 1 hour of compaction at 15.5 bar, following equation $J_{w(RO)} = A(\Delta P - \Delta\pi)$ [81]. B is the salt permeability coefficient, the calculation of which was derived as below.

Regarding effect of concentration polarization, the concentration profile of the feed and permeate solution in RO mode were described elsewhere [77].

$$\frac{c_m - c_p}{c_b - c_p} = exp\left(\frac{J_{w(RO)}}{k}\right) \quad (2.6)$$

Where, c_m and c_b are the concentrations of the feed solution at the membrane - bulk interface and in the bulk, respectively, and c_p is the concentration of solute in the permeate product, $c_p = J_s/J_{w(RO)}$ [81].

By substituting the equation of salt rejection $R = 1 - \frac{c_p}{c_b}$ [77] and Eq. (2.6) into the equation of c_p , the B value was derived herein as shown below.

$$B = \frac{J_{w(RO)}(1-R)}{R} \exp\left(\frac{-J_w(RO)}{k}\right) \quad (2.7)$$

In the present study, $J_{w(RO)}$ and R were the water flux of the permeate and salt rejection, respectively, in the RO test using 2000 ppm NaCl as the FS, at 25°C and a 1 LPM flowrate. k is the cross-flow cell mass transfer coefficient of 2000 ppm NaCl. Calculation of the k value was shown elsewhere [22, 68].

$$k = \frac{ShD_{(RO)}}{d_h} \quad (2.8)$$

Where, $D_{(RO)}$ is the solute diffusion coefficient of the 2000 ppm NaCl solution at 25°C. d_h is the hydraulic diameterof the cross-section of the RO cell of 60 mm x 100 mm x 2 mm. The Sherwood number (Sh) was determined according to the flow regime elsewhere [22, 68], which was inferred from the Reynolds number (Re). Because low Re number (Re ≈ 591) was calculated for this RO test following the equation $Re = \rho\frac{vd_h}{\mu}$, the Sh number was calculated for the laminar flow regime following the equation $Sh = 1.85\left(ReSc\frac{d_h}{L}\right)^{0.33}$, wherein v is the typical velocity of the flow in the RO channel; ρ, and μ are the fluid density and fluid dynamic viscosity of the 2,000 ppm NaCl solution at 25°C, respectively; Sc is the Schmidt number, calculated for the feed solution in the RO

test, $Sc = \frac{\mu}{\rho D_{(RO)}}$; and L is the length of the RO channel. Data for calculation of the S value are shown in Table 2.3.

2.1.3 Performance test in forward osmosis mode

The schematic diagram of the lab-scale FO system was described in Fig. 2.1. A lab-designed membrane cell with an effective area of 3 cm wide and 9 cm long was used for testing. Two gear pumps were employed to deliver 1 LPM in counter-current flows of the FS and DS, except when evaluating the effect of flowrate on performance. Temperatures of the FS and DS were controlled with a water circulator (Fisher Scientific, Isotemp 3016D). Furthermore, the membranes were configured in normal FO configuration with the active layer facing the feed solution (AL-FS), as well as in PRO configuration, with the active layer facing the draw solution (AL-DS). For most tests, sodium chloride was used as the draw solution while milli-Q water was used as the FS. Various DS concentrations from 0.1 to 5.0 M of NaCl were used to investigate the effects of DS concentration. The pH of the FS and DS were not adjusted, except for experiments specially carried out at pH 4, 7 and 10 to investigate membrane behavior under various pH conditions. Membrane performances were examined over 10 minutes of stabilizing the water flux and another 2 hours of testing.

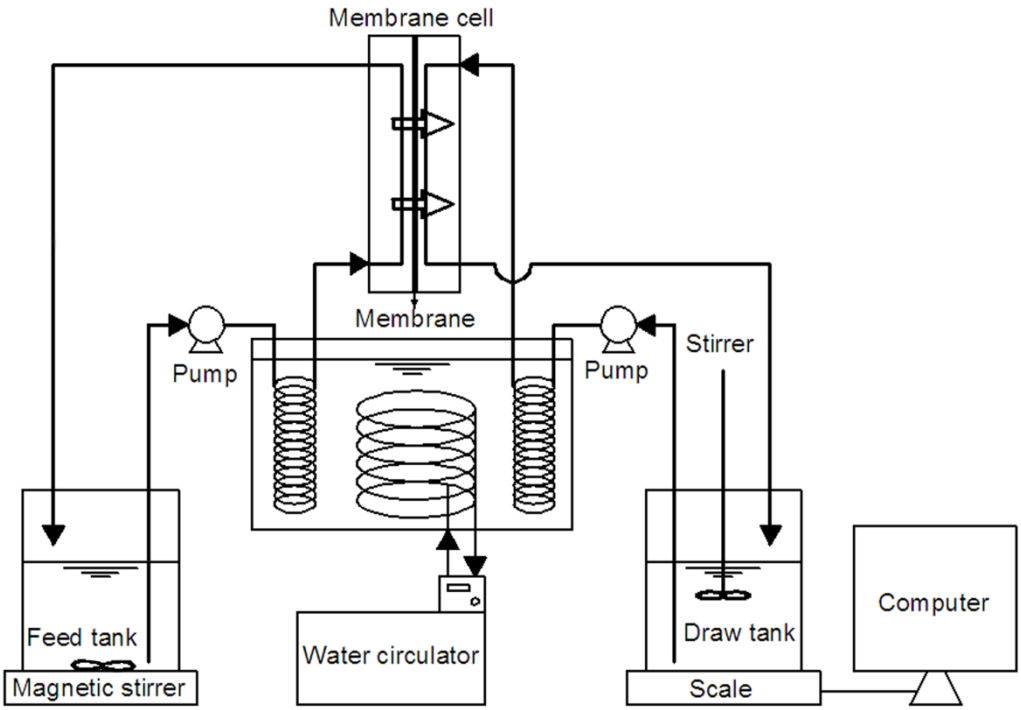

Figure 2. 1 *Laboratory-scale forward osmosis testing*

In order to investigate the fouling propensity of each membrane, BSA was used as a typical

foulant in the FS. All experiments in this investigation were conducted with 1 M NaCl as the DS, without adjustment of the pH of the FS and DS. Flowrate and temperature of both FS and DS were maintained at 1 LPM and 25°C, respectively, and the AL-FS membrane orientation was employed. A virgin membrane was first tested for 2 hour with 1 L milli-Q water as the FS, after which the FO system and the membrane were washed with DI water to remove the salt. The membrane was then taken out of the test cell, washed in milli-Q using a shaker (NB-101MT, N-BIOTEK, Korea) at 200 rpm for 5 minutes, and rinsed in milli-Q water. After the washing step, the membrane was tested for 3 hours with 1 L of 100 ppm BSA solution as the FS, followed by a washing step with ethanol 10 v/v% and DI water. Again, the membrane was taken out and washed as in the previous step. Next, the membrane was tested with milli-Q water as the FS to check the performance recovery after washing, followed by a washing step, testing with 1000 ppm BSA solution, washing again, and testing with milli-Q water.

For experiments to investigate the membrane performance under various operating conditions and to test the fouling propensity, membrane performances were evaluated in terms of the permeate flux (J_w) and reverse salt flux (RSF) (J_s). These calculations were based on the mass change of the DS and conductivity change of the FS. Calculation of the water flux followed Eq. (4.1) in section 4.1.2.2, and calculation of the RSF was described in the following equation.

$$J_s = \frac{\text{mole of NaCl}}{\text{effective membrane area} \times \Delta\text{time}} \ (\text{mole NaCl.m}^{-2}\text{h}^{-1}) \qquad (2.9)$$

Specific RSF (J_s/J_w) was also calculated to express membrane selectivity and FO efficiency, as well as draw solute loss along the permeate water product [19].

2.2 Results and discussion

2.2.1 Characterization of membrane properties

2.2.1.1 Membrane morphologies and surface characteristics

Analysis of the morphologies and surface characteristics of the membranes was carried out, which accounted for membrane separation characteristics and performance behavior under various conditions. The membrane morphologies were examined via FE-SEM. Information on the membrane morphologies was also supported by microscopic images of the bare substrates. Topographies of the membranes were revealed by AFM measurement, while the other surface characteristics of the membrane were analyzed using ATR-FTIR, XPS and a Zeta potential analyzer.

The surface, cross-section and bottom view of the membranes are shown in Fig. 2.2. The integrally asymmetric membranes, CTA-based polymer embedded on mesh (HTI1) or cast on a nonwoven fabric (HTI2), showed smooth surfaces; in contrast, the TFC membranes showed typical ridge-valley surface of the polyamide active layer (Fig. 2.2 a, d, g, j and m). Images of the bottom view showed downward diffusion of the dope solution to the bottom of the substrates during preparation, which covered the bottom side of the membranes except for HTI2, which had a thick and dense substrate. Aside from that, the bottom of the TCK-N membrane, shown in Fig. 2.2k, had patterns showing signs of another nonwoven fabric that had been peeled off from the bottom. The fabrication protocol of the TCK-N membrane has not yet been revealed, but it seemed that the membrane used a second substrate which was removed after fabrication in order to prepare a thin, air-trap free sublayer. The preparation of an air-trap free membrane has been reported through saturation of the substrate with solvent [82] or by polyvinyl pyrrolidone (PVP-K60) aqueous solution [7] to prevent the dope solution from penetrating into the substrate before solidification in a coagulation bath. Regarding the cross-sectional images, Fig. 2.2c, f, i, l and o exhibited dense structures of the integral membranes (HTI1 and HTI2) and finger-like structures of the TFC membranes (HTI3 and TCK). High magnification images in the boxed areas of the figures clearly showed that the finger-like structure of the HTI3 membrane was narrow and identical each other, while that of TCK-N was wide and even macrovoid at some areas. The finger-like structure of TCK-W was also identical, but quite wider than that of HTI3. This property may have resulted in the lower tortuosity of TCK-W compared with TCK-N and larger water pathway compared to HTI3, which will be illustrated in the performance test later.

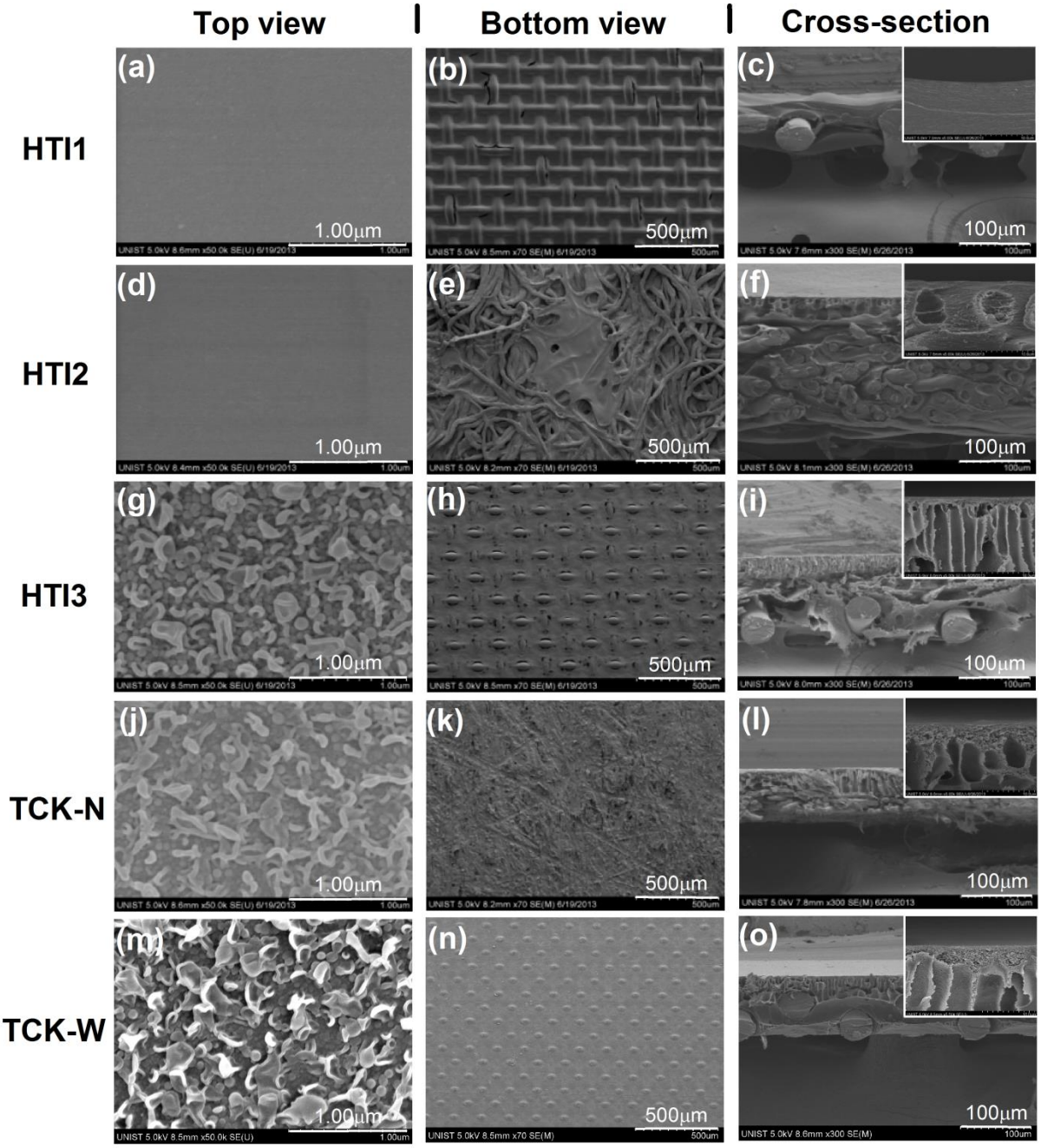

Figure 2. 2 *SEM images of the surface, cross-section, and bottom view of the integrally asymmetric membranes (HTI1 and HTI2) and the thin film composite membranes (HTI3, TCK-N and TCK-W)*

The microscopic images of the bare nonwoven and woven fabrics and their thicknesses measured by a thickness gage (Mitutoyo, Japan) are shown in Fig. 2.3 and Table 2.1, respectively. The open space ratios of the bare substrates were determined following the method in a previous study [32]. The shiny areas of the images were carefully darkened, then converted to binary images for analysis of the

white and black pixels. The woven HTI1 and HTI3 membranes showed the highest open space ratio, followed by the woven TCK-W, nonwoven TCK-N, and nonwoven HTI2. This examination revealed that the integrally asymmetric HTI1 and TFC HTI3 from HTI seemed to be prepared from the same woven polyester substrate material. TCK-N showed the thinnest thickness of both substrate and membrane. The open space ratios and thicknesses data supported the explanation of the S values of the membranes, which are discussed in Table 2.2.

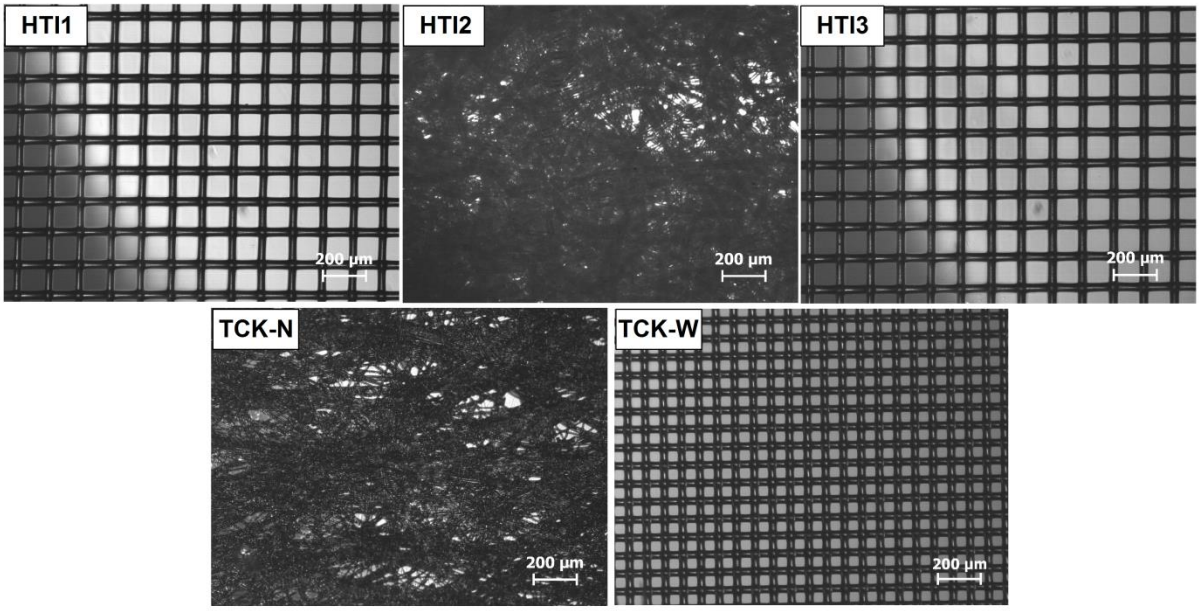

Figure 2. 3 *Microscopic images of bare nonwoven and woven fabrics of HTI1, HTI2, HTI3, TCK-N, and TCK-W membranes*

Table 2. 1 *Open space ratio and thickness of the substrates and corresponding integrally asymmetric (HTI1 and HTI2) and thin film composite membranes (HTI3, TCK-N and TCK-W)*

Membrane	**Open space ratio of substrate**	**Substrate thickness (1) µm**	**Membrane thickness (2) µm**	**Polymers thickness (*) = (2) - (1) µm**
HTI1	0.554 ± 0.006	62	90	28
HTI2	0.013 ± 0.007	154	163	9
HTI3	0.536 ± 0.003	68	113	45
TCK-N	0.028 ± 0.010	34	59	25
TCK-W	0.313±0.001	60	80	20

(*) This value did not include the thickness of the polymer occupying the substrate.

The ATR-FTIR spectra of all membranes are shown in Fig. 2.4. The CTA-based membranes, HTI1 and HTI2, were confirmed with the appearance of peaks for C=O, CH(CH_3) and C-O of acetyl groups at wavenumbers ~1740, ~1370 and ~1230 cm^{-1}, respectively. As described by TCK Company, the TCK membranes were made of a polysulfone (PSf) sublayer cast on nonwoven/woven fabric, and polyamide skin cast on the substrate. Appearance of peaks at the wavenumbers ~1660 and ~1545 cm^{-1} attributed to the amide I and amide II peaks of the polyamide skin layer were found in HTI3, TCK-N, TCK-W and commercial polyamide membranes (DOW FILMTEC^{TM} BW30 and NF90, Dow, MI, USA).The appearance of symmetric (1151 cm^{-1}) and asymmetric O=S=O stretching (1295 and 1323 cm^{-1}) of sulfone peaks was also found in the spectra of TCK-N, TCK-W and HTI3 membranes, which implied that the current TFC HTI3 membrane was comprised of a polysulfone layer and polyamide skin. However, HTI3 showed a higher intensity of O-H stretching than TCK-N and TCK-W (Fig. 2.4a), which suggested a different method of synthesizing polyamide skin layer of HTI3 compared to TCK-N and TCK-W, such as using another coating layer, additional additives, or other monomers. Comparing the three TFC membranes, the higher intensity ratio of PA/PSf at the same penetration depth of the IR beam in the ATR-FTIR measurement indicated a thicker PA layer in HTI3 compared to the TCK-N and TCK-W membranes (Fig. 2.5). The thicker PA layer of HTI3 might have resulted in the higher potential of concentration polarization effect compared to TCK-N and TCK-W, as discussed in a later part.

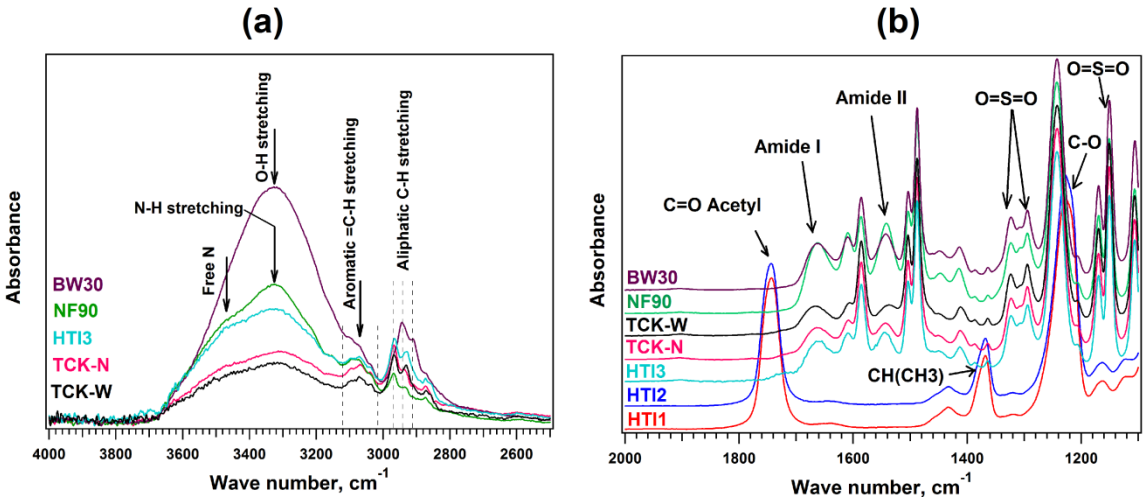

Figure 2. 4 *ATR-FTIR spectra of (a) thin film composite polyamide membranes (TCK-N, TCK-W, HTI3, NF90 and BW30) at higher wavenumber and (b) integrally asymmetric (HTI1, HTI2) and thin film composite (HTI3, TCK-N, TCK-W, NF90 and BW30) membranes at lower wavenumber*

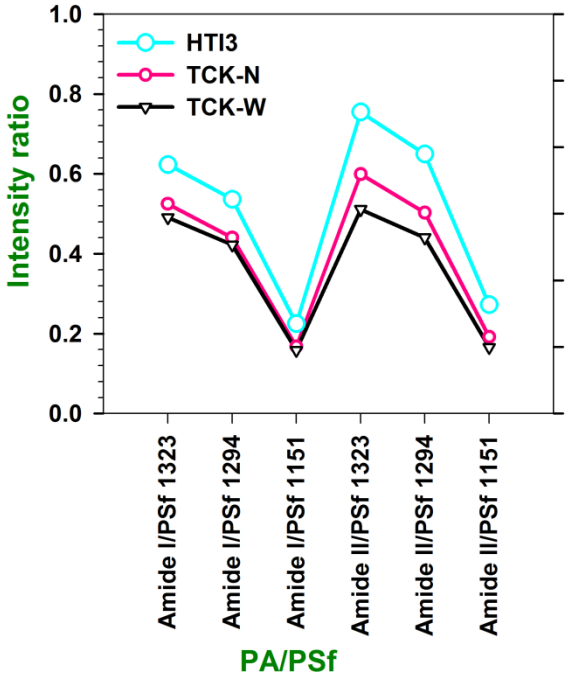

Figure 2. 5 *Amide/PSf intensity ratios of the TFC polyamide membranes (HTI3, TCK-N and TCK-W)*

Atomic percentages of the membrane surface were measured by XPS. C and O elements were detected on membranes HTI1 and HTI2, while C, O and N, which should be from amide bonds, were detected on the surface of HTI3 and TCK. It should be noted that H element cannot be detected by XPS measurement. Among the TFC membranes HTI3, TCK-N and TCK-W, the O/N of TCK-N and TCK-W (1.8 ± 0.1 and 1.3 ± 0.1) belonged to the theoretical ratio from fully-cross-linked (1.0) to fully linear polyamide (2.0) synthesized from trimesoyl chloride and 1,3-benzenediamine (m-phenylene-diamine) [83], while the ratio of HTI3 (3.2 ± 0.1) was out of the theoretical range. Furthermore, the atomic percentage of O (20.8 ± 0.4%) in the HTI3 polyamide layer also exceeded the theoretical values, which range from 12.5% for fully cross-linked to 19.1% for fully linear. Therefore, it is likely that the HTI3 membrane was prepared from another monomer other than trimesoyl chloride, with oxygen abundant additives, or with another coating layer. Regarding two the TCK membranes with the same monomer composition, the O/N value of TCK-W (1.3 ± 0.1) was closer to the theoretic value for fully cross-linked polyamide (1.0) than that of TCK-N (1.8 ± 0.1). This suggested a more cross-linked structure of TCK-W than TCK-N, which resulted in higher salt resistance, as illustrated in the later performance tests.

Topologies of all the membranes were also shown in AFM observation (Fig. 2.6). At the same scale, the surfaces of the integrally asymmetric CTA-based membranes were quite smooth (roughness R_a = 1.86 ± 0.18 nm for HTI1 and R_a = 2.00 ± 0.28 nm for HTI2), while ridge-valley rough surfaces of TFC HTI3 (roughness R_a = 26.25 ± 0.64), TCK-N (roughness R_a = 24.40 ± 0.85) and TCK-W

(roughness R_a = 34.23 ± 2.74) were observed. The smooth surface implied lower potential of fouling propensity of the integral membranes compared with the TFC membranes, which will be discussed clearly in section 2.2.3.

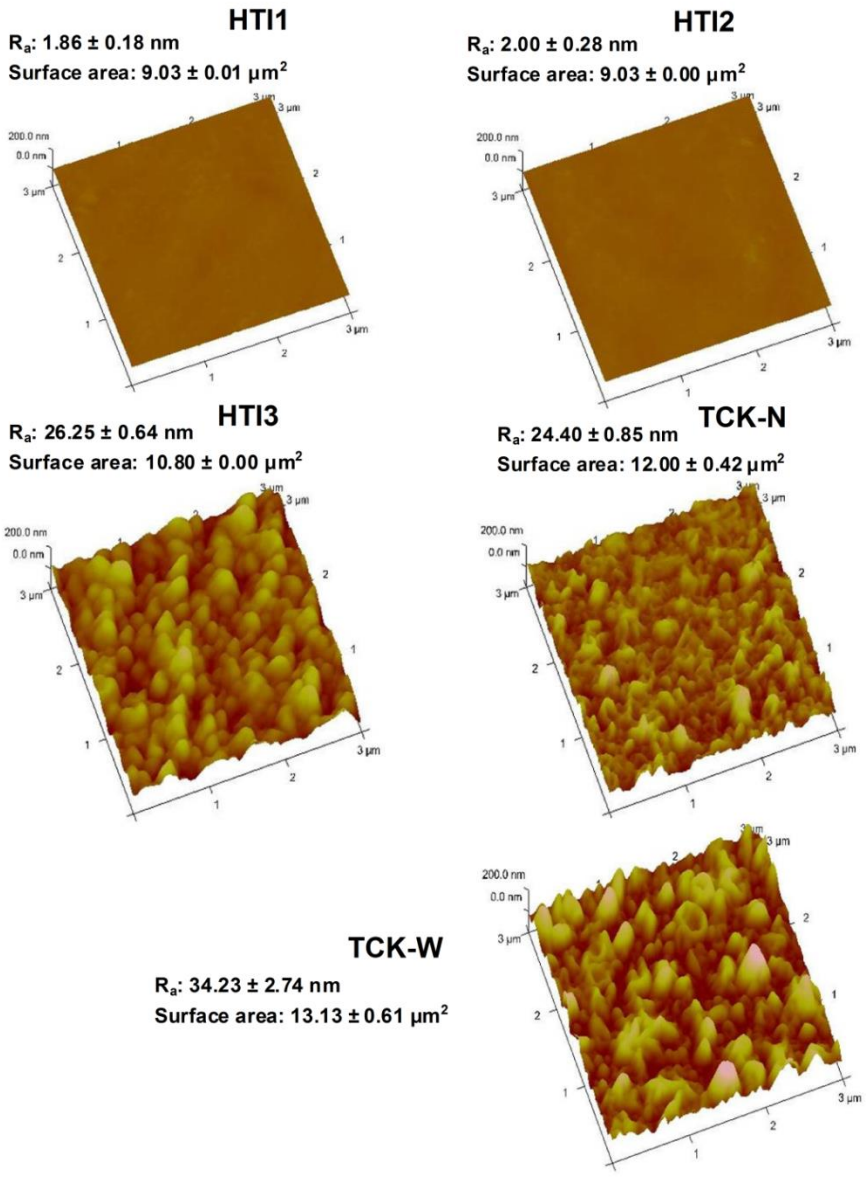

Figure 2. 6 *AFM images of the top surface of the integrally asymmetric (HTI1 and HTI2) and thin film composite membranes (HTI3, TCK-N and TCK-W)*

Zeta potentials of the membranes are shown in Fig. 2.7. All membranes showed negative potential at a pH range from pH 4 to 10, while the TFC membranes were more negative compared to the integrally asymmetric CTA-based membranes. The negative zeta potential of cellulose diacetate/cellulose triacetate-based reverse osmosis membrane was reported by other researchers [84]. The acetyl (CH_3CO-R) and hydroxyl (R-OH) groups do not dissociate (ionize) in aquatic systems, and thus the negative surface charge of the CTA-based HTI membrane likely resulted from adsorption of

electrolyte anions (OH^- and Cl^-) during measurement, and/or traces of acetic acid from acetylation and/or acidic functional additives during fabrication [32]. Meanwhile, the negative surface charges of the TFC membranes were due to the dissociation of the carboxylic acid groups R-COOH of the polyamide following $R\text{-}COOH = R\text{-}COO^- + H^+$ [84]. At high pH, more carboxylic acid groups dissociated, causing the membranes to become more negative, while positive charge was observed due to the amine functional group at extremely low pH. The TCK membranes showed more negative surface charge compared with the HTI3 membrane. The more negative surface charge of the TCK membranes was due to the different surface chemical composition from HTI3, which likely had another coating layer, some oxygen abundant additives, or different monomers from those of the TCK as described in XPS analysis. The zeta potential of the TCK membranes showed less negative values at basic pH compared to neutral pH. This observation was likely due to swelling of the membranes at high pH. More dissociation of the R-COOH groups at high pH led to more repulsion between negatively charged membrane materials causing swelling of the membranes, which resulted in movement of the electrokinetic shear plane far from the membrane surface and reduction in the membrane zeta potential [85], as described in the Gouy-Chapman theory of the exponentially decreasing electric potential upon increasing shear plane thickness.

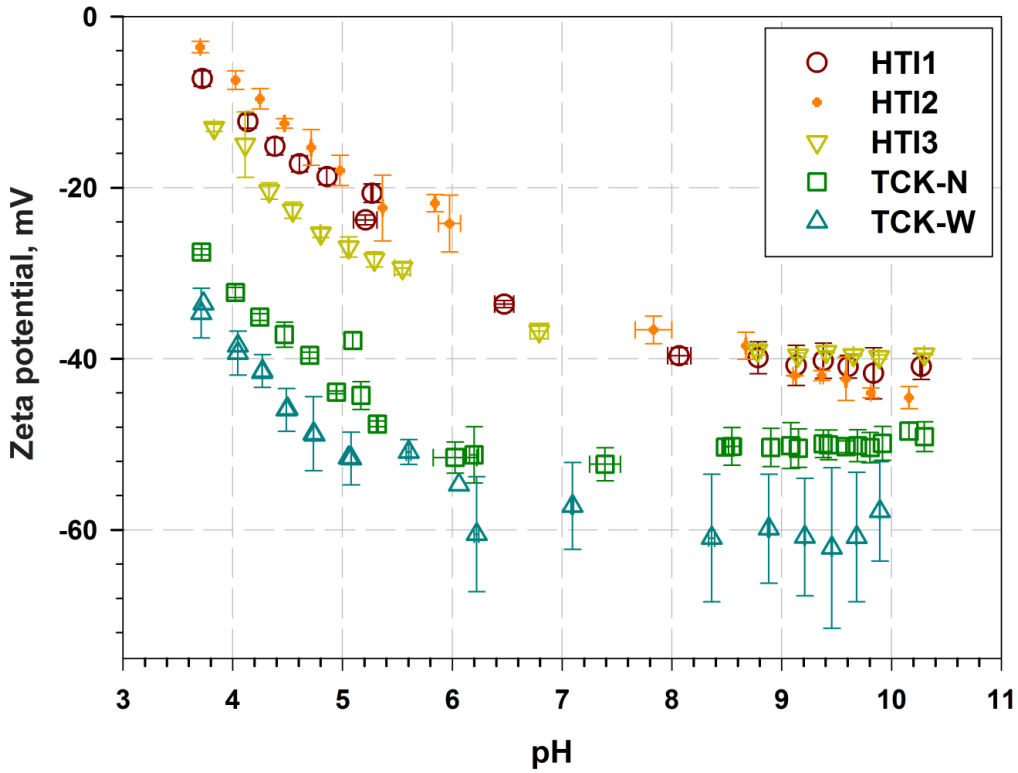

Figure 2. 7 *Zeta potential of the integrally asymmetric (HTI1 and HTI2) and thin film composite membranes (HTI3, TCK-N and TCK-W)*

2.2.1.2 Separation properties of membranes

The separation properties of the TFC membranes, as related to the pore size and/or surface charge, were systematically investigated. The intrinsic water permeability coefficient A, salt permeability coefficient B and membrane structure parameter S were obtained. The relationship of membrane properties and concentration polarization effect on the membranes were also examined via performance tests with two different membrane orientation modes.

Performance tests with the three TFC FO membranes were carried out in RO mode using ionic and nonionic solutes to illustrate the effects of surface charge on salt rejection of the membranes, the results of which are shown in Fig. 2.8. Water fluxes of the TCK membranes were much higher than that of HTI3 in RO mode, which could be explained by the fact that TCK membranes were thinner than the HTI3 membrane (Table 2.1) and had wider finger-like structures or macrovoids than HTI3 (Fig. 2.3). It was noted that the rejection of isopropanol observed in HTI3 was higher than TCK-N and similar to TCK-W, while the NaCl rejection of HTI 3 was comparable to the TCK membranes. Rejection of an ionic solute is determined by both membrane pore size and surface charge while rejection of a nonionic solute is determined by pore size. According to Fig. 2.7, the surface charges of the TCK membranes were more negative, which should have led to higher rejection of ionic solute due to repulsive interaction between the membrane and salts. Thus, the lower isopropanol rejection of TCK-N suggested larger pore size of this membrane compared to HTI3 and TCK-W.

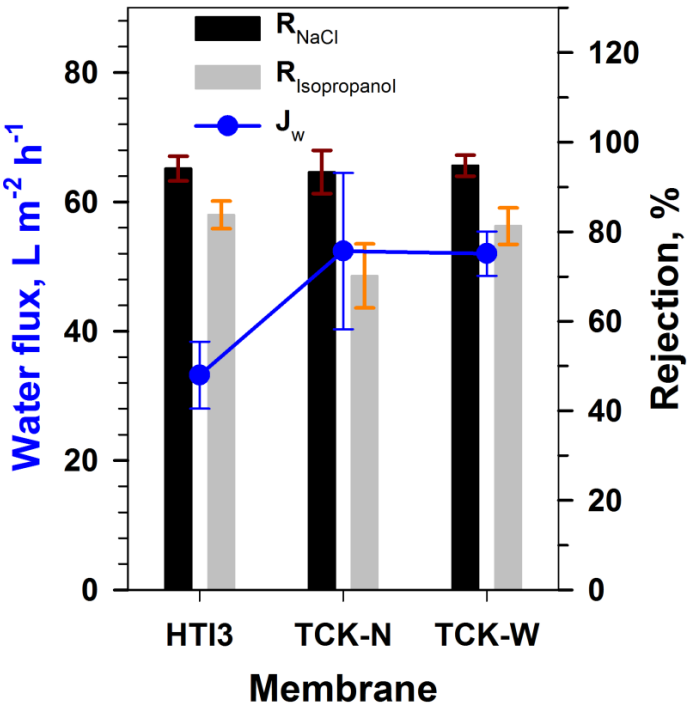

Figure 2. 8 *Performance of TFC membranes (HTI3, TCK-N and TCK-W) in the RO test using NaCl and isopropanol as ionic and nonionic solutes. A 50 L mixture of 2,000 ppm of NaCl and*

2,000 ppm of isopropanol was used as feed solution. Applied pressure was 15.5 bars. Flowrate was 1.0 LPM

The intrinsic water permeability coefficient A and salt permeability coefficient B of all membranes are shown in Table 2.2. The higher A values of the TFC FO membranes (3.036 LMH.bar^{-1} for HTI3, 6.601 LMH.bar^{-1} for TCK-N and 5.362 LMH.bar^{-1} for TCK-W) indicated superior water permeability to the integrally asymmetric membranes (0.460 and 0.436 LMH.bar^{-1} for HTI1 and HTI2, respectively). The water fluxes of HTI3, TCK-N and TCK-W in both RO and FO modes were much higher than the integrally asymmetric membranes, while the salt permeability coefficients B were still comparable, which inferred superior potential of the TFC membranes over the CTA-based integrally asymmetric membranes for use in FO.

Table 2. 2 *Membrane performance in FO and RO modes and intrinsic membrane properties of the integrally asymmetric (HTI1 and HTI2) and thin film composite membranes (HTI3, TCK-N and TCK-W)*

Membrane	R% (RO)	J_w (RO) LMH	A LMH.bar^{-1}	B x10^{-7}ms^{-1}	D x10^{-9}m^{2}s^{-1}	k x10^{-5}ms^{-1}	$\pi_{D,b}$ bar	J_w(FO) LMH	S µm
HTI1	85.73	7.13	0.460	2.924				9.29	454
HTI1-n	96.89	8.69	0.666	0.670				12.50	390
HTI2	95.35	6.75	0.436	0.816	1.480	1.652	47.39	6.33	968
HTI3	96.53	35.20	3.036	1.968				15.85	730
TCK-N	94.74	72.23	6.601	3.306				27.59	461
TCK-W	95.84	61.42	5.362	2.633				37.75	266

It should be noted that a new HTI1 (HTI1-n) was recently purchased from HTI (USA), while the old one was supplied before. HTI1-n showed different A, B and S values than the previous samples. The new HTI1 exhibited higher water flux but better salt resistance than the old one. This integrally asymmetric CTA-based HTI membrane type has been commonly used in other studies, and the properties were reported to be slightly different in each study (Table 2.3) [4, 16-18, 22, 27, 53, 78, 86-90]. Table 2.3 provides a short review which illustrates that the CTA-based membranes from HTI, which are well-known to be embedded on woven fabric, yielded variation of the permeability coefficients and structure parameters (A, B and S values).

Table 2. 3 *Summary of intrinsic water permeability coefficient, salt permeability coefficient and structure parameter of integral CTA-based HTI membranes at 25oC*

Membrane	A LMH.bar^{-1}	B x10^{-7}ms^{-1}	S µm	Reference
HTI1	0.460	2.924	454	This study
HTI1-n	0.666	0.670	390	This study
CTA	~1.089	-	-	[4]
CA-50^{o}C	2.048	-	-	[22]
HTI	1.110	1.273	-	[16]
CTA	0.312	-	-	[86]
HTI-CTA	0.44 ± 0.12	0.725 ± 0.169	481	[18]
HTI	0.80	1.7	-	[17, 87]
HTI-CTA	0.355 ± 0.109	0.889 ± 0.306	595 ± 114	[78]
CA	1.296	-	-	[53]
CTA-HW	1.19 ± 0.19	2.56 ± 0.14	720 ± 150	[27]
CTA-W	0.33 ± 0.04	0.4 ± 0.09	1000 ± 540	
HTI-CTA	0.611	1.91	498	[88]
HTI-CTA-20^{o}C	0.65 ± 0.10	0.681 ± 0.011	~525	[91]
HTI-CTA-40^{o}C	0.70 ± 0.03	0.992 ± 0.025	~525	
HTI-CTA	0.46 ± 0.02	0.26 ± 0.07	327 ± 41	[90]

Table 2.2 also shows that the structure parameters of the HTI1 (S = 454 µm), TCK-N (S = 461 µm) and TCK-W membranes (S = 266 µm) were lower than those of HTI2 (S = 968 µm) and HTI3 (S = 730 µm). The structure parameters and water flux of FO membranes are known to be related to membrane thickness (t_s), porosity (ε) and tortousity (τ) of the substructure, as shown in the equation $S = \frac{t_s \tau}{\varepsilon}$. Lower S values can come from higher porosity, lower tortousity, and/or thinner thickness. The structure parameter likely implies a characteristic distance which solutes must pass from the bulk draw solution to reach the active layer [78]; therefore, reduction of the S value is related to reduction of concentration polarization effect, resulting in high effective osmotic pressure difference through the membrane. This result could be clearly observed in the performance tests operated under the different membrane orientations, as discussed later in Fig. 2.9.

According to Table 2.1, the HTI1 and HTI3 substrates possessed similarly high open space ratio (0.536 ~ 0.554), but HTI1 demonstrated a low S value (454 µm), the S value of HTI3 was quite high (730 µm). Meanwhile, the S value obtained for TCK-N, with a low open space ratio (0.028 ± 0.010), was low (461 µm). The high substrate and membrane thickness of HTI3 (68 and 113 µm) and

extremely thin substrate (34 μm) and membrane (59 μm) of TCK-N may account for these results. This investigation suggested that besides open space ratio, having an extremely thin substrate is very important for fabricating FO membranes in order to reduce the membrane structure parameters or, in other words, the effect of concentration polarization. TCK-W, adapting a high open space ratio (0.313 ± 0.001) with a thin substrate and membrane (60 and 80 μm), exhibited the lowest S value (266 μm).

The concentration polarization effect on each membrane was evaluated via performance tests with two different membrane orientations, namely, AL-FS and AL-DS (Fig. 2.9). The water flux and RSF of all the membranes were lower for the AL-FS conditions than for AF-DS because the draw solute could easily become trapped and diluted inside the support layer in the case of AL-FS. Dilution of the draw solution at inner side of the active skin layer of the membrane in AL-FS mode lowered the concentration difference, and thus, the effective osmotic pressure difference across the membrane. The suppressed osmotic pressure difference between both sides of the active skin layer in the AL-FS mode decreased the driving force for water transport through the active layer.

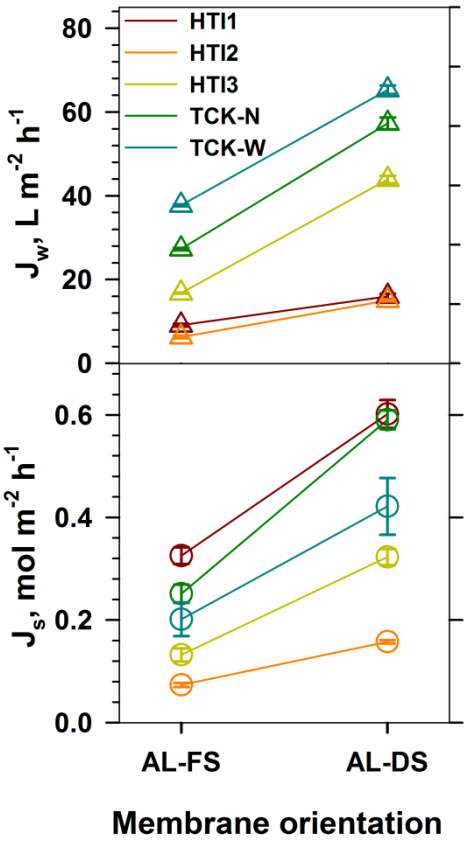

Figure 2. 9 *Effect of concentration polarization on membrane performance. Conditions: The DS was 1 M NaCl and the FS was milli-Q water, both at 25°C. The flowrate of 1.0 LPM was used with vertical orientation of the membrane cell*

Schematic salt passage through the membrane was illustrated in Fig. 2.10. As described for

osmosis process by Lee at al. [12], RSF through the substrate ($J_{s(sub)}$) is a function of the diffusive flow from high concentration to low concentration as Fick's first law, $D_s \frac{dC(x)}{dx}$, and the convective flow coupled with water flux from low concentration to high concentration, $J_w C(x)$.

$$J_{s\,(sub)} = D_s \frac{dC(x)}{dx} - J_w C(x) \tag{2.10}$$

For an asymmetric membrane, the active layer plays an important role in salt transport. At the steady state, salt leakage cross the active layer ($J_{s(AL)}$) was equal to salt flux in the porous layer, which was equal to the RSF through the membrane ($J_{s(net)}$).

$$J_{s\,(sub)} = J_{s(AL)} = J_{s(net)} \text{ or } D_s \frac{dC(x)}{dx} - J_w C(x) = B|c_{AP} - c_m| \tag{2.11}$$

Where, c_m and c_{AP} are concentrations of solutions at the bulk-AL interface and the AL-porous layer interface, respectively; D_s, $\frac{dC(x)}{dx}$, and $C(x)$ are the diffusion coefficients of the solute, concentration gradient across the membrane, and concentration profile at distance x from DS bulk-membrane interface, respectively. In the case of the AL-DS orientation, $|c_{AP} - c_m|$ was higher than for the AL-FS configuration. Therefore, higher RSF was observed in AL-DS compared to AL-FS.

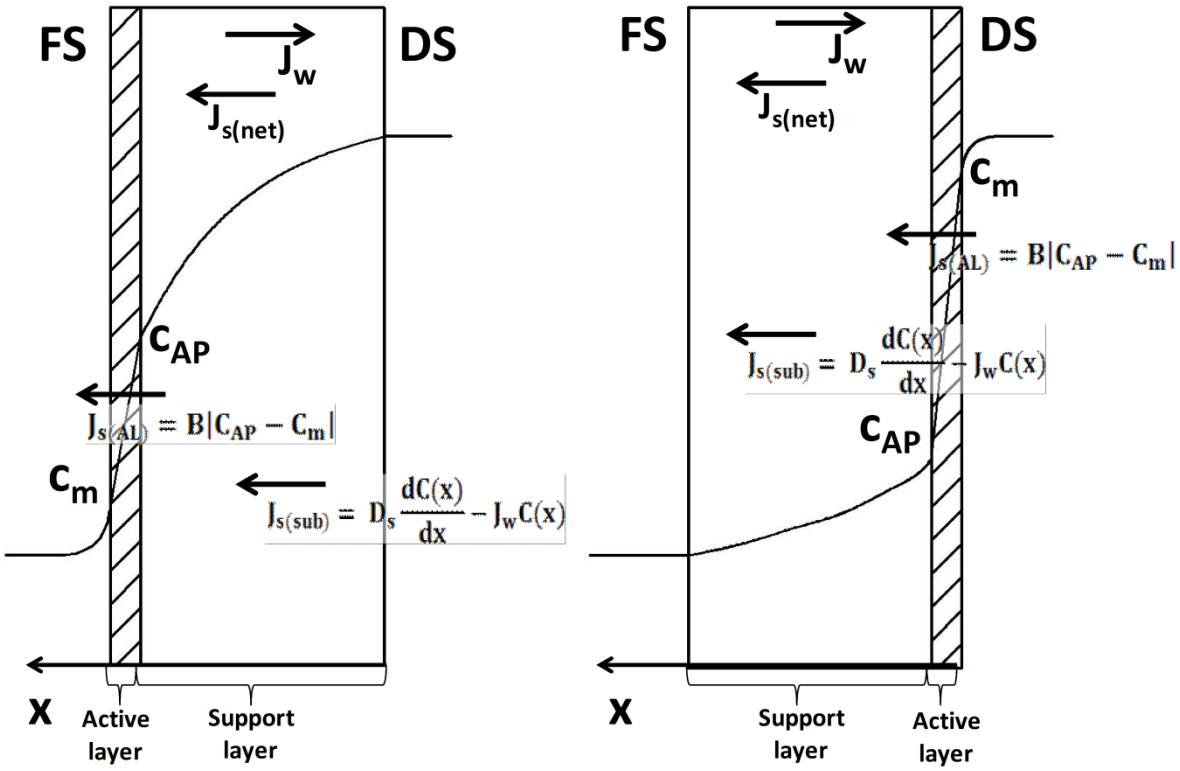

Figure 2. 10 *Schematic salt passage through asymmetric membranes with two different membrane configurations, active layer facing feed solution (AL-FS) and active layer facing draw solution (AL-DS). cm and cAP are concentrations of solutions at the bulk-AL interface*

and the AL-porous layer interface, respectively. Ds, $\frac{dC(x)}{dx}$ *and C(x) are the diffusion coefficients of the solute, concentration gradient across the membrane, and concentration profile at distance x from the DS bulk-membrane interface, respectively*

In this study, the concentration polarization effect factor was suggested for quick evaluation of the effect of concentration polarization on membrane performance. The concentration polarization effect factor was defined as the ratio of water flux in the case of AL-DS to that in AL-FS ($J_{w(DS)}/J_{w(FS)}$). The concentration polarization effect factor of TCK-W was the lowest among the membranes, indicating the lowest effect of concentration polarization on this membrane. Figure 2.11 shows the relationship among membrane structure parameter (S), membrane thickness (t_s) and porosity/tortousity parameter ($\varepsilon/\tau = t_s/S$) with water flux (J_w), concentration polarization effect factor ($J_{w(DS)}/J_{w(FS)}$) and specific reverse salt flux (J_s/J_w). Figure 4.10 appeared to show a consistent trend of the structure parameter S, reverse value of water flux $1/J_w$ and concentration polarization effect factor $J_{w(DS)}/J_{w(FS)}$. As they were supposed to have the same CTA-based polymer, the higher effect of concentration polarization found in HTI2 compared to HTI1 was due to thicker and denser support layer (Table 2.1 and Fig. 2.9). The HTI1 and HTI3 membranes had the same substrate (Fig. 2.2) but different membrane thickness and membrane structure, which led to higher effects of concentration polarization on the thicker TFC HTI3 compared to the effects on the thinner integrally asymmetric HTI1. Comparison of the three TFC membranes revealed that even though the HTI3 membrane possessed a higher open space ratio of substrate than that of the TCK membranes (Table 2.1), the concentration polarization effect factors of the HTI3 membrane were higher than TCK-N and TCK-W. As explained earlier, this was attributed to the thicker substrate, thicker membrane, and thicker polyamide layer of the HTI3. The second row of Fig. 2.11 illustrated the relationship between specific reverse salt flux and the physical properties of the membranes. Specific reverse salt fluxes of both integrally asymmetric and TFC membranes exhibited the same pattern as $1/t_s$ rather than the porosity/tortousity parameter (ε/τ). This suggested that thin membrane thickness t_s including substrate thickness and/or polymer thicknesses, is meaningful for the reduction of concentration polarization and specific reverse salt flux.

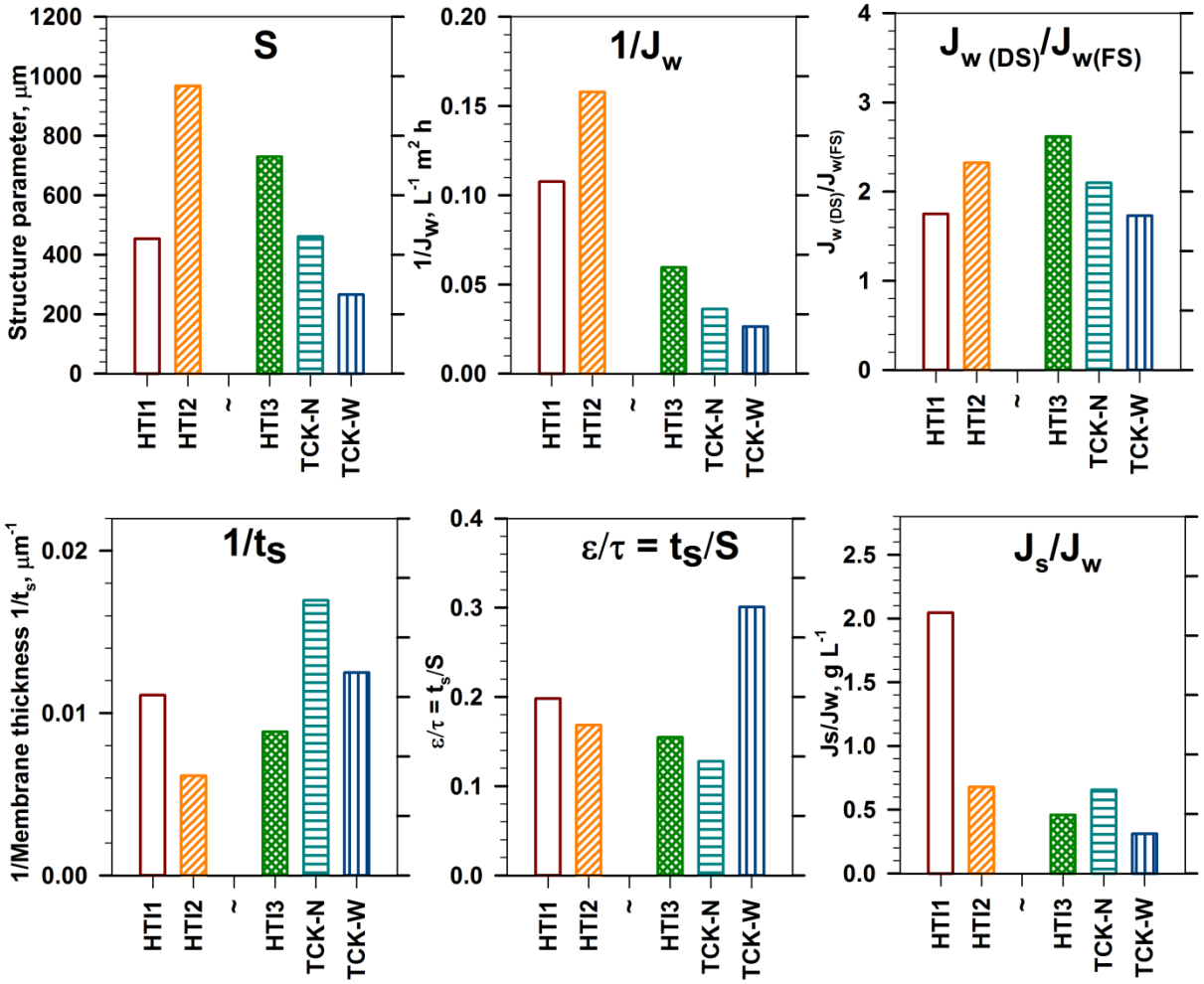

Figure 2. 11 *Relationship between membrane properties and membrane performance of the integrally asymmetric (HTI1 and HTI2) and thin film composite membranes (HTI3, TCK-N and TCK-W) in FO mode*

2.2.2 Performance of integrally asymmetric and TFC membranes under various physico-chemical conditions of FS/DS

Performance measurements of FO membranes were carried out under various conditions of FS/DS, and the effect of physico-chemical conditions of the solutions on the performance was systematically investigated.

In order to compare the performance behavior of the integrally asymmetric and TFC membranes under various solution chemistries of FS/DS, the FO membranes prepared on woven and nonwoven fabric for each membrane type (HTI1 and HTI2 for integrally asymmetric, HTI3 and TCK-N for TFCs representatives) were tested in FO mode. The performances of these membranes operated under

various flowrates of FS and DS are shown in Fig. 2.12. Both J_w and J_s of the integrally asymmetric and TFC membranes increased with increasing flowrate. The high flowrate might have reduced the dilutive external concentration polarization, causing high osmotic pressure difference to remain. The reduction of dilutive external concentration polarization caused high concentration of DS at the membrane and DS bulk interface, which resulted in higher draw solute flux at high flowrate. However, the thickest membrane, HTI2, did not show much change in performance upon increasing the flowrate. The effect of flowrate on the concentration polarization effect in the thicker membrane, in which the internal concentration polarization was more dominant than the external concentration polarization effect, was almost negligible.

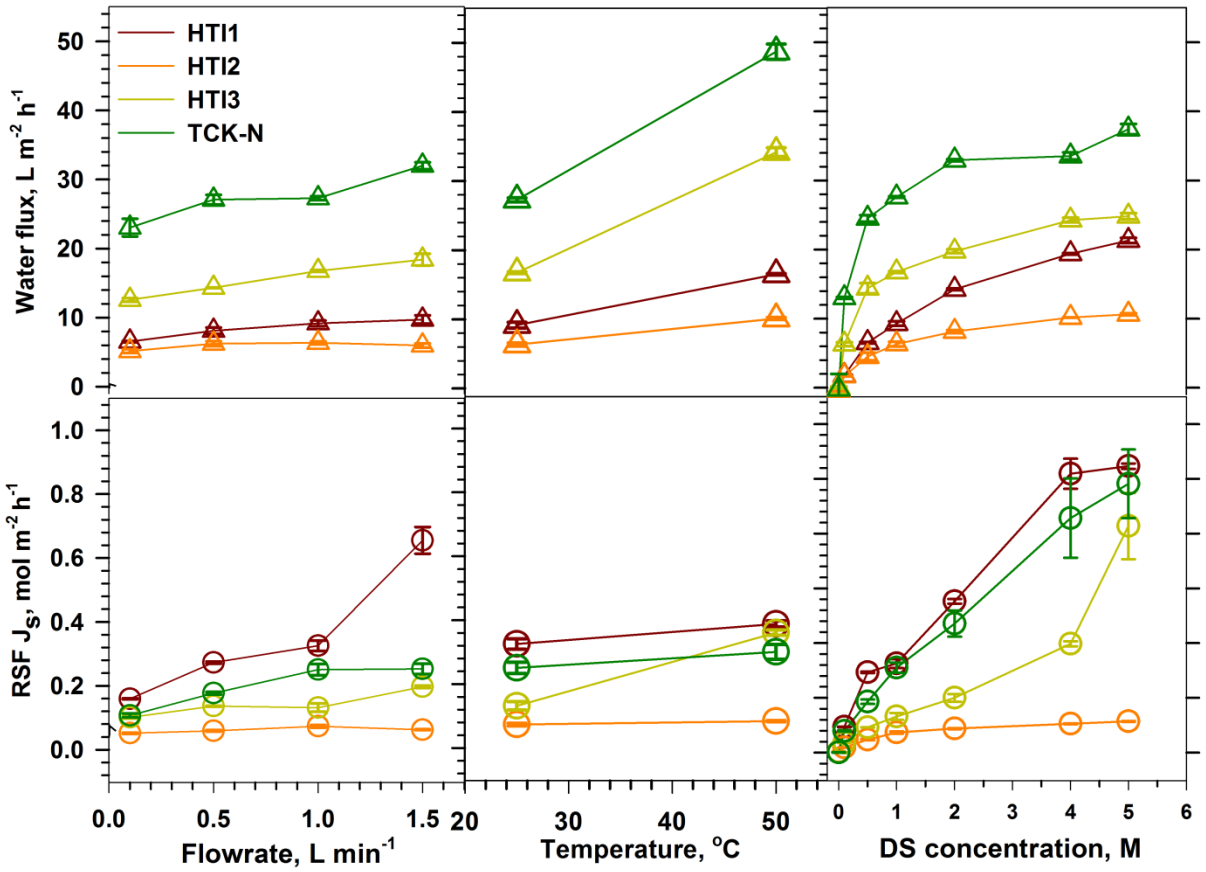

Figure 2. 12 *Membrane performances at various FS/DS temperatures, FS/DS flowrates and concentrations of DS. The DS was NaCl and the FS was milli-Q water. Membranes were oriented with active the layer facing the FS. Note that 6 M NaCl cannot be dissolved*

Performance changes of the integrally asymmetric and TFC membranes according to temperatures of the FS and DS were also examined. Both J_w and J_s of these membranes increased with increasing temperature from 25°C to 50°C. The thermodynamic energies of water molecules and solute molecules increased with increasing temperature, resulting in increasing diffusivity of the

solute and water molecules and reduction in the viscosity of the solutions. This phenomenon resulted in increase of the J_w and J_s of the membranes. This result was consistent with other studies using commercial CTA-based FO membranes [89, 92].

The integrally asymmetric and TFC membranes were also tested under various DS concentrations. Water flux of the membranes sharply increased with an increase of the DS concentration up to 1 M NaCl, after which gentle increases were observed. This observation could be explained by more severe effects of concentration polarization at higher concentration of DS, which would result in reduced osmotic pressure difference across the active layer of the membranes. However, the RSF of these membranes exhibited different patterns with water flux upon DS concentration change. RSF (J_s) is related to the diffusion coefficient (D_s) (Eq. 2.11), but insignificant change in the diffusion coefficient of DS was observed with increase of the concentration, from 0.1483E-9 m^2/s at 0.1 M NaCl to 1.590E-9 m^2/s at 5 M NaCl (Fig. 2.13). Meanwhile, RSF (J_s) is proportional to the concentration difference of solutes across the membrane active layer (C_{AP} - C_m) (Eq. 2.11). In turn, C_{AP} is proportional to the DS concentration. Therefore, RSF might increase proportionally to the increase of DS concentration (Fig. 2.12). Nevertheless, due to the high salt resistance characteristic of HTI2, the RSF was maintained at a low level regardless of increase of the DS concentration. The highly dense active layer of HTI2 might account for this phenomenon.

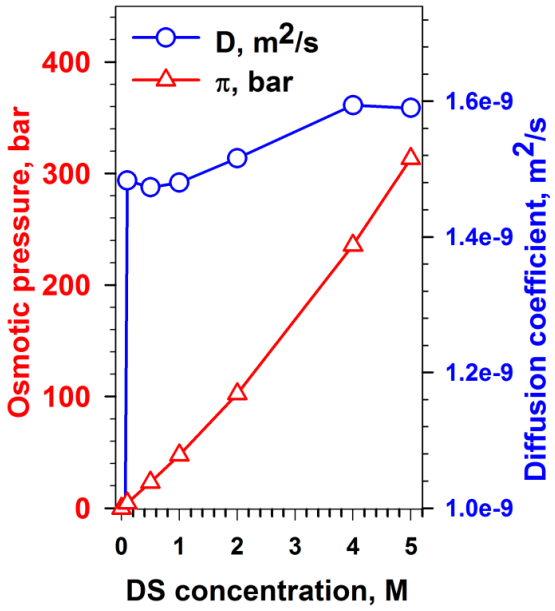

Figure 2. 13 *Osmotic pressures and diffusion coefficients D of NaCl solute at various concentrations [92]*

Membrane performance change was also investigated at various pH values of the FS and DS. The pH values of the FS and DS were adjusted by adding 1 M HCl and/or 1 M NaOH. Figure 2.14 shows the normalized water flux and normalized RSF of the membranes under different pH conditions of the

FS and DS. Water flux and RSF were normalized at pH 7, because the membranes were first tested at pH 7, washed with DI, tested at pH 4, and then washed and tested again at pH 10. This protocol aimed to minimize the effects of solute accumulation in the membranes or membrane degradation upon test time. Integrally asymmetric CTA membranes yielded the same behavior to pH effect. Insignificant performance change was observed upon change of the FS/DS pH. Both TFC membranes yielded the same behavior as an effect of the pH, wherein water flux was slightly increased while RSF decreased upon increase of pH. This phenomenon was also attributed to the electrostatic interaction between the membrane active layer and either solutes of DS or FS passing the membrane active layer. When the pH of the solutions increased, the surface charges of the membranes were more negative (Fig. 2.7), resulting in more repulsive force of the membrane to anions. On the other hand, the negative charge of the membrane was repulsive to itself, causing the membrane to become more swollen, giving a larger pathway to water molecules, which subsequently caused increased water flux. Figure 2.14 clearly shows that the TFC membranes showed good performance at basic pH conditions.

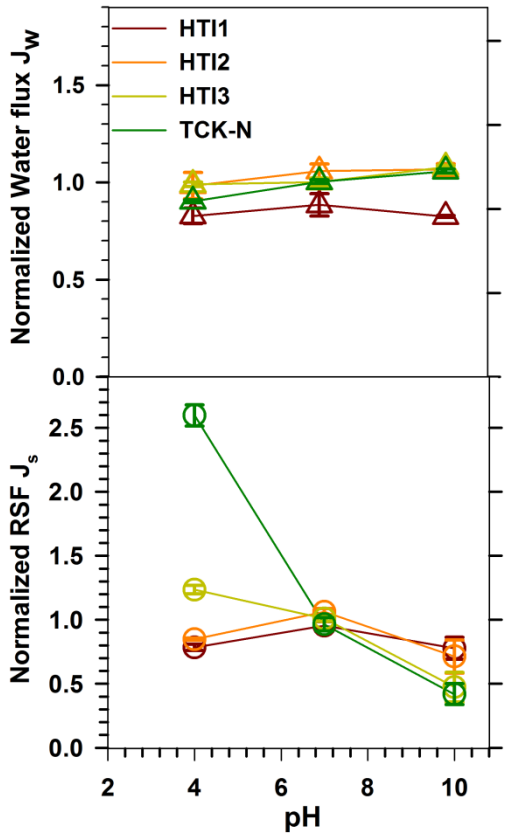

Figure 2. 14 *Membrane performance at various pH conditions of the FS and DS. Conditions: The DS was NaCl and the FS was milli-Q water, with both at 25 °C. The flowrate of 1.0 LPM was used with vertical orientation of the membrane cell, and the active layer facing the FS*

2.2.3 Organic fouling of membranes

Membrane performance change due to organic fouling was observed in experiments using BSA as a typical organic foulant. Figure 2.15 exhibited the normalized water flux and RSF profiles of the membranes during five sequent tests. All membranes yielded high water flux in virgin tests with DI water as the FS, followed by low flux with 100 ppm BSA solution as the FS, high flux after washing, low flux again in tests with 1000 ppm BSA solution, and finally, high water flux after washing. The RSF of the membranes were high in DI tests, low in tests with BSA, and high again after washing. Formation of a cake layer and/or pore blocking by BSA on the membranes might resist water flux and solutes passing through membranes during testing with BSA. Physical washing with DI water helped recover the water flux of the membranes. Sharper decrease of the water flux and RSF in the fouling test was found for the TCK-N and TCK-W membranes compared with the others. The rough surfaces of TCK-N and TCK-W observed in the AFM measurement (Fig. 2.6) help explain this phenomenon. The valley-ridge morphologies of these polyamide membranes were more attractive to the deposition of foulant, resulting in more resistance to water flow and salt flow compared to the smooth integrally asymmetric membranes HTI1 and HTI2. However, regarding the two TFC membranes which had similar roughness (Ra = 26.25 ± 0.64 nm for HTI3 and R_a = 24.40 ± 0.85 nm for TCK-N), a more severe effect of fouling was observed on TCK-N compared to HTI3. This can likely be attributed to the existence of a coating layer and/or oxygen abundant additives, and/or the monomer of the HTI3 membrane. This hypothesis is consistent with the XPS and zeta potential data presented in section 2.2.1. Comparing the two TCK membranes, TCK-W was rougher than TCK-N (roughness R_a = 34.23 ± 2.74 nm for HTI3 and R_a = 24.40 ± 85 nm) and more negatively charged, but showed less fouling propensity than TCK-N. As hypothesized earlier in testing the rejection of isopropanol, the TCK-N membrane had larger pore size, which might cause severe pore blocking of the membrane by foulant than TCK-W. Pore blockage is difficult to mitigate by physical washing with DI. This hypothesis was consistent with the lower water recovery after the washing of TCK-N compared to TCK-W observed in Fig. 2.15.

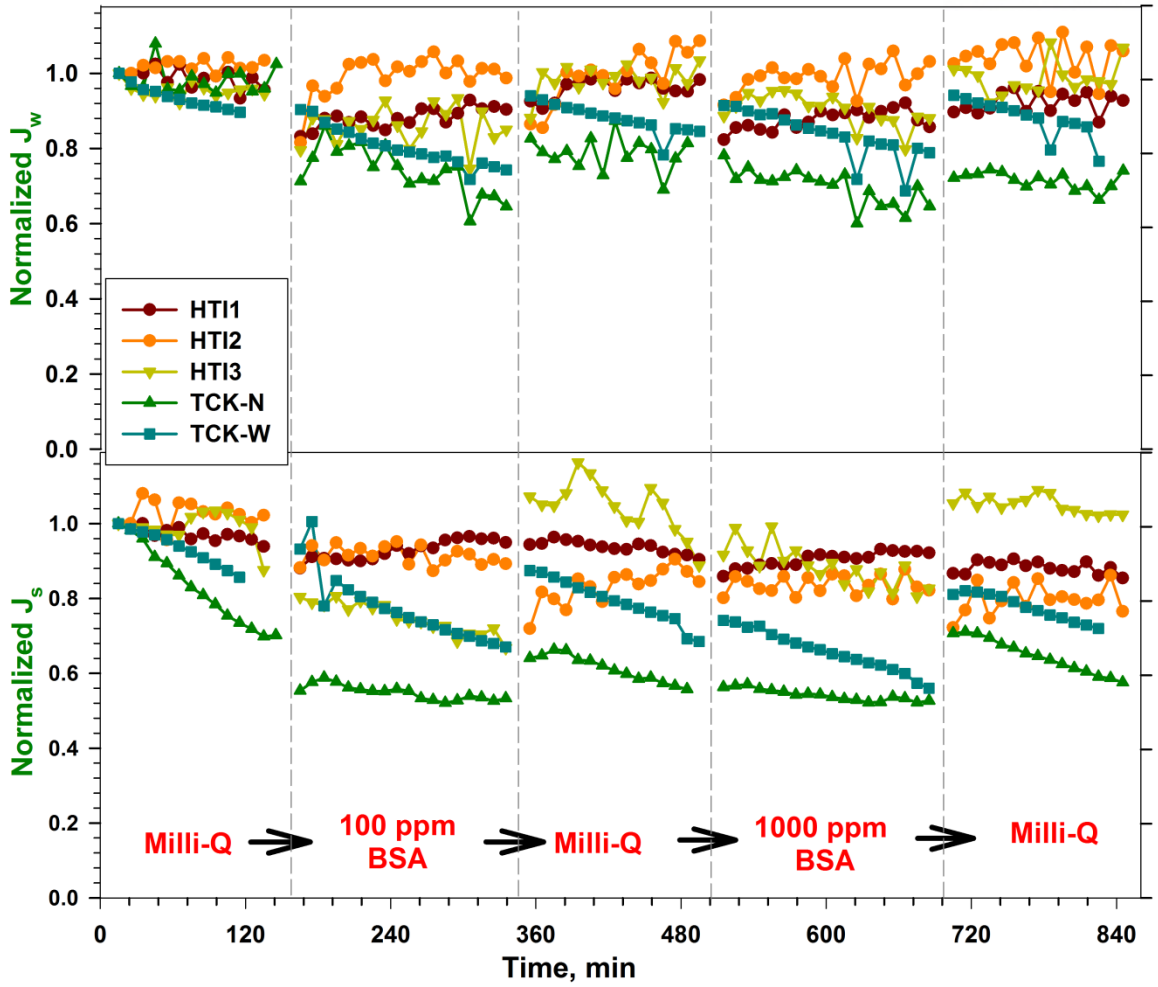

Figure 2. 1 *Fouling performance of the integrally asymmetric (HTI1 and HTI2) and thin film composite membranes (HTI3, TCK-N and TCK-W) in FO mode using Bovine Serum Albumins (BSA) as a foulant*

2.3 Conclusions

The physico-chemical properties and performance of integrally asymmetric and TFC FO membranes were systematically investigated in order to better understand the FO transport mechanism and to figure out appropriate characteristics for a desirable FO membrane. The effects of solution chemistry and operational conditions such as temperature, pH, flowrate of FS/DS and DS concentration on the performance of integrally asymmetric and TFC membranes were also evaluated. Integrally asymmetric membranes, which were fabricated with CTA-based polymer on either a woven fabric (HTI1) or nonwoven fabric (HTI2), were denser and smoother, causing lower water flux compared to the commercial polyamide TFC membrane (HTI3) or TCK membranes. However, the smoothness of the membranes conferred lower fouling propensity. The TFC membranes showed

superior performance than the integrally asymmetric membranes under various test conditions, while the difference in performance between the two types of membranes became more pronounced during operation under alkaline conditions due to repulsive interactions within the negatively charged membrane and with solute anions. The commercial TFC membrane (HTI3) still had low water flux compared to the TCK membranes, but higher water flux than the integral CTA-based membranes, while the RSF of HTI3 was very low. It is likely that the HTI3 was prepared from another monomer rather than trimesoyl chloride, or prepared with additives or a coating layer, which resulted in an increase of the O content in the polyamide layer, decrease of the negative charge, and improvement of fouling resistance.

The HTI2 membrane had the largest structure parameter, followed by HTI3, TCK-N, HTI1 and TCK-W, which showed gradually lower values. Among the factors t_s, τ and ε, membrane thickness t_s was suggested to be the main factor contributing to low S values, associated with low concentration polarization effects and high water flux for FO membranes. In particular, t_s was the main contributor to the specific reverse salt flux of the FO membranes. The data from SEM, XPS and rejection tests with isopropanol addressed that the woven fabric type possesses more advantages than nonwoven fabric to obtain identical finger-like structures of the substrate, more fully cross-linked polyamide on the substrate, and narrower pore size. Thus, it is suggested that besides the requirement of a porous support layer for FO membranes, (i) ultra-thin substrate and small membrane thickness and (ii) woven type fabrics were important factors for the design of FO membranes. The TCK-W membrane, comprised of a thin woven substrate (60 μm thickness), a polysulfone middle layer, and a polyamide skin layer with a total membrane thickness of 80 μm, yielded greatly higher water flux and lower RSF than commercial FO membranes. However, the TCK-W membrane was still sensitive to fouling, yielding large decline of the water flux in desalination. That is one of the drawbacks of polyamide membranes, and challenges more study for improvement of the antifouling characteristic of polyamide membranes rather than CTA-based membranes.

III. DEVELOPMENT OF INTEGRALLY ASYMMETRIC CTA/CA-BASED MEMBRANES FOR FO

This section presents the development of integrally asymmetric CTA/CA-based FO membranes with enhanced performance: higher permeate water flux, high salt rejection and low RSF than the commercial integrally asymmetric FO membranes. Flat-sheet membranes were prepared by immersion precipitation using a solution with an optimized composition in terms of 1,4-dioxane/acetone ratio and CTA/CA ratio. Preparation conditions – casting thickness, evaporation time and annealing temperature – were also optimized so as to generate thin and dense membranes by tailoring the highly porous support layer. The membrane performance and surface properties were compared with those of commercial FO membranes.

3.1 Experimental materials and methodology

3.1.1 Materials

CTA (43-49 wt.% acetyl) and CA (39.8 wt.% acetyl, average Mn ~30,000) were from Aldrich (MO, USA) and used without further purification. 1,4-dioxane (≥99.5% purity), acetone (≥99% purity), maleic acid (≥99% purity) and methanol (≥99.8% purity) were from Sigma-Aldrich (MO, USA). Sodium chloride (NaCl, 99% purity, Bioshop, Canada) and potassium bromide (KBr, 99.0%~100.2% purity, Junsei, Japan) were used for membrane performance testing. Disodium carbonate (Na_2CO_3, Sigma-Aldrich, MO, USA) was used as an effluent for ion chromatography (ICS 3000, Dionex, CA, USA).

Three nonwoven fabrics, labeled NWF1, NWF2 and NWF3, and three woven fabrics, labeled WF1, WF2 and WF3, were used as support layers for the membranes. The major difference among three nonwoven fabrics or woven fabrics is their porosities. The prepared membranes were tested against two commercially available membranes (Hydration Technology Innovations, HTI): a cartridge CTA-based membrane (090128-NW-1, HTI1) comprising CTA supported by an embedded polyester screen and a pouch CTA-based membrane (081118-SS-2, HTI2) comprising CTA cast on nonwoven polyester fibers individually coated with polyethylene.

3.1.2 Preparation of flat-sheet CTA/CA-based membranes

Flat-sheet membranes were prepared by immersion precipitation [68]. The casting solution comprised CTA and CA polymers dissolved in 1,4-dioxane and acetone with maleic acid and

methanol additives. The solution was kept in Erlenmeyer flask that was stoppered by hollow plugs and Teflon tape to prevent evaporation of the solvents. The solution was homogenized using a rotator (RT-10, WiseMix®, Korea). Other than for the assessment of different support materials, woven fabric WF1 (200 µm x 200 µm pore) was used as a support layer attached to a glass plate by sticky tape. The casting dope was then cast on to this substrate using an adjustable thickness casting knife (YBA-5, Baker applicator, Yoshimitsu, Japan) in a constant temperature (set up at 25°C) and humidity (70% relatively humidity) chamber (Fig. 3.1). After partial evaporation of the solvent, the casting film was immersed in a coagulation bath containing 1 ± 0.3°C water for 24 hours. The membrane was then removed to a room-temperature bath of deionized water, which was changed every 4 hours for 24 hours to wash out the solvents. Subsequently, the membrane was annealed for 15 minutes at 85°C in water before being stored in deionized water prior to performance testing.

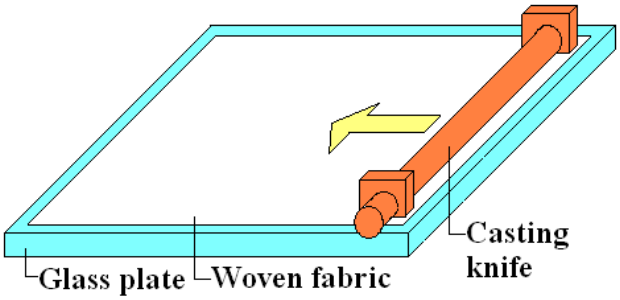

Figure 3. 1 *Casting an asymmetric membrane by employing NIPS method*

Membrane compositions were optimized to enhance performance by testing various ratios of CTA/CA (1:5, 1:2, and 1:1) and 1,4-dioxane/acetone (2:1, 2.9:1, 3:1, and 5:1) with other parameters being kept constant. The range of ratio for CTA/CA and 1,4-dioxane/acetone was chosen based on preliminary experiments and several literatures [93-98]. The effects of preparation conditions – support material, casting thickness, evaporation time and annealing temperature – were investigated using a casting solution of 6.3 wt.% CTA, 12.6 wt.% CA, 49.9 wt.% 1,4-dioxane, 17.2 wt.% acetone, 3.7 wt.% maleic acid and 10.3 wt.% methanol. Three nonwoven fabrics (NWF1, NWF2 and NWF3) and three woven fabrics (WF1, WF2 and WF3) were tested as substrates for the CTA/CA membranes. Solution was cast to thicknesses of 100, 150, 200 and 250 µm. Evaporation times from 10 to 240 seconds were tested. Membranes annealed for 15 minutes at 50, 60, 70, 80, 85 and 90°C were compared with an unannealed membrane.

3.1.3 Performance test in FO mode

The prepared membranes were tested in FO mode (Fig. 2.1 in the previous section.) using a test

cell with 27 cm^2 effective area (width, 3 cm; length, 9 cm). The feed tank was placed on a hotplate (Cimarec, Thermo Scientific, USA) for stirring. The DS tank placed on a balance (XP8002S, Mettler Toledo, USA) at a similar height to the FS tank to eliminate any gravitational effects. The mass of the DS tank was logged by a computer. The DS was stirred by a standing stirrer. Flow rates of both solutions were set at 1 $L.min^{-1}$ by two gear pumps (81808, Cole-Parmer, USA). Counter-currents of 18.5 cm/s were applied to both solutions to maintain the highest concentrations of both solutions in contact with each other when flowing along the membrane cell [99]. A circulator (Fisher scientific, Isotemp 3016D) maintained both solutions at 25 ± 0.5°C. The DS faced the support layer, and the FS faced the active layer – a normal FO configuration for desalination and water treatment [8].

Milli-Q water (Millipore®, USA) FS and 1 M NaCl DS and were generally used and membrane performances were assessed over 1 hour by measuring permeate water flux (J_w) and RSF (J_s). Calculated data were taken after 10 minutes of stabilizing water flux. The permeate water flux was calculated by the weight change of the DS due to the permeate passing through the effective membrane surface during an interval of time as Eq. (3.1).

$$J_w = \frac{\Delta \text{ weight}}{\text{water density} \times \text{effective membrane area} \times \Delta \text{ time}} \ (Lm^{-2}h^{-1} \text{ or LMH}) \qquad (3.1)$$

The concentration of NaCl in the FS was also determined during the 1 hour tests using a calibrated conductivity electrode (856 Conductivity module, Metrohm, Switzerland) connected to the computer. From the feed concentration, RSF was defined in Eq. (3.2) as the number of mole of NaCl diffusing from the DS tank to the FS tank per unit time per unit membrane area.

$$J_{s\text{-}NaCl} = \frac{\text{mole of NaCl}}{\text{effective membrane area x } \Delta\text{time}} \quad \left(\text{mole NaCl}.m^{-2}h^{-1}\right) \qquad (3.2)$$

The mass of DS and conductivity of FS were measured and stored on a computer every 10 seconds. At least two membrane coupons were tested for each parameter.

The optimized membrane was tested at various pH values by soaking it for 10 hours in 500 ml deionized water adjusted to pH 4, 7, or 10 using NaOH 1 M and/or HCl 1 M. Performance was assessed in terms of permeate water flux, RSF and salt rejection (R) using a DS of 1 M KBr and a FS of 0.1 M NaCl. Salt rejection and RSF were determined by ion chromatography (ICS-3000, Dionex, USA), which analyzed the concentrations of chloride and bromide ions in both tanks. 1 ml samples of each solution were collected before testing and after one hour. The Cl^- concentration of the permeate flow was determined from the permeate water mass passing through the membrane and the Cl^-

concentration in the DS tank. Salt rejection and RSF were calculated as Eq. (3.3) and Eq. (3.4), respectively.

$$R = \left(1 - \frac{[Cl^-]_{permeate}}{[Cl^-]_{feed}}\right) \times 100 \quad (3.3)$$

$$J_{s\text{-}Br^-} = \frac{\text{mole of } Br^- \text{ in FS}}{\text{effective membrane area x } \Delta\text{time}} \qquad (\text{mole } Br^- .m^{-2}h^{-1}) \quad (3.4)$$

The membrane performances were compared against commercial FO membranes under similar conditions.

The effects of different substrates were tested using the membranes in reverse osmosis of which schematic diagram was similarly described elsewhere [59]. Four 66.56 cm^2 effective area membrane coupons were tested together at an applied pressure of 225 psi (15.5 bar). The 50 L 2,000 ppm NaCl FS flowed at 1.0 LPM at 25^{o}C. Permeate water was collected using a Falcon tube after 1 hour. Water flux was calculated by the mass change of the Falcon tube per unit effective membrane area per unit time, similar to in the FO test. The conductivity of the collected samples and the feed solution were measured using a calibrated conductivity meter (Ultrameter II^{TM}, Myron L Company, USA). NaCl rejection was calculated from the feed concentration and the permeate concentration as Eq. (3.5).

$$R = \left(1 - \frac{[NaCl]_{permeate}}{[NaCl]_{feed}}\right) \times 100 \quad (3.5)$$

3.1.4 Analytical tools

- **Scanning Electron Microscope (SEM)**

Top surface and cross-section images of the membranes were observed using SEM (Quanta 200, FEI, USA). Each membrane sample was dried at 50^{o}C for 24 hours in an oven to dehydrate it. Then, the membrane was rigidly mounted on a specimen by conductive adhesive carbon tape. In order to clearly observe the cross-section image, the membrane was carefully cut in liquid nitrogen by using a knife before being mounted on the specimen. For reducing image artifacts caused by electrostatic charge, all samples were Pt-coated at 20 mA and $2x10^{-3}$ mbar for 60 seconds in a Turbo Pumped High-Resolution Chromium Sputter Coater (K575X, EMITECH, Germany).

- **Attenuated total reflectance - Fourier Transform Infrared spectroscope (ATR-FTIR)**

ATR-FTIR spectra were obtained by an elsewhere reported method using a Nicolet 6700 spectrometer (Thermo Scientific, USA) equipped with a flat plate germanium ATR crystal [65]. OMNIC 8.1 software was used to record the spectra, correct their baselines, normalize the spectra and find the peaks. Samples were repeatedly scanned under a moisture-free, continuously purged, nitrogen gas environment and average spectra were generated at wave numbers 600 – 4000 cm^{-1} with a resolution of 4 cm^{-1}.

- **Zeta potential analyzer**

The zeta potential of each membrane surface was measured using Surpass equipment (Anton Paar, Austria). Wet membrane samples soaked in 1 mM potassium chloride solution for 24 hours were attached to an adjustable gap cell, and the zeta potential was evaluated by Fairbrother and Mastin method at pH 4 – 7 and separately at pH 7 – 10 in a background electrolyte of 1 mM potassium chloride. The acidic pH values were adjusted using 0.1 M HCl. Basic pH values were adjusted using with 0.1 M NaOH. The membrane samples and the system were thoroughly rinsed between testing in acidic and basic conditions without detaching the membranes.

- **Contact Angle instrument**

Hydrophilicity of a membrane was confirmed by average contact angle measurements (Phoenix 300Plus, Surface & Electro Optics Co. Ltd., Korea) using sessile drops method. Membrane samples were dehydrated at 50^{o}C for 24 hours in an oven before measurement. Two replicates were used, and five drops per replicate were measured.

- **Atomic force microscope (AFM)**

Surface morphologies of membranes were examined using a Multimode V (Veeco, USA) AFM capable of imaging at vertical lateral resolutions of 0.1 Å. After being dried at 50^{o}C for 24 hours in an oven, membranes were cut into approximately 1 cm x 1 cm pieces which were mounted on a sample stage. Measurement was in tapping mode using a cantilever tip oscillating at its resonant frequency. Changes of oscillation amplitude of the cantilever due to the interactions between the sample and the cantilever tip were recorded, and topography of each sample was obtained by mapping the corresponding deviations from the target amplitude in voltage.

- **Optical microscope**

The substrates were observed using an optical microscope at 5x magnification (Axio scope, Carl Zeiss Microimaging GmbH, Germany). The dry substrate was held between two plain glass slides.

The images were collected using a visual program DMC Advanced (INS Co., Ltd. AxioVision software, Axio Vs40 V4.8.0.0, Carl Zeiss Imaging Solutions GmbH, Germany). The program measured open spaces of the substrates. The HTI membranes were supplied "glycerol wet-treated"; they were soaked in milli-Q water for 48 hours and measured with a few water drops on the glass slides.

- **Viscosity of polymer solution**

Viscosities of the polymer solutions were measured using a Bop and Cup Rheometer (Haake Mars III Rheometer, Thermo Fisher Scientific Inc., MA, USA) at applied shear rates of 0.001 to 1000 1/s at 25^{o}C.

- **Ultraviolet-Visible (UV-Vis) absorbance of annealing solution**

The leaching out of solvents and additives during annealing was assessed by measuring the ultraviolet-visible (UV-Vis) absorbance of the annealing nonsolvent before and after annealing using a UV-Vis spectrophotometer (Scinco S-3100, Scinco Co. Ltd., Korea). The individual absorbance of each chemical used to prepare the casting dope solution – 1,4-dioxane, acetone, maleic acid and methanol – were also analyzed qualitatively.

3.2 Results and discussion

3.2.1 Effects of composition on membrane performance

Figure 3.2a shows the performance of FO membranes prepared with 1,4-dioxane/acetone ratios of 2.0 to 5.0. Mixed solvents were used to dissolve the CTA/CA blend, as using either solvent alone could not completely dissolve the polymer mixture. Solvent ratios below 2.0 also failed to completely dissolve the blend. Water flux and RSF of membranes increased 21.62% and 470%, respectively, with increasing 1,4-dioxane/acetone ratio of the solvent from 2 to 5. Plotting specific reverse solute flux ($J_{s\text{-}NaCl}/J_w$) clearly displayed increasing draw solute loss with increasing 1,4-dioxane/acetone ratio. Specific RSF, the ratio of RSF to permeate water flux ($J_{s\text{-}NaCl}/J_w$) [19], reflects a membrane selectivity, FO efficiency and draw solute loss per unit permeate water product. A high value indicates poor selectivity, low FO efficiency and high draw solute loss. Therefore, increasing 1,4-dioxane/acetone ratio was shown to lead to low membrane selectivity, low FO efficiency and high draw solute loss, implying an increase of membrane pore size.

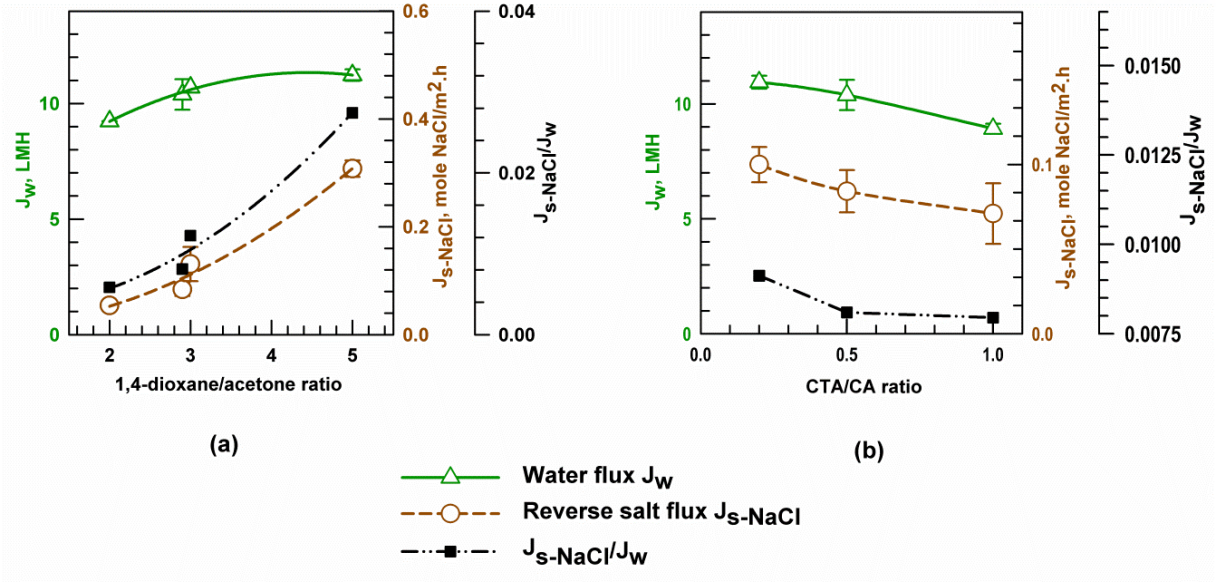

Figure 3. 2 *Performance of CTA/CA-based FO membranes prepared with 18.9 wt.% polymers, 67.1 wt.% solvents, 3.7 wt.% maleic acid and 10.3 wt.% methanol. Various (a) 1,4-dioxane/acetone and (b) CTA/CA ratios were tested. DS was 1 M NaCl and FS was milli-Q water; both at 25 ^{o}C. 1.0 LPM flowrate was used with cells vertically oriented, and active layer faced FS*

Two possible mechanisms related to miscibility of the polymers in the solvents and volatility of solvents likely determined membrane porosity. First, compared with acetone in the solvent mixture, 1,4-dioxane is more favored for CTA and CA. Both solvents are proton acceptors and thus could easily form hydrogen bonds with the polymers, however, 1,4-dioxane was a better solvent for the polymers than acetone due to compatibility between its ring system and the pynarose rings of CTA and CA [94]. Acetone can dissolve CA, but poorly dissolves CTA [100]. Once a polymer is well dissolved in a solvent, its chains become greatly disengaged and extended, increasing their hydrodynamic volume and so increasing viscosity of the solution [101]. Such behavior was shown by the polymers tested in solvents with different 1,4-dioxane/acetone ratios (Fig. 3.3): viscosity increased with increasing 1,4-dioxane content of the solvent. Furthermore, as a casting film is immersed into the coagulation bath, there are the diffusions of solvent (outflow) and nonsolvent (inflow) in the polymer matrix to and from coagulation bath due to the chemical potential difference [68]. Good dissolution of a polymer in a solvent leads to strong interactions between the polymer and the solvent molecules [101], which decelerate outflow of the solvent during phase separation. Therefore, inflow of nonsolvent is allowed to diffuse into the polymer matrix more rapidly [102], and polymer solution reaches the two-phase region more quickly at lower polymer concentration in the phase diagram of ternary system, which is so-called instantaneous liquid-liquid demixing. As a result, a porous membrane is obtained [68]. Through such behavior, the higher 1,4-dioxane/acetone ratios led to more porous membranes and higher water flux (Fig. 3.2a). This result is consistent with previous studies of

polysulfone using DMF/NMP solvent mixtures – NMP is a better solvent for polysulfone than DMF is, and membrane porosity increased with increasing NMP content of the casting solution [102].

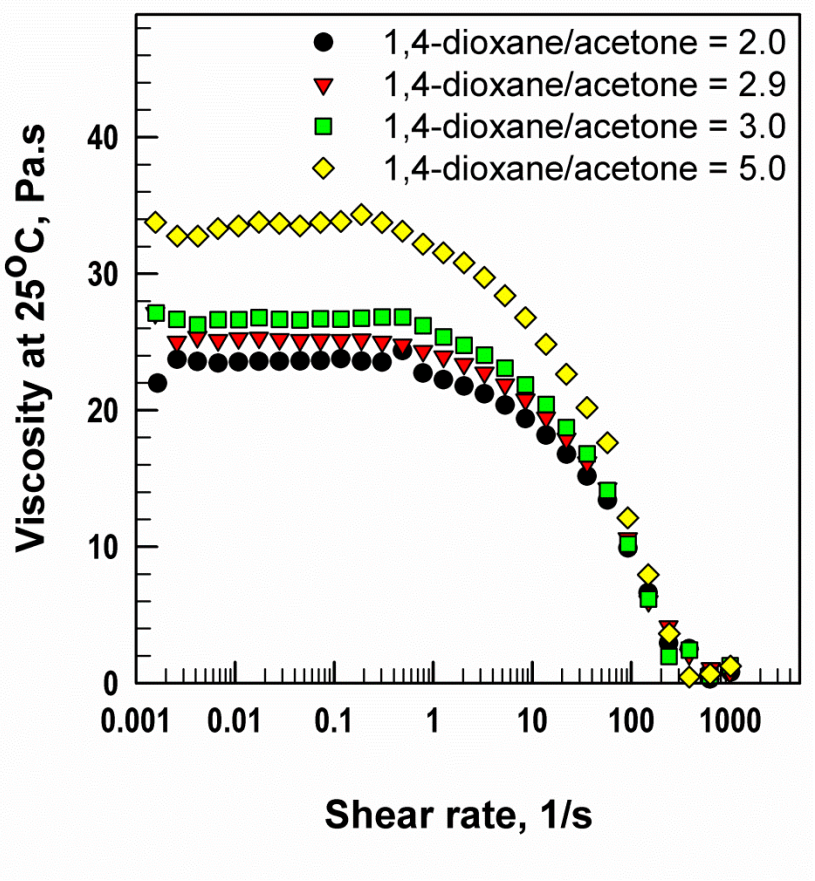

Figure 3. 3 *Viscosity of polymer solutions with respect to 1,4-dioxane/acetone ratio*

The second mechanism relies on acetone having greater volatility than 1,4-dioxane. Increasing 1,4-dioxane content of the solvent resulted in less solvent evaporation and hence a lower polymer concentration on the membrane surface. The lower polymer concentration leads to less advanced gelation in the polymer/solvent/nonsolvent ternary phase and the formation of a less dense skin membrane [103]. Furthermore, when the casting film was immersed in the coagulation bath, precipitation occurred due to the low miscibility between the polymers and the nonsolvent and solidification simultaneously occurred due to the diffusional flow of the solvents and the nonsolvent [104]. Higher contents of less volatile 1,4-dioxane led to less solvent loss through evaporation, and so solidification was more favored over precipitation; therefore, more porous and thicker membranes resulted. Higher salt resistance of membranes would, therefore, likely be achieved at lower 1,4-dioxane contents. The optimum ratio of 1,4-dioxane to acetone was found to be 2.9; the resulting membranes would allow high flux and reasonable RSF.

Figure 3.2b shows the performance of FO membranes formed using CTA/CA ratio of 0.2 to 1.0.

Water flux, RSF and specific RSF decreased with increasing CTA content of casting solutions, implying increased selectivity. This was likely due to the formation of less porous membranes at higher CTA/CA ratios. Backbones of the two polymers have different numbers of hydrogen bond forming hydroxyl (-OH) and acetyl (-$COCH_3$) functional groups [105]. The different hydrogen bonding levels lead to different hydrogen bonding solubility parameters of CA (11.87 $(MPa)^{1/2}$) and CTA (10.64 $(MPa)^{1/2}$) (Table 3.1).

Table 3. 1 *Hansen solubility parameter of liquids at 25°C and polymers [81]*

Compounds	**Components of solubility parameter, $(MPa)^{1/2}$**			**Solubility parameter, $(MPa)^{1/2}$** δ
	Dispersive δ_D	**Polar** δ_P	**Hydrogen-bonding** δ_H	
Acetone	15.5	10.4	7.0	20.1
1,4-dioxane	19.0	1.8	7.4	20.5
Cellulose acetate	15.55	***	11.87	19.56
Cellulose triacetate	15.55	***	10.64	18.84

***, indicate data for which only dispersive and polar contributions are available as in the expression of Hildebrand [100]

The solubility parameter of CA was higher than that of CTA and closer those of the solvents (Table 3.1). Therefore, there was greater affinity between CA and the solvents than between CTA and the solvents; CA was more miscible in the solvent mixture than CTA was. As CTA/CA ratio of the polymer solution increased, miscibility of the polymer solution with the solvents decreased, leading to more rapid outflow of solvent into the coagulation bath and slower inflow of nonsolvent into the casting film during phase separation. As a result, delayed demixing was advanced to take place and denser membranes formed with increasing CTA/CA ratio.

Different polymers/solvents ratios were tested at constant ratios of CTA/CA (0.5) and 1,4-dioxane/acetone (2.9) (Table 3.2). Additives were consistently present at 14%, leaving 86% polymers and solvents. Differing levels of precipitation and solidification contributed to different structures and performances of the membranes. Increasing overall polymer content of the solution from 9% to 18.9% promoted precipitation, hindered solidification and led to denser membranes. At total polymer content of 21% could not be dissolved in the 65% solvents. Overall solution contents of around 6.0% to 6.3% CTA and 12.0% to 12.6% CA were considered optimal to obtain membranes showing high water flux and reasonable RSF.

Table 3. 2 *Membrane performances corresponded to polymer and solvent content*

Membrane	Composition% w/w				J_w ($Lm^{-2}h^{-1}$)	$J_{s\text{-}NaCl}$ (mole $NaCl.m^{-2}.h^{-1}$)
	CTA	CA	1,4-Dioxane	Acetone		
1	3	6	57.3	19.7	4.939 ± 0.246	9.146 ± 0.303
2	4	8	55.0	19.0	9.497 ± 0.344	4.008 ± 0.163
3	5	10	52.8	18.2	12.089 ± 0.236	0.477 ± 0.005
4	6	12	50.6	17.4	9.811 ± 0.194	0.071 ± 0.002
5	6.3	12.6	49.9	17.2	10.390 ± 0.661	0.084 ± 0.013
6	7	14	48.4	16.7	-	-

3.2.2 Effect of preparation conditions on membrane performance

Six support layers, three nonwoven fabrics (NWF1, 2, 3) and three woven fabrics (WF1, 2, 3), were tested in the fabrication of FO membranes. Surface images of the various support layers and cross-sectional images of FO membranes constructed on each support layer were observed by optical microscopy and SEM, respectively (Fig. 3.4). The support layer fabrics showed porous structures, which were analyzed using Igor Pro software (Igor Pro 4.01, WaveMetrics, Inc., USA) after converting the original images to binary images. Pore areas of the samples were measured by summing the white pixels within a given area of the binary microscopic images, and open space ratio was computed as a ratio of the pore area to the analyzed area of the membrane. To the knowledge of the authors, this is the first study on the effects of the support layer fabric on FO membrane performance using optical microscopy coupled with computerized quantitative image analysis.

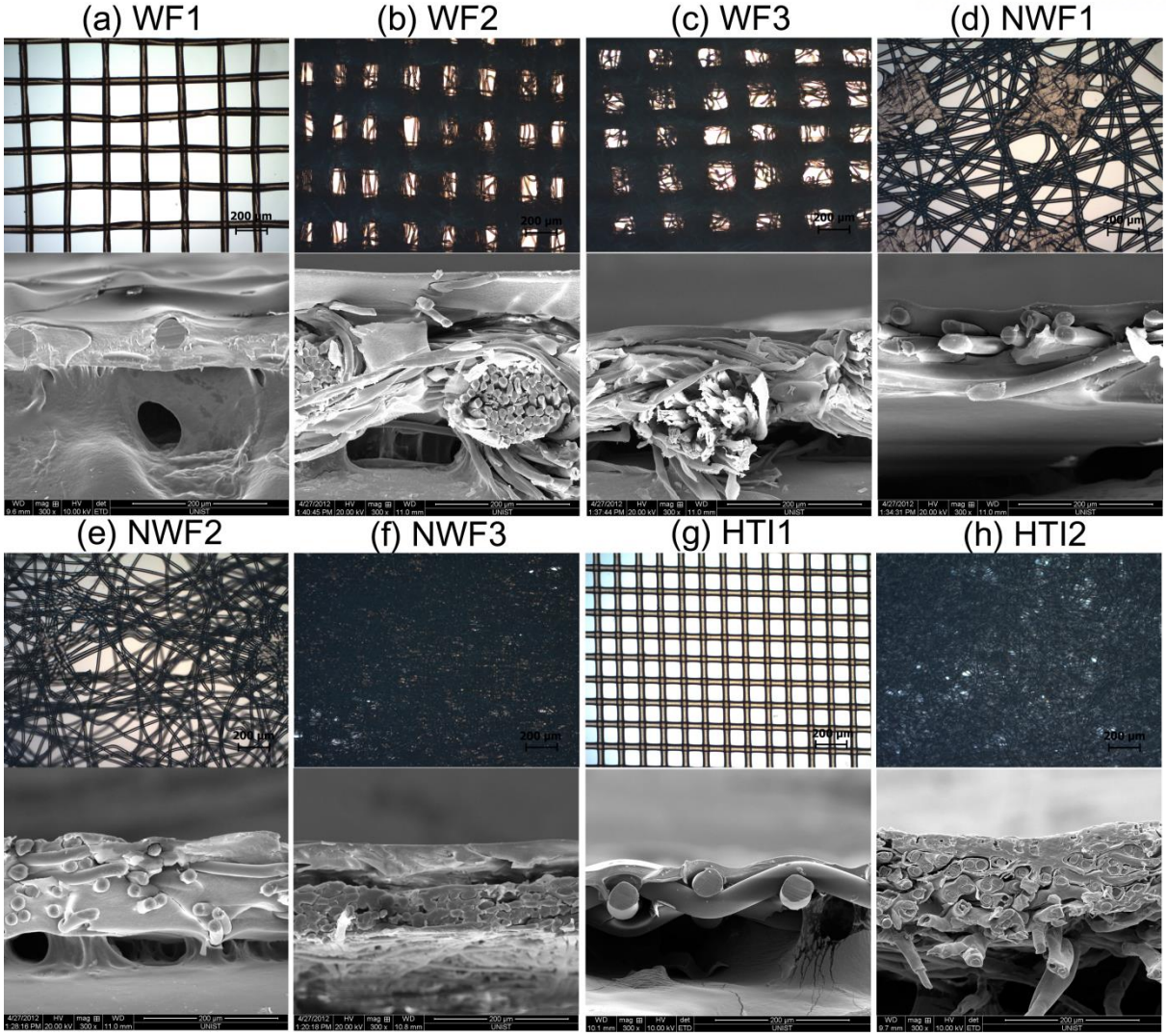

Figure 3. 4 *Microscopic surface images of support layers (first row) and SEM cross-sectional images of FO membranes (second row) fabricated on the corresponding support layers. a, b, and c show the woven fabrics WF1, 2, and 3, respectively; d, e, and f show the nonwoven fabrics NWF1, 2, and 3, respectively; g and h show HTI membranes 1 and 2, respectively.*

Membrane performances in forward and reverse osmosis modes were assessed with respect to their open space ratios (Fig. 3.5). In FO mode, the open space ratio of the support layer greatly affected water flux. The loosest fabric (open space ratio: 0.624 ± 0.012) resulted in the highest water flux (10.390 ± 0.661 LMH); conversely, the most tight fabric (open space ratio: 0.002 ± 0.002) led to the lowest water flux (1.171 ± 0.289 LMH). A low open space ratio may have led to trapped DS within the support layer and prevented the exchange of the trapped diluted DS with bulk DS, causing dilutive internal concentration polarization, which would have severely impaired performance [4]. RSF of the membranes was not related to their open space ratio; it was, however, closely related (correlation coefficient, -0.987) to salt rejection during reverse osmosis. This implies that RSF values

of the membranes were determined by the tightness of their skin layers. WF3 led to the highest RSF (0.3707 ± 0.0574 mole NaCl.m^{-2}.h^{-1}) and the lowest salt rejection (31.583 ± 5.618 %). In reverse osmosis mode, driven by a hydraulic pressure gradient rather than osmotic pressure, dilutive internal concentration polarization within the support layer did not occur to decrease the water flux. Therefore, the water flux of membranes in reverse osmosis mode showed the reverse trend of their salt rejection. The membrane prepared with WF3 showed the lowest salt rejection (31.583 ± 5.618 %) and the highest water flux (21.905 ± 7.177 LMH). The commercial membranes showed similar behavior to the lab-made membranes. Both HTI membranes were made from the same polymer composition on different support materials. During forward osmosis, HTI1 showed higher water flux (9.075 ± 0.408 LMH) and RSF (0.270 ± 0.004 mole NaCl.m^{-2}.h^{-1}) than HTI2 showed (6.027 ± 0.300 LMH and 0.067 ± 0.003 mole NaCl.m^{-2}.h^{-1}). However, they both showed comparable water flux during reverse osmosis: 6.378 ± 0.189 LMH and 6.134 ± 0.522 LMH, respectively. The effects of dilutive internal concentration polarization due to the thick and dense support layer of HTI2 (Fig. 3.4h) disappeared during reverse osmosis. These results show that an FO membrane should have a thin and tight skin layer supported by a porous substrate which can be woven or nonwoven.

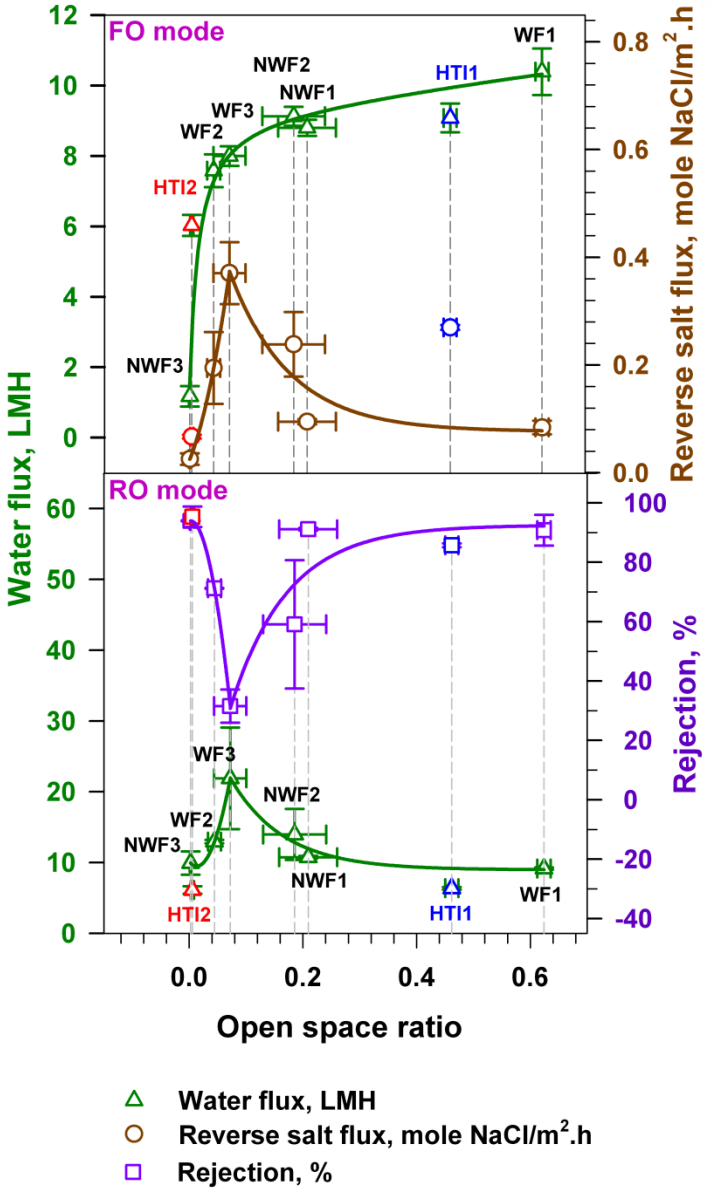

Figure 3. 5 *Performances of FO membranes in forward and reverse osmosis modes. The open space ratio of the support layer is defined as the ratio of the pore area to the analyzed area of the material*

The effects of preparation conditions – casting thickness, evaporation time and post-treatment temperature – on membrane performance were investigated (Fig. 3.6). Decreasing casting thickness facilitated water flux and RSF (Fig. 3.6a) because the thinner membranes showed less resistance against water and salt transport. The highest water flux (13.765 ± 0.599 LMH) and RSF (0.159 ± 0.011 mole $NaCl.m^{-2}.h^{-1}$) were shown by the membrane cast with 50 µm thickness. Water flux and RSF then decreased as casting thickness increased to 250 µm. The cast layer should be sufficiently thick to cover the support layer without defects occurring in the polymer layer. The WF1 support layer was approximately 50 µm thick. Therefore, 200 – 250 µm casting thickness was suggested for preparing membranes with low specific RSF values.

Allowing up to 120 s for the evaporation of the casting solution before immersing samples in the coagulation bath showed no significant effects on water flux of membranes (Fig. 3.6b). Longer evaporation times decreased water flux, RSF and specific RSF as the increased concentration of polymers on the drier surface of the casting solution favored precipitation over solidification during phase inversion. The denser membrane structures that resulted due to precipitation yielded lower water flux and RSF.

Membranes were tested after annealing at different temperatures (Fig. 3.6c). Annealing provided thermal energy to the membranes, which enhanced hydrogen bonding between the polymer chains, so increased salt rejection and decreased water flux [106]. Water flux and RSF decreased as annealing temperature increased from 70 to 90^{o}C. Cooler annealing differently affected performance: water flux increased with increasing temperature up to 70^{o}C because increased annealing allowed the release of trapped solvents and additives from the polymers. At room temperature, the solvents and additives – 1,4-dioxane, acetone, methanol and maleic acid – embedded within the polymer matrix were not completely washed out during rinsing for 24 hours and so clogged the membrane pores and reduced water flux. Low-temperature annealing (50^{o}C) provided some thermal energy to the membrane to allow the rearrangement of its structure. Some pores were enlarged so that trapped chemicals were released. Under rearrangement due to provided thermal energy, these pores were large enough to enhance water pathway but not salt pathway, which increased water flux but not reverse salt flux. Such releases were likely increasingly aided with increasing annealing temperature up to 60-70^{o}C, close to the boiling points of methanol (65^{o}C) and acetone (56-57^{o}C). Annealing above 60-70^{o}C offered no beneficial removal of chemicals; it only decreased water flux through increased hydrogen bonding. These results suggest that rinsing for 24 hours did not remove all the residual solvents and additives. They were, however, removed by adequate annealing, which led to improve membrane performance.

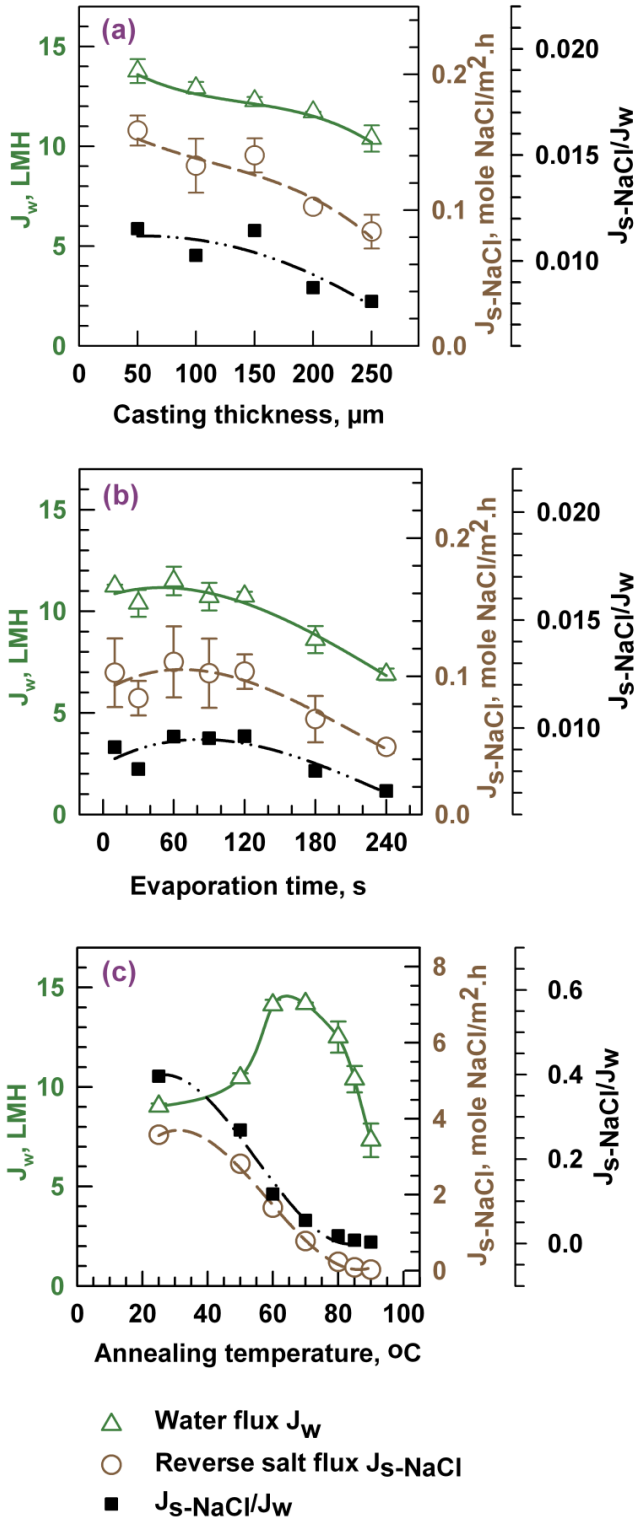

Figure 3. 6 *Effects of preparation conditions on membrane performance: (a) casting thickness, (b) evaporation time, and (c) annealing temperature. DS was 1 M NaCl and FS was milli-Q water; both at 25 °C. 1.0 LPM flow rate was used with the cell vertically oriented, and active layer faced FS*

The leaching out of solvents and additives was assessed by ultraviolet-visible (UV-Vis) absorbance spectroscopy of annealing nonsolvent (water) measured before and after annealing (Fig. 3.7). Detection of solvents and additives implied that the chemicals were released into the water bath during annealing. The absorbance peaks could be divided into two groups: those occurring at 50 and 60^{o}C and those occurring during hotter annealing. The partial release of chemicals was observed below 70^{o}C and complete release was observed at 70^{o}C and hotter. Therefore, the absorbance spectra after annealing at 70, 80, 85 and 90^{o}C are largely similar. Qualitative characterization of the UV absorbance of the solvents and additives is also shown in Fig. 3.7. The absorbance spectrum of the nonsolvent, water, in the annealing bath was deconvoluted into three sub-peaks at 192, 212 and 264 nm using SPXPEAK 4.1 software. The peak at 264 nm was attributed to acetone; that at 212 nm was attributed to maleic acid; and methanol, 1,4-dioxane and acetone all showed absorbance around 190 nm. The three peaks contributed approximately equally to the absorbance spectra. The release of residual chemicals may have been due to the enhanced rotational freedom (flexibility) of the polymer chains and/or the increased thermal dynamic properties of the chemicals during annealing. Annealing provided thermal energy to the residual chemical and polymer molecules, which increased their internal energy and accelerated their motion and so facilitated the release of chemicals from the membranes.

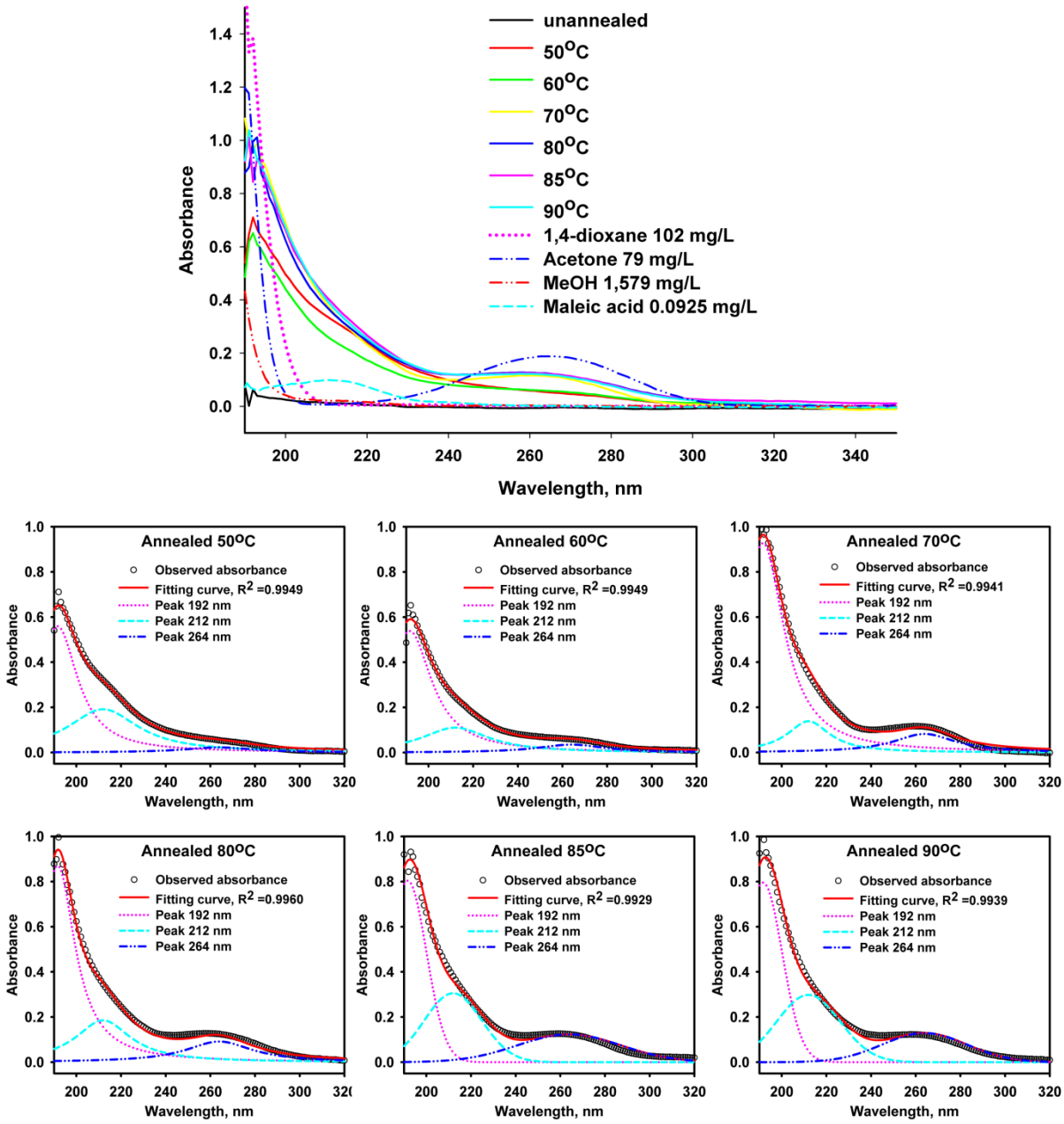

Figure 3. 7 *Deconvoluted UV absorbance spectra of nonsolvents in annealing bath after post-treatment*

3.2.3 Performance and surface properties of the optimized membrane

The optimized composition and preparation conditions were assessed in previous sections by forming membranes under various conditions using differently proportioned casting solutions. The optimized membrane was formed by casting 6.3 wt.% CTA, 12.6 wt.% CA, 49.9 wt.% 1,4-dioxane, 17.2 wt.% acetone, 3.7 wt.% maleic acid and 10.3 wt.% methanol to a thickness of 250 μm on a

porous woven (WF1) support layer with subsequent evaporation for 30 seconds at 25°C and 70% relative humidity, and annealing at 85°C.

The performance of the optimized membrane was compared against the commercial membranes at various pH conditions (Fig. 3.8). Membrane HTI1 showed good water flux but poor salt rejection; HTI2 showed poor water flux but good salt rejection. The lab-made membrane showed higher flux than HTI1 and comparable salt rejection to HTI2.

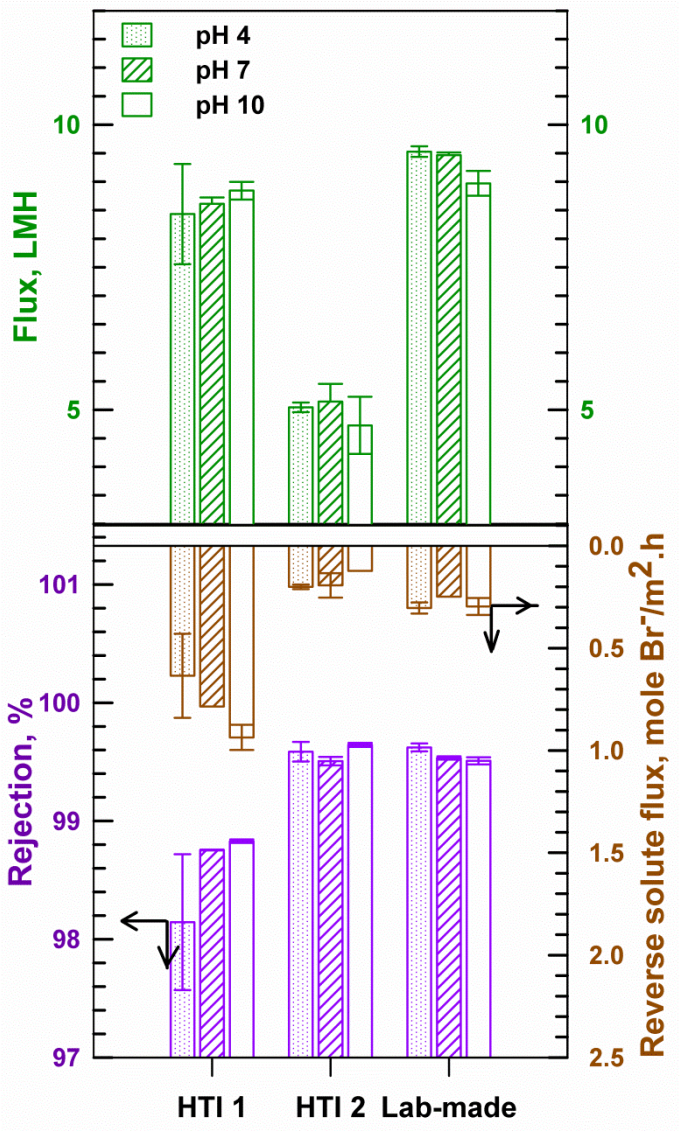

Figure 3. 8 *Membrane performances at various pH conditions. DS was 1 M KBr; FS was 0.1 M NaCl; both at 25°C. Flow rate of 1.0 LPM was used in a vertically oriented cell with active layer faced FS*

Surface properties of the membrane were characterized by SEM, ATR-FT-IR, AFM, Zeta potential analysis and contact angle analysis. The cross section of the optimized lab-made membrane

is shown in Fig. 3.4a; its high water flux, low RSF and high salt rejection were achieved through its thin and dense structure. The asymmetric CTA/CA-based membrane was originally cast to 250 µm thickness using a casting knife, but its final thickness was approximately 50 µm, comparable to that of HTI1 (Fig. 3.4g) and thinner than that of HTI2 (Fig. 3.4h). ATR-FTIR confirmed CTA and CA structure of the membrane. The lab-made membrane showed similar surface functional groups to the two commercial membranes. Acetyl groups in the CTA and CA structure showed signals at 1744 cm^{-1} (–C=O), 1368 cm^{-1} (CH_3), and 1228 cm^{-1} (C-O). The lower contact angle of the lab-made membrane shows it was slightly more hydrophilic than membrane HTI1 (contact angle 51.3° ± 3.3^o vs. 53.5° ± 0.6^o). Zeta potentials of the CTA/CA-based membrane and membrane HTI1 (Fig. 3.9) were negative at every tested pH. They became more negative with increasing pH. HTI1, a CTA-based membrane, showed more negative values than the lab-made CTA/CA-based membrane. The negative zeta potentials of cellulose diacetate/cellulose triacetate reverse osmosis membranes have been reported elsewhere [84]; acetyl (CH_3CO-R) and hydroxyl (R-OH) groups of that membrane did not dissociate (ionize). Surface charge, therefore, may have arisen from (i) the adsorption of electrolyte anions (OH^- and Cl^-); (ii) from traces of acetic acid from the acetic anhydride used during acetylation; or (iii) from the acidic functional additives in the polymer solution. Nonlinear structure of a water molecule and higher electronegativity of oxygen (3.44) than that of hydrogen (2.20) on the Pauling scale lead to negatively charged oxygen of a polar water, which is strongly attracted to positively charged cations. However, two positively charged hydrogen atoms of the water molecule spread out and so weakly attract anions. Therefore, anions were less hydrated than cations and could more favorably approach a hydrophobic surface than a hydrophilic one. On the other hand, low contact angle values of both lab-made and HTI1 membranes definitely exhibit these membranes are hydrophilic, and hence, the anions (OH^- and Cl^-) are not favorable to absorb on these membrane surfaces. The negative charges of the membrane, therefore, may have arisen from traces of acetic acid and/or acidic functional additives. Additives used to prepare HTI1 membrane were not stated, but traces of maleic acid in the lab-made membrane probably contributed to its negative charge.

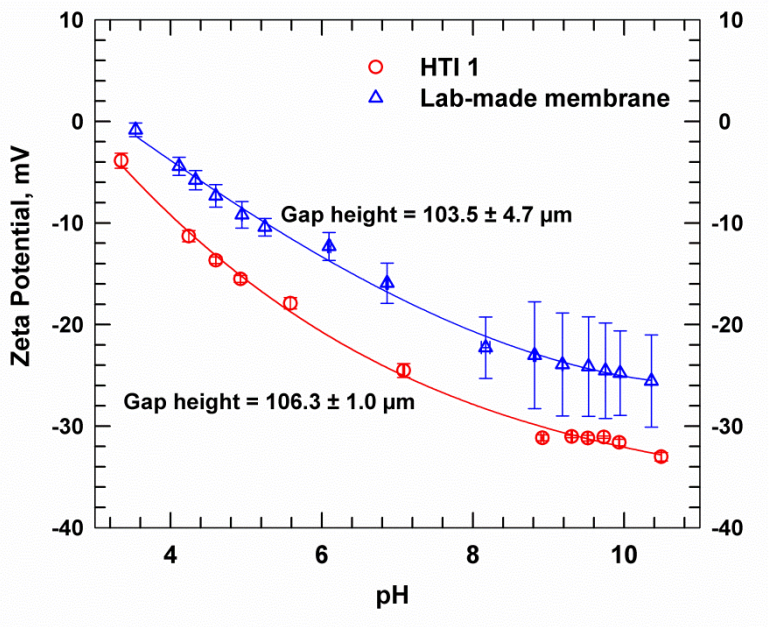

Figure 3. 9 *Zeta potentials of the lab-made and HTI1 membranes*

The lab-made membrane was smoother than the HTI1 membrane (Fig. 3.10), which implies its fouling is less likely. The large-scale surface roughness of a thin film composite polyamide membrane likely contributed to higher fouling during reverse osmosis than the smooth surface of a cellulose acetate membrane [53, 107]. The smoother surface of the lab-made membrane (Fig. 3.10a) is expected to allow less fouling than the commercial membrane (Fig. 3.10b).

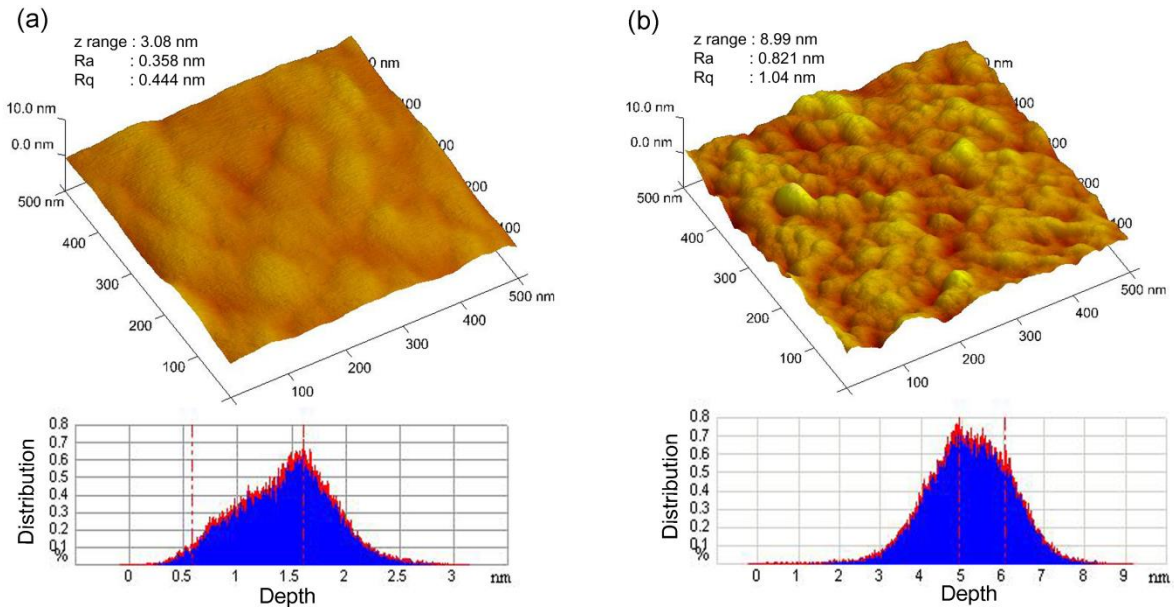

Figure 3. 10 *AFM images of (a) lab-made and (b) HTI1 membranes*

3.3 Conclusions

CTA/CA-based forward osmosis membranes were prepared by immersion precipitation using different casting compositions and preparation conditions, which were optimized to result in membranes with high water flux and low reverse salt flux. The optimized membrane was made by casting 6.3 wt.% CTA, 12.6 wt.% CA, 49.9 wt.% 1,4-dioxane, 17.2 wt.% acetone, 3.7 wt.% maleic acid, and 10.3 wt.% methanol to a thickness of 250 μm on a porous woven (WF1) support layer with subsequent evaporation for 30 seconds at 25 ^{o}C and annealing at 85 ^{o}C.

The optimized membrane showed 10.39 LMH water flux and 0.084 mole NaCl/m^2.h RSF using an FS of milli-Q water and a DS of 1 M NaCl. 9.270 LMH water flux, 0.248 mole Br^-/m^2.h RSF and 99.533% NaCl rejection were achieved with an FS of 0.1 M NaCl and a DS of 1 M KBr. The optimized membrane showed a more hydrophilic and smoother surface than a commercial FO membrane, indicating its likely lower fouling and, therefore, suggesting its potential applicability to such as treating wastewater. Future work could improve the membrane performance through modification, basing on suggestions below, and assess its performance in wastewater treatment and desalination.

(i) Assessment of the constituent polymers showed that higher CTA content led to higher salt resistance.

(ii) Testing different solvent mixtures showed that 1,4-dioxane promoted the membrane porosity.

(iii) Casting the membranes on thin, porous, woven or non-woven fabric support layers with an open space ratio greater than 0.24 led to great performance. Computerized image processing analysis of optical microscope images was useful in assessing the nature of the support layer and the relationship between membrane performance and support layer structure.

(iv) The casting thickness is dependent on intended application of membranes as water flux and RSF increased proportionally with casting thickness.

(v) Allowing the solvents to evaporate for up to 120 seconds did not affect on membrane performances.

(vi) Longer evaporation of solvents in cast films decreased performance. Annealing at 70^{o}C not only allowed the release and removal of residual solvents and additives from the membranes but also improved performance of the membranes.

IV. EFFECT OF CONCENTRATION POLARIZATION AND PREFERRED MEMBRANE CONFIGURATION

It was believed that the AL-DS membrane configuration yield higher effective osmotic pressure difference and higher water flux than AL-FS. However, the effect of concentrative ECP was ignored in AL-DS configuration. This section presents systematical investigation of the effect of CP, especially concentrative ECP in AL-DS configuration, to reveal whether the AL-DS configuration is always preferable for PRO operation. Several integrally asymmetric and TFC membranes were tested in both AL-FS and AL-DS configurations. Theoretical water fluxes were calculated based on a model adopting both ICP and ECP. Furthermore, the effects of CP on the application of PRO using real river water and real seawater as FS and DS, respectively, or in desalination using real seawater as FS were systematically studied. Cleaning efficiency of the membranes was investigated to support the suggestion of proper membrane configuration for osmotic processes.

4.1 Experimental materials and methodology

4.1.1 Membranes

Three commercially available membranes were purchased from Hydration Technology Innovations (OR, USA). Those were a CTA-based membrane embedded with polyester woven support (denoted as HTI1, 62 μm support thickness, 90 μm membrane thickness, and 390 μm structural parameter [40]), a CTA-based membrane cast on nonwoven polyester fabric support (denoted as HTI2, 154 μm support thickness, 163 μm membrane thickness, and 968 μm structural parameter [40]), and a polyamide TFC membrane (denoted as HTI3, 68 μm support thickness, 113 μm membrane thickness, and 730 μm structural parameter [40]). Two polyamide TFC membranes supplied from Toray Chemical Korea (South Korea) were prepared on a polyester nonwoven fabric support (denoted as TCK-N, 34 μm support thickness, 59 μm membrane thickness, and 461 μm structural parameter [40]) or on a polyester woven fabric support (denoted as TCK-W, 60 μm support thickness, 80 μm membrane thickness, and 266 μm structural parameter [40]). The properties of these membranes have been thoroughly characterized and reported in the section 4.2. Cross-sectional structures of these membranes are displayed in Fig. 2.2, and structures of the supporting layers are displayed in Fig. 2.3.

4.1.2 Chemicals

For most experiments of membrane performance, sodium chloride (NaCl, 99% purity, Bioshop, Canada), potassium bromide (KBr, 99.0%~100.2% purity, Junsei, Japan), or seawater were used as DS while sodium chloride, milli-Q water, seawater, or river water were used as FS. Milli-Q water was produced with 18.2 MΩ resistivity by a purification system (Millipore®, Merck Millipore, Germany). River water samples were collected from Nakdong river (Busan, Korea), Suyeong river (Busan, South Korea), and Taehwa river (Ulsan, South Korea). Seawaters were collected from Ilsan beach and Jeong-ja beach (Ulsan, South Korea). River and seawater samples were filtered by using GF/C™ glass microfiber filters (Whatman™ grade 1.2 μm, GE Healthcare Bio-Sciences, PA, USA). For the investigation of fouling effect on membrane performance, river water and seawater were filtered by using ultrafiltration membranes (Toray Chemical Korea, South Korea) in dead-end filtration cells (Amicon® 8400, Merck Millipore, Germany) at 4 bar applied pressure. The properties of the water samples were characterized, which were shown in Table 5.1, and stored at 4°C for later usage. The pH, conductivity and total dissolved solids (TDS), turbidity, total organic carbon (TOC) and total nitrogen (TN), and osmolarity were measured by using a calibrated pH probe (Orion 4 Star, Thermo Scientific, MA, USA), an Ultrameter II™ 6P meter (Myron L, CA, USA), a TC-3000e tri-meters (Lamotte, MD, USA), a TOC-V analyzer (Shimadzu, Japan), and a VAPRO® Vapor Pressure Osmometer (ELITechGroup, France), respectively.

Table 4. 1 *Characteristics of seawater and river water*

	Ilsan beach	**Jeong-ja beach**		**Suyeong river**	**Nakdong river**	**Taehwa river**	
	After GF/C filter	**After GF/C filter**	**After UF filter**	**After GF/C filter**	**After GF/C filter**	**After GF/C filter**	**After UF filter**
pH	8.08 ± 0.09	8.06 ± 0.07	8.10 ± 0.08	7.64 ± 0.07	7.92 ± 0.02	7.90 ± 0.22	8.02 ± 0.15
Conductivity (μS/cm)	51,085 ± 689	49,178 ± 166	49,110 ± 45	676 ± 0	356 ± 1	322 ± 1	321 ± 0
TDS (ppm)	32,278 ± 407	31022 ± 106	31,000 ± 20	351 ± 1	183 ± 1	165 ± 0	165 ± 0
Turbidity (NTU)	0.06 ± 0.05	0.07 ± 0.06	0.01 ± 0.01	0.09 ± 0.05	0.09 ± 0.07	0.17 ± 0.06	0.07 ± 0.07
TOC (ppm)	1.40 ± 0.04	1.59 ± 0.11	1.54 ± 0.08	2.78 ± 0.06	2.54 ± 0.13	1.99 ± 0.17	1.81 ± 0.08
TN (ppm)	0.14 ± 0.05	0.18 ± 0.00	0.19 ± 0.00	8.20 ±0.04	2.81 ± 0.00	2.65 ± 0.11	2.61 ± 0.08
Osmolarity (mmol/kg)	999.0 ± 12.7	958.0 ± 0.6	962.0 ± 6.9	12.3 ± 0.9	10.3 ± 0.8	6.0 ± 0.7	6.0 ± 1.2

4.1.3 Membrane performance test

Membranes were tested in a lab-scale system of which schematic diagram was described in the previous study [32]. Counter-current flows of the FS and DS were maintained at 1 $Lmin^{-1}$ by two gear pumps (81808, Cole-Parmer, IL, USA). The FS and DS temperature were controlled and maintained at 25°C by a water circulator (Isotemp 3016D, Fisher Scientific, MA, USA). The membranes were tested in both AL-FS and AL-DS configurations. NaCl, KBr, or seawater were used as DSs while milli-Q, low concentration NaCl, seawater, or river water were used as FSs. Initial 10 minutes water flux (in conditioning step) was removed for the calculation of average permeate water flux (Supplementary figure). The permeate water flux (J_w) was calculated by the weight change of the DS, which were automatically recorded every 10 seconds, using Eq. (4.1). At least two membrane coupons were tested for repeatability of each experiment. Except for the application tests using real seawater/river water or 2 M KBr/seawater operated over 24 hours, membrane performance tests for investigating concentrative ECP were performed over 1 hour.

$$J_w = \frac{\Delta \text{ weight}}{\text{water density} \times \text{effective membrane area} \times \Delta \text{ time}} \quad (Lm^{-2}h^{-1}) \tag{4.1}$$

Intrinsic membrane parameters, such as water permeability coefficient A, salt permeability coefficient B, and structural parameter S, were determined by reverse osmosis and FO tests (Table 4.2)

4.1.4 Theoretical calculation of membrane water flux

Lonsdale et al. [12] derived a general equation of water J_w for PRO (Eq. (4.2)), which considered the ICP effect on membrane performance but ignored the effect of ECP.

$$J_w = A\left[\pi_{D,b}\frac{1-\frac{C_{F,b}}{C_{D,b}}\exp(J_wK)}{1+\frac{B}{J_w}[\exp(J_wK)-1]} - \Delta P\right] \tag{4.2}$$

S. Loeb et al. [79] assumed the concentration ratio between two different phases in Eq. (4.2) were equivalent to the osmotic pressure ratio ($\frac{C_{F,b}}{C_{D,b}} = \frac{\pi_{F,b}}{\pi_{D,b}}$) and derived a water flux equation for PRO (Eq. (4.3)) and for FO (Eq. (4.4)). In these equations, ECP effect was not considered as in the Eq. (4.2). The osmotic pressure profile of this assumption was adapted and described in the model (1) of Fig. 5.1, and Eq. (4.3) and (4.4) were used to predict water flux using model (1) in this study.

$$J_w = \left(\frac{1}{K}\right)\left(ln\frac{B+A\pi_{D,b}-J_w}{B+A\pi_{F,b}}\right) \tag{4.3}$$

$$J_w = \left(\frac{1}{K}\right)\left(ln\frac{B+A\pi_{D,b}}{B+J_w+A\pi_{F,b}}\right) \tag{4.4}$$

Where K is solute resistivity ($s.m^{-1}$) and K = DS [78]. D is diffusion coefficient of draw solute or feed solute (m^2s^{-1}). D depends on concentration of solute solution, and Table 4.2 shows the dependence of D upon concentration of NaCl solutes [80]. Structural parameter S (m), water permeability coefficient A ($Lm^{-2}h^{-1}bar^{-1}$), salt permeability coefficient B (ms^{-1}) expressed by $B = \frac{J_{w(RO)}(1-R)}{R}\exp\left(\frac{-J_w(RO)}{k}\right)$, salt rejection R, and cross-flow cell mass transfer coefficient k ($m.s^{-1}$) were obtained from our previous study [40].

Table 4.2 *Diffusion coefficient at various concentration of NaCl* [80]

NaCl concentration M	**D m^2s^{-1}**
0.1	1.483E-09
0.5	1.473E-09
1	1.480E-09
2	1.516E-09
4	1.594E-09
5	1.590E-09

Recently, McCutcheon and Elimelech have derived a water flux equation considering effect of both ICP and ECP on membrane performance [15]. A detailed clarification of definition of concentrative or dilutive ICP and concentrative or dilutive ECP was proposed in their study. However, in their calculation to predict water flux behavior, two assumptions were made: (i) salt was rejected completely and thus the concentrative modulus was expressed as $\exp\left(\frac{J_w}{k}\right)$; and (ii) there was no concentrative ECP on the outer surface of the porous support layer in AL-DS configuration and no dilutive ECP on the porous support layer in AL-FS configuration. Regardless of the assumption (i), the assumption (ii) was employed in the model (2) in this study (Fig. 4.1), in which rejection R of the membranes was adapted from previous our studies [40] and concentration polarization modulus was calculated based on $\frac{exp\left(\frac{J_w}{k}\right)}{R+(1-R)exp\left(\frac{J_w}{k}\right)}$ [77]. Thereby, the water fluxes of model (2) were calculated using Eq. (4.5) and Eq. (4.6) in AL-DS and AL-FS configurations, respectively.

$$J_w = \left(\frac{1}{K}\right)\left[ln\frac{B+A\pi_{D,b}exp\left(-\frac{J_w}{k}\right)\times(R+(1-R)exp\left(\frac{J_w}{k}\right)-J_w}{B+A\pi_{F,b}}\right] \quad (4.5)$$

$$J_w = \left(\frac{1}{K}\right)\left[ln\frac{B+A\pi_{D,b}}{B+J_w+A\pi_{F,b}\frac{exp\left(\frac{J_w}{k}\right)}{R+(1-R)exp\left(\frac{J_w}{k}\right)}}\right] \quad (4.6)$$

In this study, we introduced another model with the addition of concentrative ECP in the case of AL-DS to propose the model (3), and the model is shown in Fig. 4.1. From our previous study, except integrally asymmetric HTI1 and HTI2 membranes, TFC membranes yielded high water flux [40]. In AL-DS configuration, feed solutes transported and accumulated inside support layer due to the high convective water transport across TFC membrane, causing concentrative ICP in the porous support layer. The solute concentration in the support layer was always higher than FS bulk concentration because of the trap of FS in the support layer and replenishment of FS outside of the membrane. The solutes in the support layer diffused back to the FS bulk due to concentration gradient. High water transport against the solute back diffusion likely resulted in the occurrence of concentrative ECP on the outer surface of the porous support layer. The higher permeate flux was obtained from the membrane, the more FS solutes was built-up in the porous support layer. Subsequently, the big concentration gap of FS solutes in the interface between support layer and FS bulk resulted in the more severe concentrative ECP. The rejection of the membrane was used to calculate the modulus of the concentrative ECP. Thereby, the concentrative ECP modulus in this model became $\frac{exp\left(\frac{J_w}{k}\right)}{R+(1-R)exp\left(\frac{J_w}{k}\right)}$. Water fluxes in the model (3) were calculated following Eq. (4.7) in Al-DS and Eq. (5.6) in AL-FS.

$$J_w = \left(\frac{1}{K}\right)\left[ln\frac{B+A\pi_{D,b}exp\left(-\frac{J_w}{k}\right)\times(R+(1-R)exp\left(\frac{J_w}{k}\right)-J_w}{B+A\pi_{F,b}\frac{exp\left(\frac{J_w}{k}\right)}{R+(1-R)exp\left(\frac{J_w}{k}\right)}}\right] \quad (4.7)$$

Assuming 100% rejection of membrane can change the CP modulus from $\frac{exp\left(\frac{J_w}{k}\right)}{R+(1-R)exp\left(\frac{J_w}{k}\right)}$ to $exp\left(\frac{J_w}{k}\right)$ in Eq. (4.6) and (4.7) to obtain the model (4). Theoretical flux data were shown and discussed in Section 4.2.1.

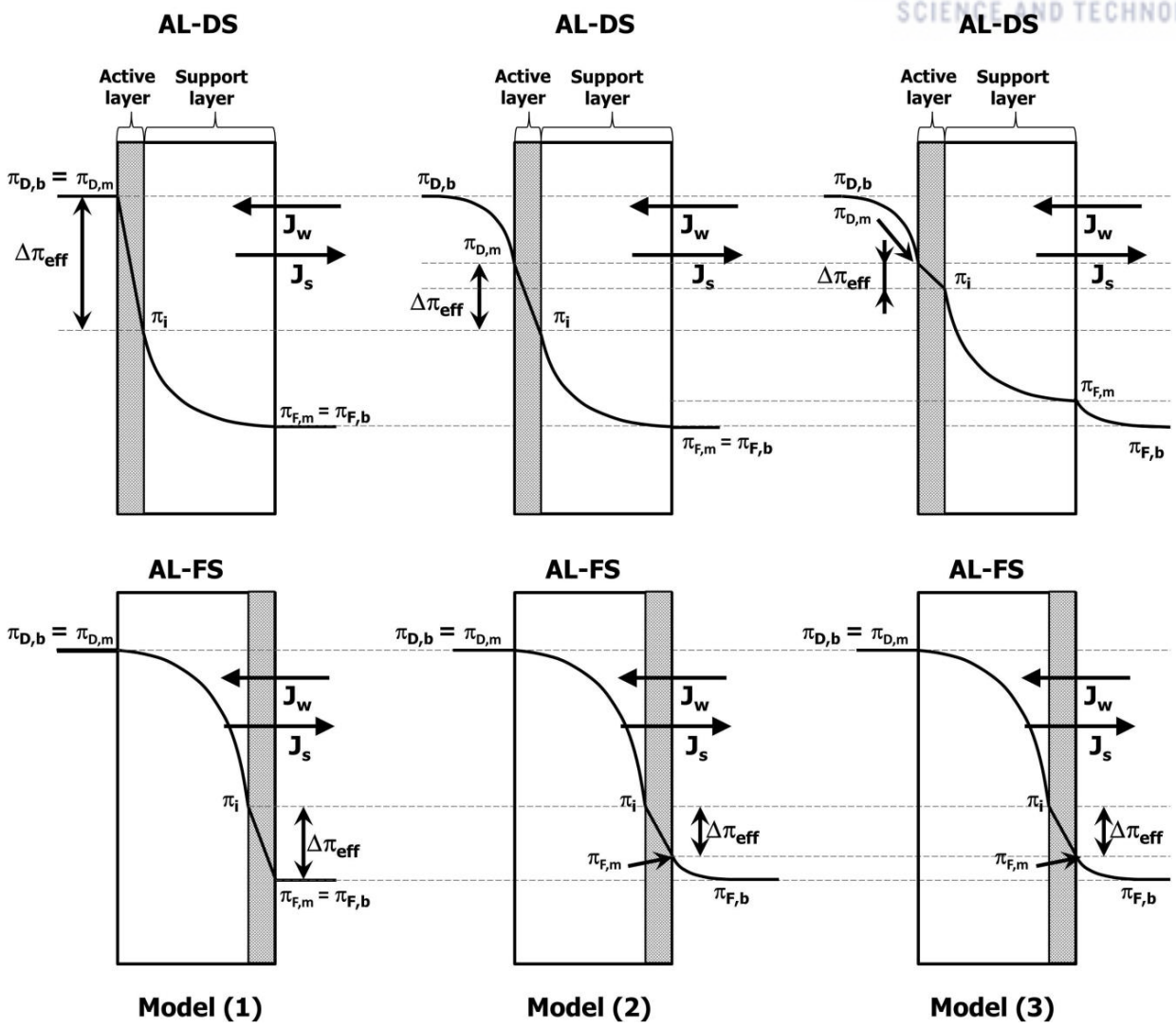

Figure 4. 1 *Illustration of concentration polarization of the membranes in AL-FS and AL-DS configurations with various calculating approaches. Model (1) assumes no ECP; model (2) introduces dilutive ECP in AL-DS and concentrative ECP in AL-FS; model (3) introduces dilutive and concentrative ECP in AL-DS and concentrative ECP in AL-FS.* $\pi_{D,b}$, $\pi_{D,m,}$ π_i, $\pi_{F,m}$ *and* $\pi_{F,b}$ *are osmotic pressures of bulk draw solution, of draw solution at membrane active layer-bulk draw solution interface, of active layer-support layer interface, of feed solution at support layer-bulk feed solution interface, and of bulk feed solution, respectively.*

4.2 Results and Discussion

4.2.1 Effect of concentrative external concentration polarization on membrane performance

Figure 4.2 shows the performance of TCK-W in different membrane configurations, i.e., AL-FS and AL-DS, using 2M NaCl as DS and various concentrations from 0 to 1.0 M of NaCl as FSs. When milli-Q was used as FS, the water flux in AL-DS configuration was approximately 1.7 times higher than that in AL-FS. The higher water flux in AL-DS than AL-FS could be well explained by the less dilutive ICP occurring in the support layer of the membrane. The dilutive ICP of AL-FS reduced effective osmotic pressure difference across the membrane. With increasing FS concentration from 0 to 0.01 M NaCl, the water flux of AL-FS insignificantly changed but that of AL-DS dramatically declined, and the water flux gap of two membrane configurations became negligible. Further increase of FS concentration over 0.01 M lowered the water flux of AL-DS below the water flux of AL-FS.

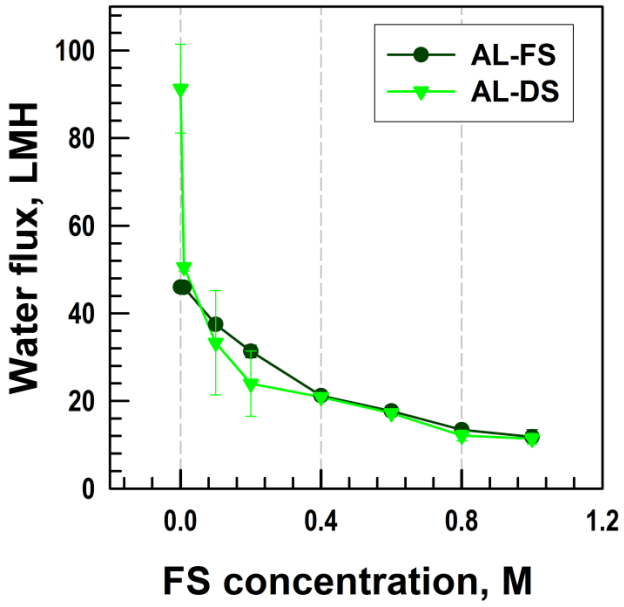

Figure 4. 2 *Performance test of TCK-W membrane in AL-FS and AL-DS membrane configurations, using 2M NaCl as DS and various concentrations from 0 to 1.0 M of NaCl as FSs*

Theoretical calculation of water flux for model (1) (no ECP), model (2) (dilutive ECP in AL-DS and concentrative ECP in AL-FS), model (3) (dilutive and concentrative ECP in AL-DS and concentrative ECP in AL-FS), and model (4) (model (3) with 100% rejection assumption) were shown in Fig. 4.3a, b, c and d, respectively. Model (1) showed a big gap in the theoretical and experimental values (Fig. 4.3a). As mentioned elsewhere [15], model (1) was only valid if the permeate flux was very low. The membrane TCK-W showed high water flux and thus the model (1) was insufficient to

describe the water flux of the membrane. Figure 4.3b showed better matching of the theoretical flux and experimental flux but there was still a gap between the theoretical line and experimental data in AL-DS configuration. According to this model (2), the water flux in AL-DS is always higher than that in AL-FS, which cannot explain the reversal of water flux in the two configurations. Model (3) showed the best calculation of water flux in both membrane configurations. The two water flux modeling lines in two membrane configurations intersected at 0.066 M NaCl as FS, and the water flux line of AL-DS moved downward the water flux line of AL-FS. The difference between model (2) and (3) is the existence of concentrative ECP effect in AL-DS configuration. Model (3) estimated the water flux of the TCK-W membrane more accurately at high FS concentration than model (2). Assuming that rejection of membrane was 100% as other studies have assumed to theoretically estimate the water flux of the membranes [12, 15, 38], concentrative ECP modulus of model (3) was changed from $\frac{exp\left(\frac{J_w}{k}\right)}{R+(1-R)exp\left(\frac{J_w}{k}\right)}$ to $exp\left(\frac{J_w}{k}\right)$ in model (4). The data of model (4) in Fig. 4.3d showed agreement of the experimental data with the theoretical data. Regardless of complete rejection of solutes or 95.84% rejection by membrane [40], the occurrence of concentrative ECP in AL-DS was severe when water flux was high and FS was not pure water.

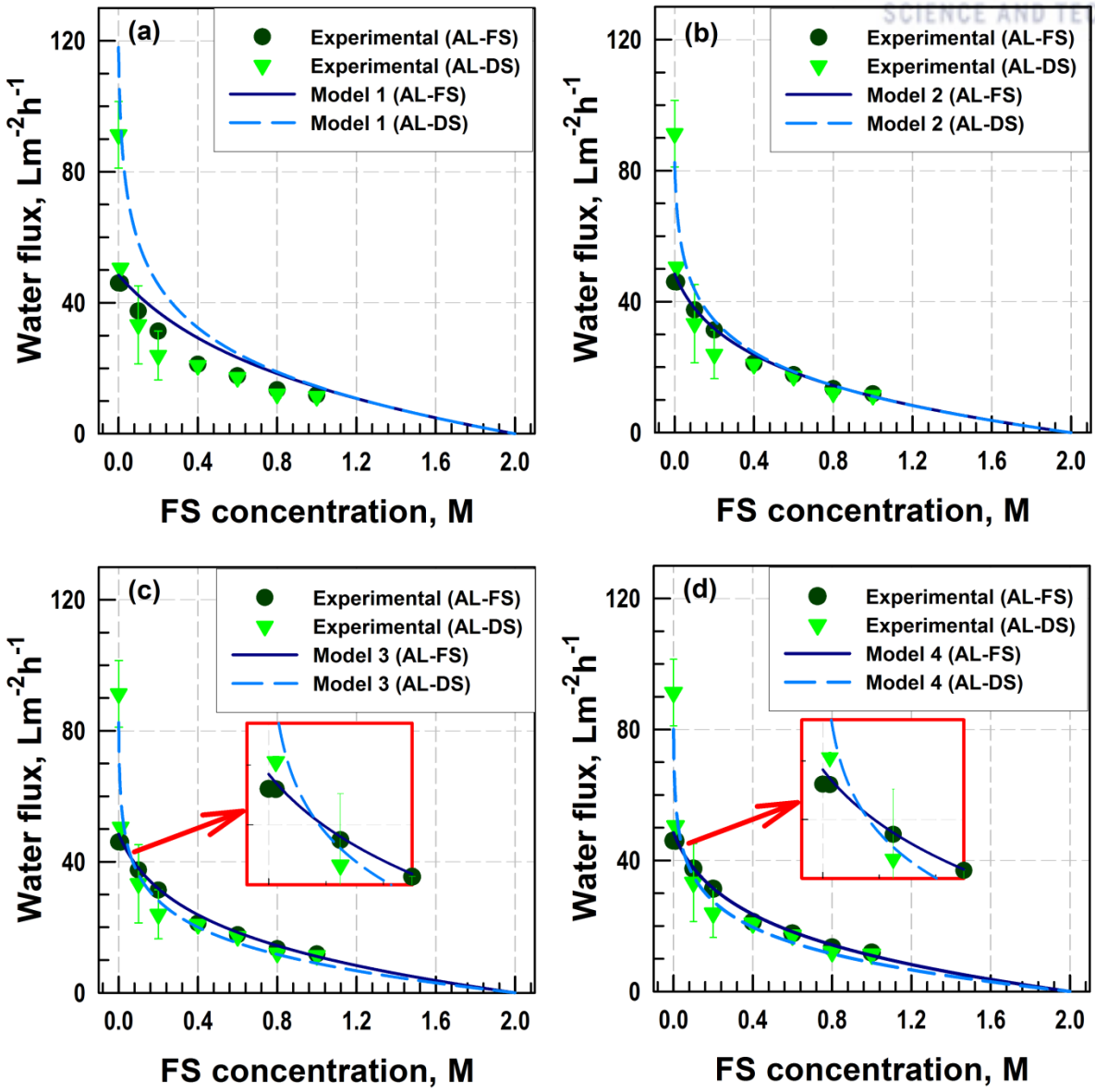

Figure 4. 3 Theoretical *flux of membrane TCK-W using (a) model (1) (no ECP), (b) model (2) (dilutive ECP in AL-DS and concentrative ECP in Al-FS), (c) model (3) (dilutive/concentrative ECP in AL-DS and concentrative ECP in AL-FS), and (d) model (4) (dilutive/concentrative ECP in AL-DS and concentrative ECP in AL-FS with 100% rejection assumption)*

Studying the effect of concentrative ECP was conducted with 5 types of membranes. The method utilized to calculate theoretical flux of Fig. 4.3c was used to calculate theoretical fluxes of various membranes using 2 M NaCl as DSs and various NaCl concentrations from 0 to 2 M as FSs. The ratios of water fluxes obtained in two membrane configurations are shown in Fig. 4.4, and the intersection point where $J_{w(AL\text{-}DS)}$ was equal to $J_{w(AL\text{-}FS)}$ was determined (Table 4.3). All the membranes displayed the intersection point, beyond which the water flux of AL-DS was beneath that of AL-FS. The

previous study showed that TFC structured membranes (HTI3, TCK-N and TCK-W) showed higher water flux than integrally asymmetric membranes (HTI1 and HTI2) [40]. FS concentrations of the intersection points in Fig. 4.4 and Table 4.3 were inversely proportional to the water fluxes of the membranes in Fig. 4.5a.

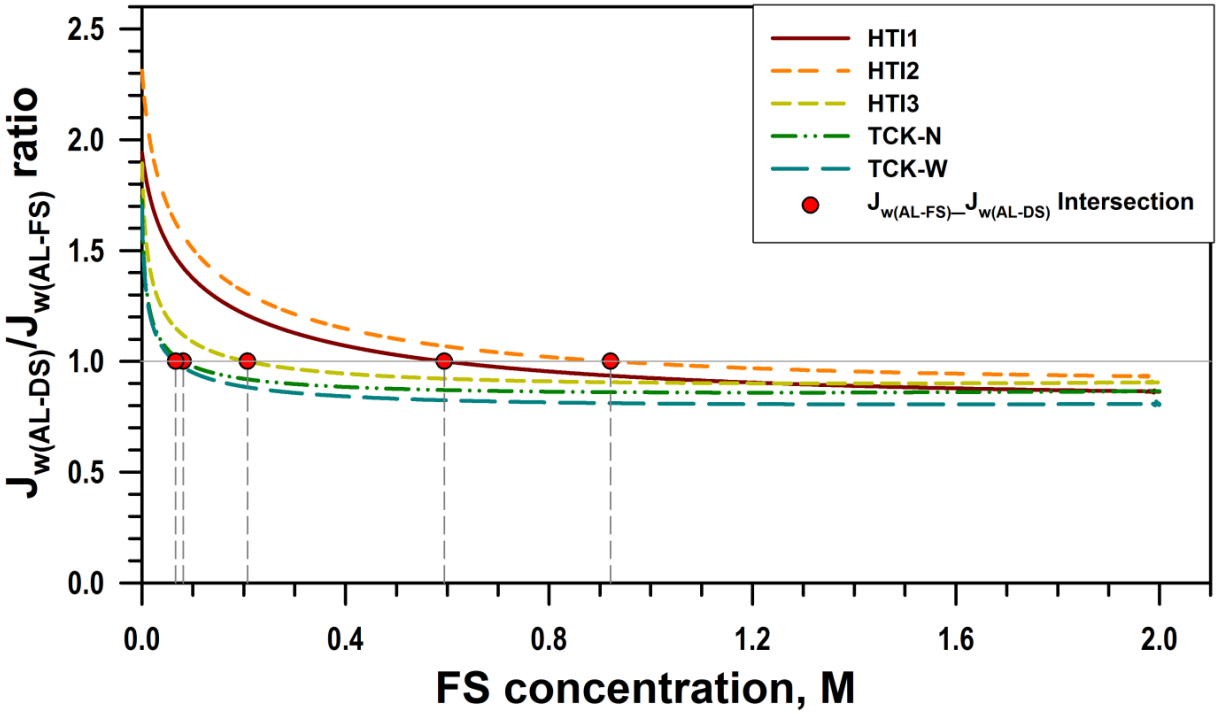

Figure 4. 4 *Modeling relationship of water fluxes between AL-FS and AL-DS membrane configurations with various membranes*

Table 4. 2 *Intersection point of water fluxes in AL-FS and AL-DS membrane configurations*

	FS concentration	$J_{w(AL-FS)} = J_{w(AL-DS)}$
	M	**$Lm^{-2}h^{-1}$**
HTI1	0.594	10.42
HTI2	0.921	3.52
HTI3	0.207	13.67
TCK-N	0.081	27.56
TCK-W	0.066	40.92

Figure 4.5 also exhibits the relationship between water flux of two membrane configurations when different DS and FS agents (1 M NaCl or 2 M KBr as DS and milli-Q water or 0.6 M NaCl as FS, respectively) were used. With 1 M NaCl as DS and milli-Q water as FS, the water fluxes of AL-

DS of all membranes were always higher than those of AL-FS from 1.7 to 2.6 times (Fig. 4.5a). On the contrary, when 2 M KBr and 0.6 M NaCl were used as DS and FS, respectively, the water fluxes of AL-DS were lower than those of AL-FS (Fig. 5.5b). Results shown in Fig. 4.2, 4.3, 4.4, and 4.5 and Table 4.3 suggest that for each type of membrane, the membrane configuration should be considered based on the FS concentrations to yield the highest water flux. For instance, when TCK-W membrane was applied with 2 M NaCl as DS and DI water as FS, AL-DS configuration was recommended to obtain high water flux, on the contrary, AL-FS configuration was recommended when 0.066 or greater than 0.066 M NaCl was used as FS.

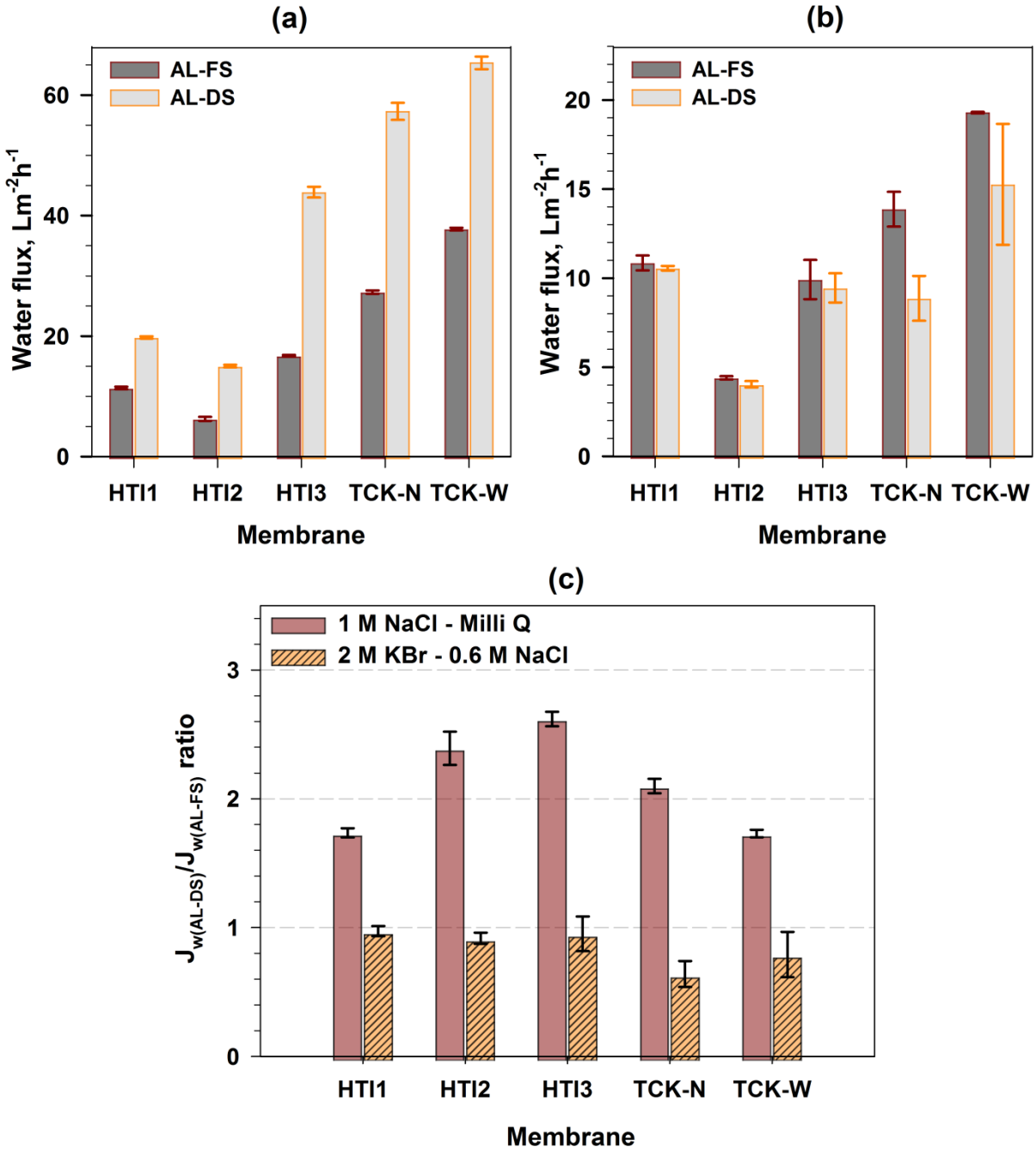

Figure 4. 5 *Effect of membrane orientation on membrane performance using 1 M NaCl and milli-Q water as DS and FS, respectively (a), 2 M KBr and 0.6 M NaCl as DS and FS, respectively (b) and water flux ratio between these two membrane configurations (c)*

Furthermore, the effect of concentrative ECP was investigated using natural source water during 24-hour test. Figure 4.6 shows water flux profiles of virgin TCK-W membrane using Ilsan seawater and Suyeong river water (Fig. 4.6a), Ilsan seawater and Nakdong river water (Fig. 4.6b), Jeong-ja seawater and Taehwa river water (Fig. 4.6c) and Jeong-ja seawater and UF-filtered Taehwa river water (Fig. 4.6d) as DSs and FSs, respectively, in different membrane configurations. All the water fluxes of membranes in AL-FS configuration slightly declined upon time; however, those in AL-DS sharply declined within few hours, and then declined below the water flux of AL-FS. This result of the TCK-W membrane could be explained by the concentrative ECP effect proposed in this study. At the initial time, the concentration of river water was still low in the support layer of the membrane operated in AL-DS configuration. The effective osmotic pressure difference in AL-DS configuration was much higher than that in AL-FS, resulting in higher initial water flux of AL-DS. However, continuous filtration of FS through the membrane in AL-DS led to the accumulation of solutes on the outer surface of the membrane support layer and the diffusion of the solute to the FS bulk, resulting in concentrative ECP. The water flux profiles versus permeate mass in Fig. 4.6 show the effect of concentrative ECP more clearly. For instance, when the same 600 g permeate mass passed through the membrane from FS to DS, the water flux in AL-DS (4.3 $Lm^{-2}h^{-1}$) was about one-fifth of water flux in AL-FS (21 $Lm^{-2}h^{-1}$) for Suyeong River (Fig. 4.6a). Moreover, the water flux profile versus permeate mass exhibited that permeate mass in AL-FS became higher than those in AL-DS within one day.

Similar tendency of performance change was observed in four cases of operations in Fig. 4.6, regardless of the properties of FS and DS (Table 4.1). Times for the occurrence of intersection points in Fig. 4.6a, b, c, and d were inversely proportional to - the conductivity, TOC, TN and osmolarity of river water, which implied the influence of either organic fouling or osmotic pressure of river waters. However, when the river water was filtered by the UF membranes to get rid of fouling effect on Fig. 4.6d, the intersection point came out slightly later than that of Fig. 4.6c, which implied insignificant effect of fouling on the decline of water flux in AL-DS configuration.

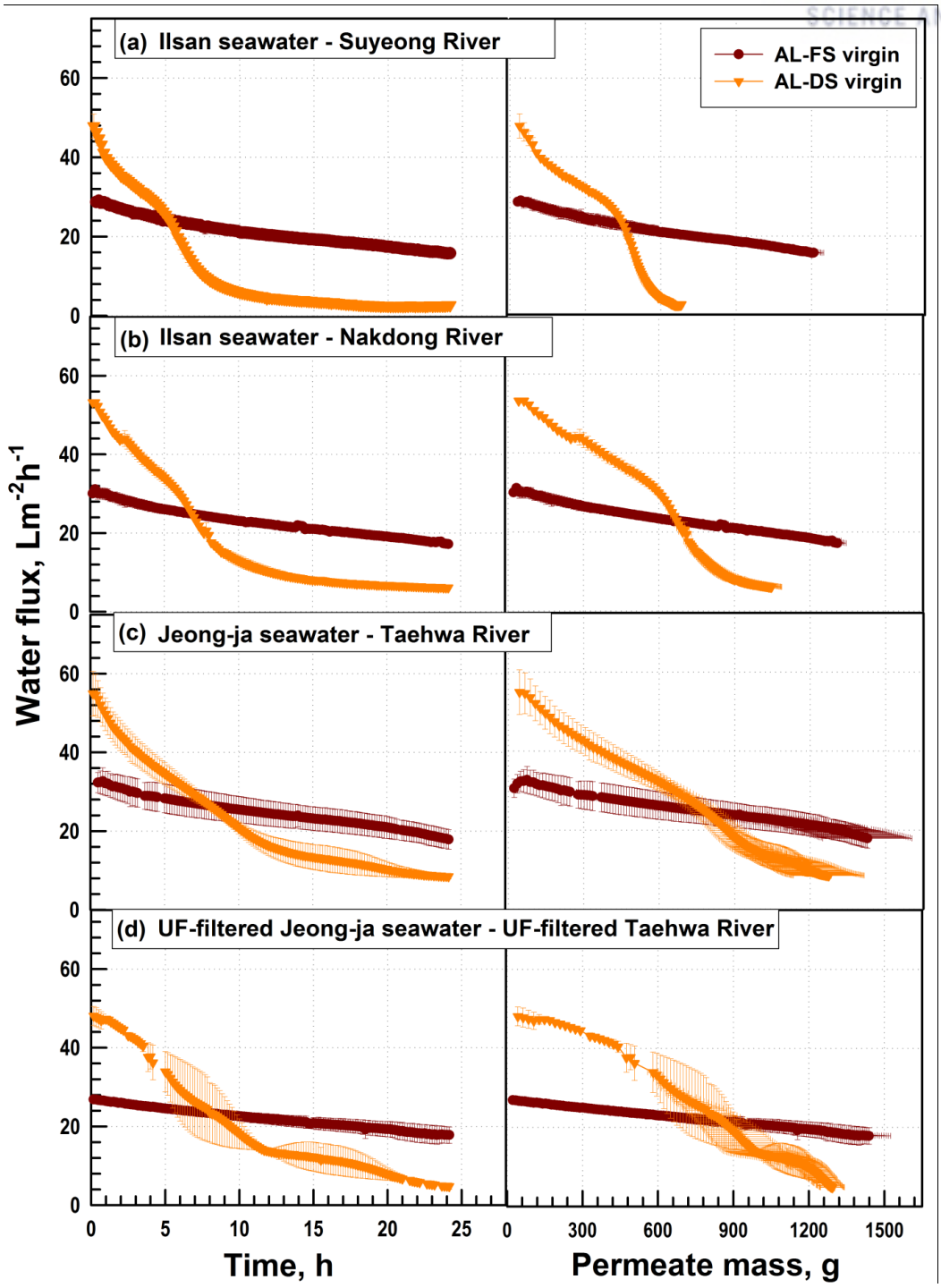

Figure 4. 6 *Effect of membrane orientation on membrane performance using Ilsan seawater and Suyeong River water (a), Ilsan seawater and Nakdong River water (b), Jeong-ja seawater and Taehwa River water (c) or Jeong-ja seawater and UF-filtered Taehwa River water (d) as DSs and FSs, respectively*

4.2.2 Effect of concentrative ECP on seawater desalination

Study on concentrative ECP effect in the field of seawater desalination was conducted using 2 M

KBr as DS and seawater as FS in AL-FS configuration and shown in Fig. 4.7. Compared with initial water flux using 1 M NaCl as DS and milli-Q water as FS (Fig. 4.5), the initial water flux using 2M KBr as DS and seawater as FS was much lower (Fig. 4.7). For instance, about 25 $Lm^{-2}h^{-1}$ was observed using 2 M KBr/seawater (~1.4 M concentration difference between DS and FS) compared with 37 $Lm^{-2}h^{-1}$ 1 using 1 M NaCl/milli-Q (1 M concentration difference). This result was likely due to the concentrative ECP effect on the boundary layer of the active layer when high FS concentration was used. The effect of concentrative ECP severely cut the actual water flux off. Figure 4.7 also shows the water flux of all membranes converges approximately after one day operation.

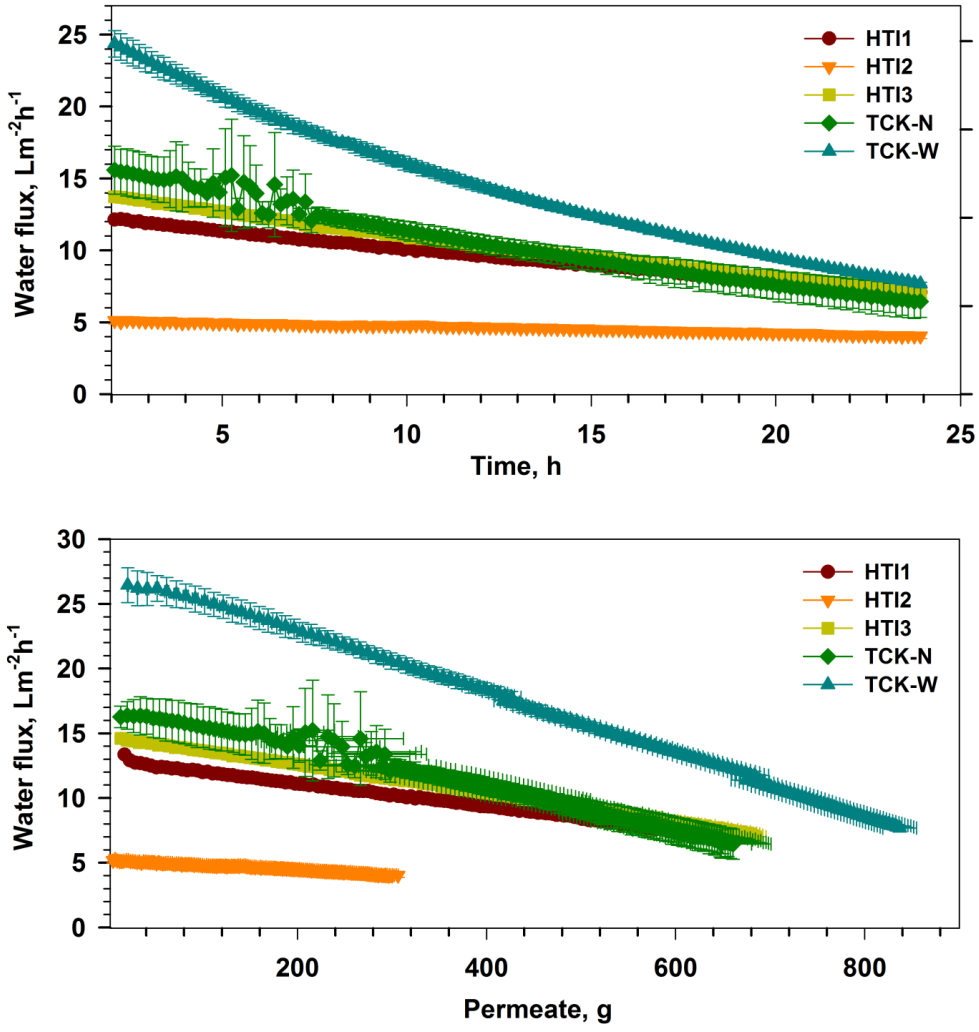

Figure 4. 7 *Performance test of all membranes with real seawater as FS and 2 M KBr as DS*

4.2.3 Cleaning efficiency of membranes in FO and PRO mode

Figure 4.6 shows the decline of water flux of membrane TCK-W after 1-day test with various sweaters and river waters in both AL-FS and AL-DS configurations. The membranes were physically

cleaned by rinsing and shaking at 150 rpm for 5 min with milli-Q water. The water flux recovery of the membranes after physical cleaning with milli-Q water was studied in this section. Normalized water flux of virgin and cleaned membrane by the initial water flux of virgin membrane was calculated and shown in Fig. 4.8. This figure clearly shows that after cleaning, the initial flux of the membranes performed in AL-FS returned to approximately 83% with Suyeong river, 90% with Nakdong river, 85% with Taehwa river and 95% with UF-filtered Taehwa river. Meanwhile, these values were 73%, 68%, 67% and 94% in AL-DS, respectively. Apparently, the Fig. 11c and d exhibited the removal of foulants in DSs and FSs by UF membranes before FO test. With the same cleaning condition, the water flux after cleaning step of the membrane using UF-filtered seawater and UF-filter river water (Fig. 4.8d) was higher than that in the case of using GF/C-filtered samples (Fig. 4.8c).

For AL-DS, the porous support layer faced to the river water, organic and inorganic foulants in river were easily trapped in porous support layer. This fouling was not easily mitigated by flushing with milli-Q water on the membrane surface or shaking during cleaning. Chemical cleaning such as using chlorine causes membrane deterioration by chlorination of polyamide membrane [65, 108]. Modification of membranes has been studied elsewhere to enhance membrane resistance to fouling and chlorine [108-111]. Therefore, the employment of AL-DS configuration in power generation using seawater as DS and river water as FS obviously faces challenges of fouling and cleaning efficiency more than the AL-FS configuration.

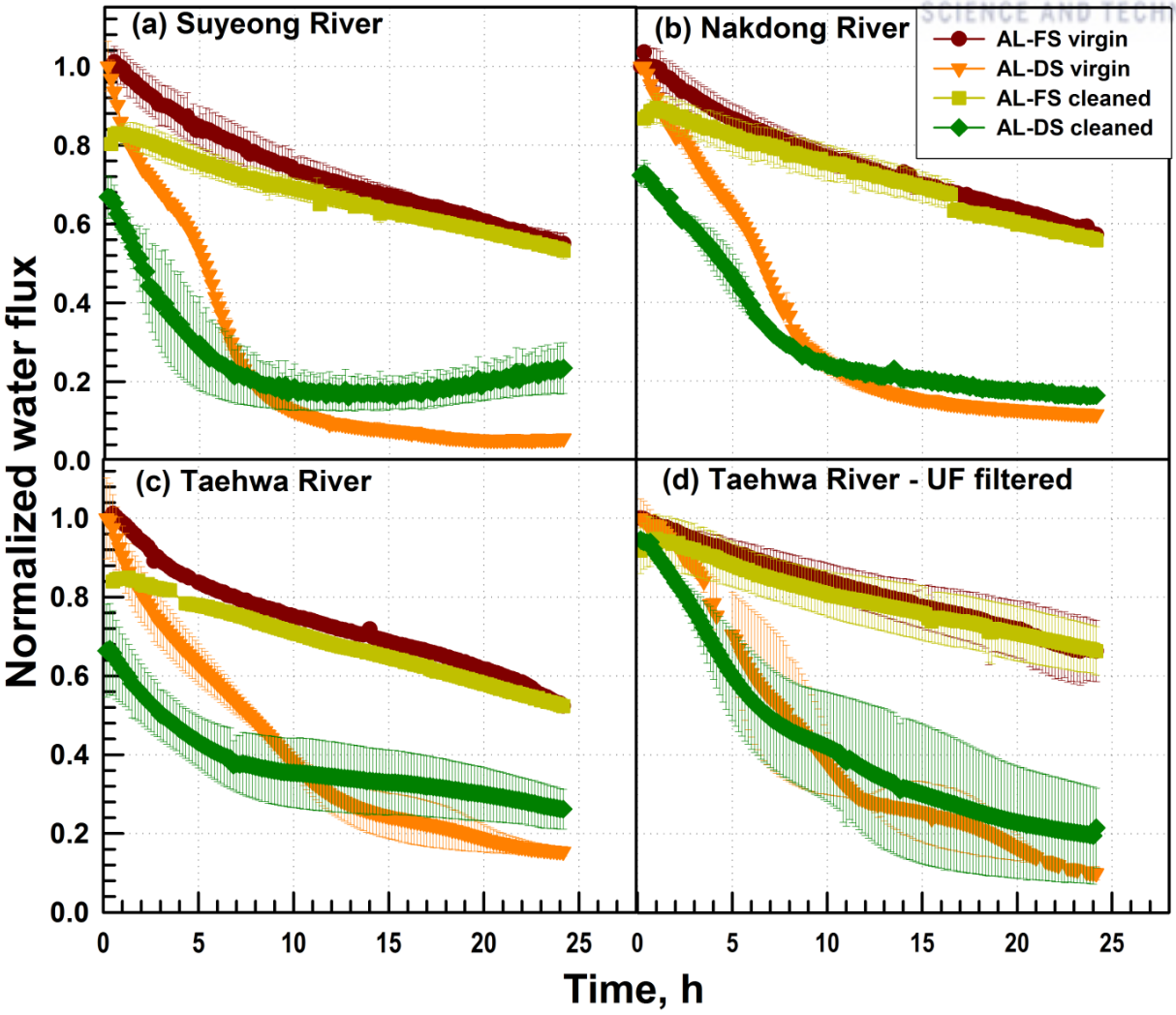

Figure 4. 8 *Effect of membrane orientation on cleaning efficiency of the membrane using Ilsan seawater and Suyeong River water, Ilsan seawater and Nakdong River water, Jeong-ja seawater and Taehwa River water or Jeong-ja seawater and UF-filtered Taehwa River water as DSs and FSs, respectively*

4.3 Conclusions

Concentration polarization effect on performance of integrally asymmetric and TFC FO membranes were thoroughly investigated in AL-FS and AL-DS configurations. When pure water was used as a FS, water flux in AL-DS was much higher than that in AL-FS due to the less dilutive ICP in the support layer of membranes. However, the presence of salts in FS depressed the water flux in AL-DS below the water flux in AL-FS. At the operation of membranes with higher initial water flux, the water flux depression was more obvious. According to a model developed in this study, the line of water flux profile in AL-DS intersected the line of water flux profile in AL-FS at certain FS concentration, which depended on membrane type. The theoretical FS concentrations, at which water fluxes in both modes were equal, were inversely proportional to the initial water flux of the membranes. The membrane with highest initial water flux (TCK-W membrane, 83 $Lm^{-2}h^{-1}$ at 2 M NaCl as DS and milli-Q as FS) showed the lowest FS concentration at the intersection point (0.066 M NaCl), while the HTI2 membrane with lowest initial water flux showed the highest FS concentration at the intersection points (21 $Lm^{-2}h^{-1}$ and 0.921 M NaCl, respectively).

When river water and seawater were used as FS and DS, respectively, the water flux of the membranes in AL-DS sharply declined and became lower than the water flux in AL-FS within about 8 hours of operation. AL-FS mode showed more stable and higher water flux after the 8-hour running time. Moreover, the membranes operated in AL-DS configuration were more easily fouled and showed lower water flux recovery after cleaning. This study suggests that the AL-FS configuration is preferable for application of PRO for optimal water flux and lower operating costs.

V. CHLORINATION OF INTEGRALLY ASYMMETRIC CTA-BASED AND TFC FO MEMBRANES

Once membranes are used in real water/wastewater treatment, membrane properties, and sequent membrane performance may be affected by various environmental factors. One of those factors is chlorine in the water. Chlorine is the cheapest and the most convenient biocide to be used in pretreatment of water/wastewater to control membrane fouling or used as cleaning agent. Chlorination has been studied and exhibited that it changed performance and properties of polyamide membranes in pressure-driven membrane processes. Up to this study, there is no publication on neither the chlorination mechanism of FO membranes nor performance changes of FO membranes under various chlorine conditions. This study aims to evidentially exhibit the pathway of chlorination of available CTA-based FO membrane as well as contribute understating of the chlorine mechanism and performance change of available CTA-based FO membrane in comparison with other commercial TFC PA-based FO and RO membranes in FO mode. The membrane performance in terms of water flux and reverse salt flux (RSF) of the membrane after being soaked in a chlorine solution was tested in FO mode, and compared with the virgin one. Membrane properties were characterized by X-ray Photoelectron Spectroscope (XPS), Time-of-Flight Secondary Ion Mass Spectrometry (ToF-SIMS), Solid-state Nuclear Magnetic Resonance (NMR), Attenuated Total Reflectance - Fourier Transform InfraRed (ATR-FTIR) and zeta potential analyzer. As the best knowledge of the authors, this is the first time ToF-SIMS is employed to study a membrane property change after chlorination..

5.1 Experimental materials and methodology

5.1.1 Chemicals and membranes

Sodium hypochlorite (NaOCl, available chlorine 10-15 %, 425044 - Sigma-Aldrich, USA) was used to prepare chlorine stock solutions. Chlorine concentration was titrated by using a titration device (888 Titrando, Metrohm, Switzerland), following Standard Methods 4500-Cl B, in which the standard sodium thiosulfate ($Na_2S_2O_3$, 35245-Fluka®, Germany) titrates (at pH 3 to 4 adjusted by glacial acetic acid (Duksan, South Korea)) the free iodine liberated from potassium iodide (KI, Duksan, South Korea) by chlorine. The pH of chlorine solutions were adjusted by adding NaOH (1 M standard solution, Daejung, South Korea) or/and HCl (concentrate 36%, Daejung, South Korea). Sodium chloride (NaCl, 99% purity, Bioshop, Canada) and milli-Q water (18 MΩ resistivity, Millipore® , Merck Millipore, Germany) were used as the DS and the FS, respectively, in FO mode.

A labmade CTA/CA-based membrane was prepared in the previous study [32] via immersion precipitation method. A 18.9 wt.% mixture (1:2 weight ratio) of CTA (43-49 wt.% acetyl, Aldrich, MO, USA) and CA (39.8 wt.% acetyl, average Mn ~ 30,000, Aldrich, MO, USA) was dissolved in a solvent mixture of 1,4-dioxane (≥ 99.5% purity, Sigma-Aldrich, MO, USA) and acetone (≥ 99% purity, Sigma-Aldrich, MO, USA) (2.9:1 weight ratio) with 10.3 wt.% methanol (≥9 9.8% purity, Sigma-Aldrich, MO, USA) and 3.7 wt.% maleic acid (≥ 99% purity, Sigma-Aldrich, MO, USA) as additives. That dope solution was cast with 250 μm casting knife at 25°C and 70% relative humidity. The casting film was immersed in a 1 ± 0.3°C water coagulation bath for 2 hours for the formation of the membrane, then, post treated with 85°C hot water for 15 minutes. The final membrane was stored in deionized water for later usage.

Three commercial FO membranes from Hydration Technology Innovations (OR, USA) were used, which are the integrally asymmetric CTA-based membrane embedded on a polyester screen (denoted as HTI1), the integrally asymmetric CTA-based membrane cast on a non-woven polyester fibers individually coated with polyethylene (denoted as HTI2) and the TFC PA-based membrane (denoted as HTI3). The surface morphologies, membrane structure and hydraulic properties of these membranes were well characterized in the previous studies [32, 40]. Other TFC membranes, i.e., NF90, NF270 and BW30 (DOW FILM-TEC™, MI, USA), were tested as references..

5.1.2 Protocol of chlorination of membranes

Chlorination can be studied via a soaking test or filtration test. In this study, only the soaking test, in which the membrane was soaked in chlorine then washed and tested performance in FO mode with membrane configuration of active layer facing the FS (AL-FS), was carried out. The chlorination test was performed twice with the virgin and the chlorinated membrane coupon.

Chlorination of the labmade membrane was tested at various values of exposure time to chlorine for chlorination mechanism study of CTA-based membranes. The membrane coupons were soaked and stirred in 2,000 ppm chlorine at pH 4 for 1, 10 or 20 hours. The performance of virgin and chlorinated membranes were compared by testing in FO mode, and characteristics were analyzed by measuring XPS, ToF-SIMS, solid-state NMR and zeta potential. Effect of chlorine concentration on CTA-based membranes was also investigated with two tests of independent and stepwise increase of chlorine concentration. In the independent test, the labmade membranes were solely soaked in various chlorine concentrations at pH 4 for 10 hours and tested performance for two hours to compare the performance with the virgin membrane. Meanwhile, in the stepwise test, the labmade membranes were soaked in a stepwise increase of chlorine concentration from 0, 2,000, 5,000 to 10,000 ppm at

pH 4. After being soaked in each chlorine concentration and physically washed by milli-Q at 150 rpm for 5 mins using a shaker, the membranes were tested FO performance before being soaking in a higher chlorine concentration. Effect of chlorination on the CTA-based membrane at various pH values was tested with 2,000 ppm chlorine at pH 4, 7 or 10 for 1 or 10-hour soaking.

Chlorination of CTA-based FO membranes (labmade, HTI1 and HTI2) in FO mode was compared with TFC PA-based FO membrane (HTI3) and other PA-based membranes (NF90, BW30 and NF270). Chlorination tests were conducted with 2,000 ppm chlorine solution at pH 4 or pH 10 for 10-hour soaking; then, 2-hour test in FO. pH of chlorine solution was adjusted by addition of NaOH and/or HCl. All FO performance tests in this study were repeated at least two times.

5.1.3 Performance test of chlorinated membranes in FO

Membranes were tested in a lab-scale system of which schematic diagram was described in Fig. 2.1. Counter-current flows of the FS and DS were maintained at 1 $Lmin^{-1}$ by two gear pumps (81808, Cole-Parmer, IL, USA). The FS and DS temperature were controlled and maintained at 25^{o}C by a water circulator (Isotemp 3016D, Fisher Scientific, MA, USA). The membranes were configured AL-FS. NaCl 1 M and milli-Q was used as a DS and FS. The membrane performance tests were performed over 2 hours. The permeate water flux (J_w) was calculated by the weight change of the DS, which were automatically recorded every 10 seconds, using the Eq. (5.1). Except the test of chlorine concentration effect, in which the performance changed during 2-hour test were observed, only the permeate mass of second hour was removed from the calculation of the average permeate water flux of the membranes for comparison among virgin and chlorinated membranes. At least two membrane coupons were tested for repeatability of each experiment.

$$J_w = \frac{\Delta \text{ weight}}{\text{water density} \times \text{effective membrane area} \times \Delta \text{ time}} \qquad (Lm^{-2}h^{-1}) \tag{5.1}$$

The concentration of NaCl in the feed solution was also determined during 2-hour experiment by a calibrated conductivity electrode (856 Conductivity module, Metrohm, Switzerland) connected with the computer. RSF (J_s) was defined as the mole number of NaCl diffusing from the DS to the FS tank per time unit and membrane area unit as Eq. (5.2).

$$J_{srd\text{-}NaCl} = \frac{\text{mole of NaCl}}{\Delta\text{time x effective membrane area}} \qquad \left(mol.h^{-1}m^{-2}\right)$$

(5.2)

5.1.4 Characterization of membrane properties

Chemical structure changes of the membranes were detected by using Attenuated Total Reflectance - Fourier Transform InfraRed (ATR-FTIR) spectrometer (Nicolet 6700, Thermo Scientific, USA) with a Germanium crystal window. The OMNIC 8.1 software was used to control measurement. ATR-FTIR spectra were collected from 32 scans after background subtraction in the range of wave number from 600 cm^{-1} to 4,000 cm^{-1} with 4 cm^{-1} resolution.

Atomic percentages and high-resolution X-ray spectra of the elements on the membrane active layer were measured by using an X-ray Photoelectron Spectroscope (XPS) (K Alpha, Thermo Scientific, USA) with 5 ~ 10 nm penetration depth of X-ray beam into the membrane active layer.

Zeta potential of the membrane surface was measured by Surpass equipment (Anton Paar, Austria). The zeta potential value was evaluated by Fairbrother and Mastin method from pH 4 to 10 with KCl 1 mM electrolyte solution. The wet membrane sample was mounted on a 10 mm × 20 mm adjustable gap cell by adhesive tape. Zeta potential data were firstly determined from neutral pH to acidic pH value of electrolyte and then washed and again from neutral pH to basic pH value.

Atom and fragments of the polymer before and after chlorination were detected by using Time-of-Flight Secondary Ion Mass Spectrometry (Tof-SIMS, TOF.SIM^5, ION-TOF GmbH, Germany) in negative charge mode with a Cesium ion (Cs^+) gun. Surface composition and depth profile were analyzed. Measurements were conducted under a condition of 2,000 Voltage. Working distance is 8.2 mm.

^{13}C and ^{1}H Nuclear Magnetic Resonance (NMR) spectra of the virgin and chlorinated membranes were analyzed by using 500 MHz Solid State NMR (Varian Unity INOVA, CA, USA). In both MAS NMR of ^{1}H and ^{13}C, samples were spun at 20 kHz, 5 seconds of the delay time, and 4 μs for π/2 pulse. Samples were placed in a 3.2 mm Chemagnetics MAS Probehead for measurement. Data were calibrated as 0 ppm with ^{1}H and ^{13}C in the tetramethylsilance (TMS). ^{13}C NMR was operated at 125.7 MHz of frequency and 18,000 scans each increment while those of ^{1}H NMR are 499.8983 MHz of frequency and 40,000 scans.

Membranes used for ATR-FTIR, XPS, ToF-SIMS and solid-state NMR were freeze-dried for at least 40 hours in a vacuum freeze dryer (Biocryos, Korea); whereas, wet membranes were used for zeta potential measurements.

5.2 Results and discussion

5.2.1 Chlorination mechanism of the integrally asymmetric CTA-based FO membranes

5.2.1.1 Chlorination of the integrally asymmetric CTA-based FO membranes at various chlorine exposed time

The mechanism of chlorination of the integrally asymmetric CTA-based FO membranes was studied with chlorination of the labmade membrane under various exposure time to hypochlorite solutions at pH 4. Upon increasing exposure time from 1, 10 to 20 hours contacting with 2,000 ppm chlorine solution at pH 4, the chlorine dosages increased from 2,000, 20,000 to 40,000 ppm.h. XPS data in Fig. 5.1 shows the atomic content of chlorine binding on membrane surfaces increased with the increase of exposure time. As shown in this figure, chlorine content rapidly increased in the initial gap of the graph and gradually reached to constant content after 1-hour exposure. This result indicated that chlorine quickly bound on the membrane at the preliminary time, then slowly deposited continuously.

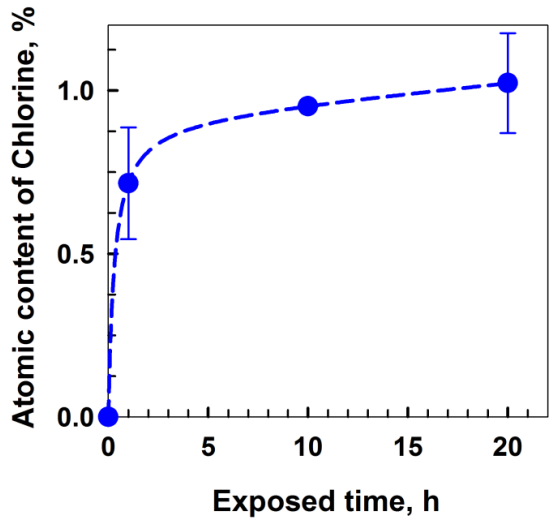

Figure 5.1 *Atomic content of chlorine in the virgin and chlorinated CTA-based labmade membranes upon exposure time to the 2,000 ppm chlorine solutions at pH 4*

Corresponding to the increase of chlorine content on membranes in Fig. 5.1, the membrane performances of the labmade membrane declined more severely. The normalized J_w and J_s of the membranes upon increasing exposure time to the chlorine were shown in Fig. 5.2. The water flux increased little (0.4, 8.5 and 18.5% after 1, 10, 20-hour exposure time, respectively) but the RSF increased incredibly (12, 96 and 576% after 1, 10 and 20-hour exposure time, respectively). The dramatic decreasing salt resistance of this CTA-based FO membrane is consistent with elsewhere

study on cellulose acetate (CA) RO membranes under various immersed time in chlorine, in which the longer immersed time was carried out, the lower salt rejection absented due to cut-off of polymer chain to smaller molecular weight by chlorine, i.e. the chlorinated CA RO membrane by 1,000 ppm Cl at pH 7 showed similar salt rejection with the virgin membrane (about 99%) after 7 hours but 98% after 24 hours and 68% after 48 hours of immersion [112]. In the present work, the membrane performance of the labmade membrane slightly changed at 20,000 ppm.h (2,000 ppm chlorine for 10-hour exposure time) and dramatically changed at 40,000 ppm.h (2,000 ppm chlorine for 20-hour exposure time) of chlorine dosage at pH 4. Increase of both J_w and J_s of the labmade in Fig. 5.2 were attributed to be a result of damage of polymer chain due to chlorine as mentioned in the CA RO membrane above, and chlorination mechanism of the TCA-based will be discussed later with data of zeta potential, high resolution XPS, ToF-SIMS, NMR and more FO tests.

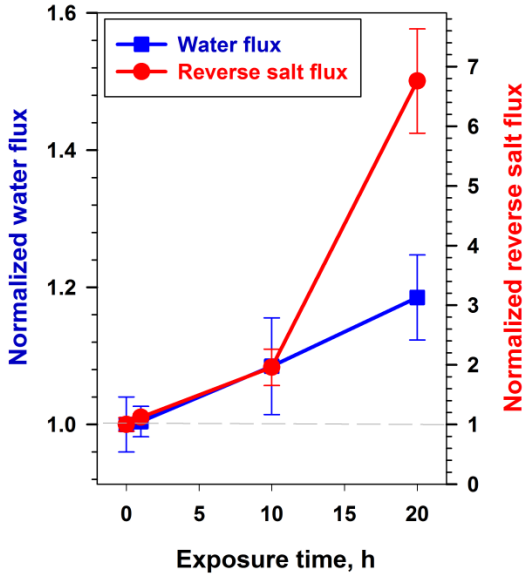

Figure 5.2 *Normalized J_w and J_s of the chlorinated CTA-based labmade membranes upon exposure time to the 2,000 ppm chlorine solution at pH 4. The membrane performances were normalized by the 1 hour average data after 1 hour conditioning of the virgin membrane*

Figure 5.3 shows more negative charge of the chlorinated CTA-based labmade membranes soaked longer in 2,000 ppm chlorine solution at pH 4. The increase of both J_w and J_s in Fig. 5.2 suggested an enlargement of pore size of the membranes after chlorination. This enlargement has been similarly studied elsewhere in which an ultrafiltration CA membrane was enlarged pore size resulting in more negative streaming potential of the membrane after being cleaned with hypochlorite [58]. Thus, the increase of negative charge of the chlorinated CTA-based labmade membranes upon the increase of exposure time in Fig. 5.3 confirmed the hypothesis of the enlargement of membrane pore

size as the result of the effect of hypochlorite. On the other hand, hypotheses of chlorination pathway has suggested the formation of carboxylic end-group in the CTA or CA-based membranes after chlorination [57, 58], which is supposed to dissociate as the following reaction resulting in negative charge of the membrane.

$R\text{-}COOH = R\text{-}COO^- + H^+$ [113].

Hence, the CTA-based labmade membranes were likely more negative charged due to formation of carboxylic end-group after chlorination.

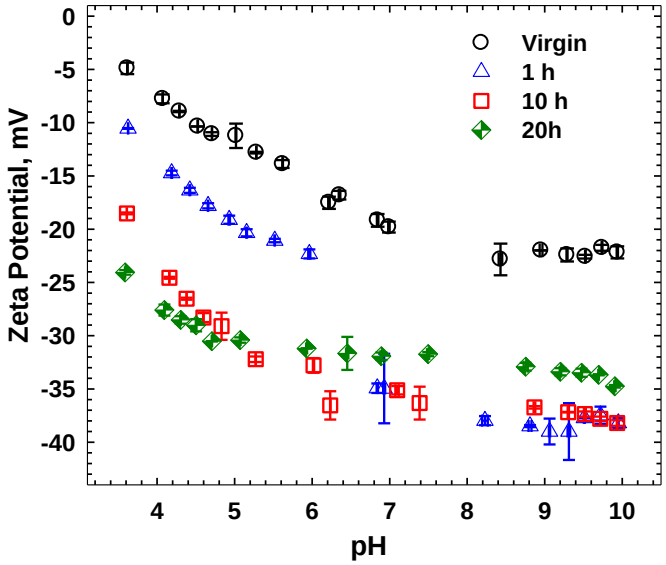

Figure 5.3 *Zeta potential of the virgin and chlorinated CTA-based labmade FO membranes at various exposure times to the 2,000 ppm chlorine solutions at pH 4*

The high resolution XPS of peak C1s, O1s and Cl2p were shown Fig. 5.4. The C1s and O1s peaks of chlorinated samples were less intensity than the virgin sample, and specially, their binding energies shifted to the lower energy regions. Those lower binding energies inferred that interaction of C bond and O bond in the polymer molecules were weakened, which requires low energy to break those bonds by the X-ray beam during XPS measurement. This weakness of binding energy got along with the increase of exposure time in chlorine solution. Therefore, chlorine likely affected on the C and O bonds in the CTA/CA polymer.

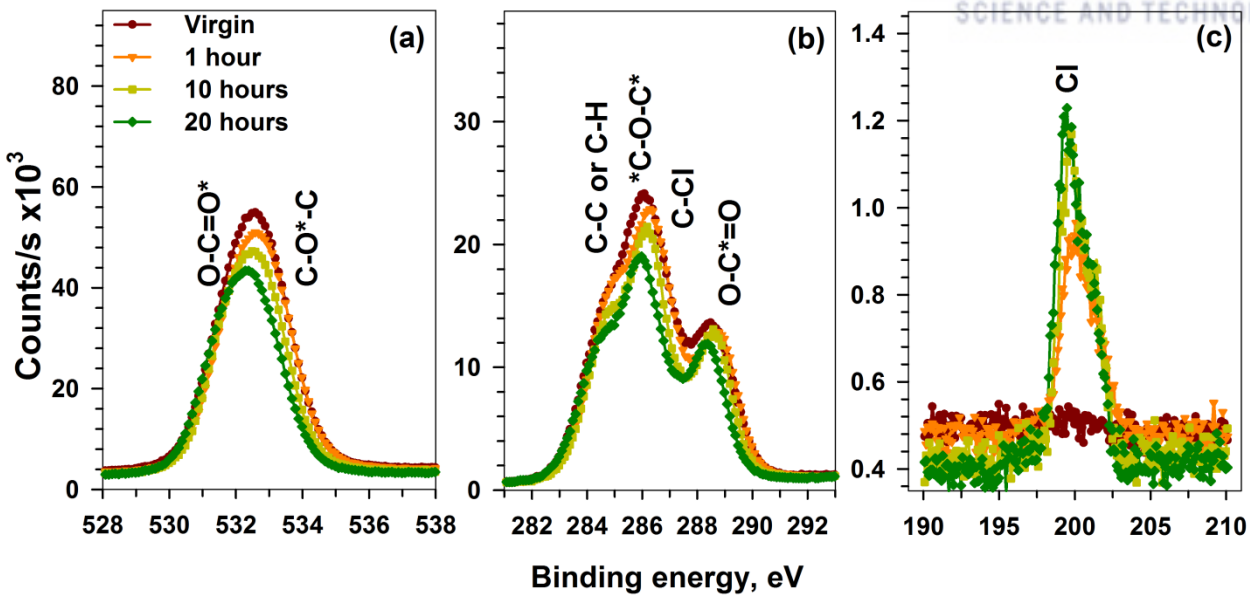

Figure 5.4 *XPS high resolution of O1s (a), C1s (b) and Cl2p (c) of the virgin and chlorinated CA-based labmade membranes at various exposure time to the 2,000 ppm chlorine solutions at pH 4*

By deconvoluting XPS spectra of membranes with SPXPEAK 4.1 software and showing in Fig. 5.5, this study estimated how C bond and O bond changed when chlorine attacked the polymers. All sub-peaks of carbon arising from C-C bond at 284.9 eV, *C-O-C* at 286.4 eV, or O-C*=O at 288.6 eV shifted to the left region with lower binding energy. With the similar trend, sub-peaks O-C=O* at 531.7 eV and C-O*-C at 532.7 eV also shifted to lower binding energy. This resulted implied a less interaction between O and C in the chlorinated membranes. Whereas, the C-Cl sub-peak appeared at chlorinated samples indicated that chlorine was chemically bound to the polymer.

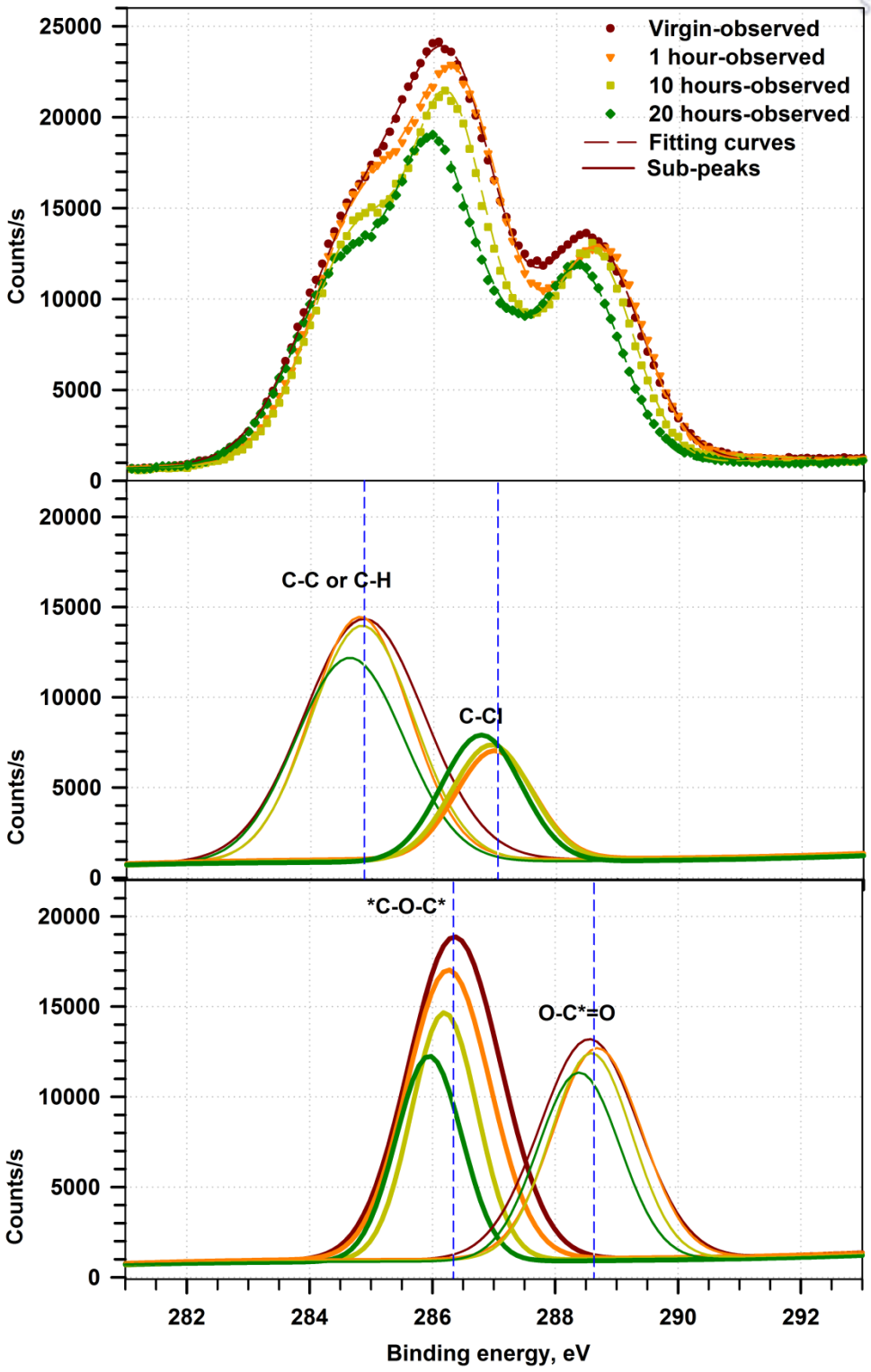

Figure 5.5 *Deconvoluted sub-peaks of C1s the virgin and chlorinated CA-based labmade membranes at various exposure time to the 2,000 ppm chlorine solutions at pH 4*

Three hypothetic mechanisms proposed for chlorination of CTA-based membrane and

schematized in Fig. 5.6 are (i) Cl reacted with acetyl/acetate group leading to break H-bonding, (ii) Cl reacted with CH_3 or acetate sites, and (iii) Cl reacted with pyranose ring. The pathway of chlorination of CA membrane has been proposed elsewhere to form carboxyl COOH, ketone C=O or aldehyde –CHO but still deficient proof of this reaction [57, 58]. This study employed ToF-SIMS measurement that could detect the elements and fragment species of the polymer after being treated with an ion beam in a strong electric field. The most affected by chlorine will be earliest fractured from the polymer structure. Therefore, fragment intensity confirms the reaction site order of CA-based membrane with chlorine.

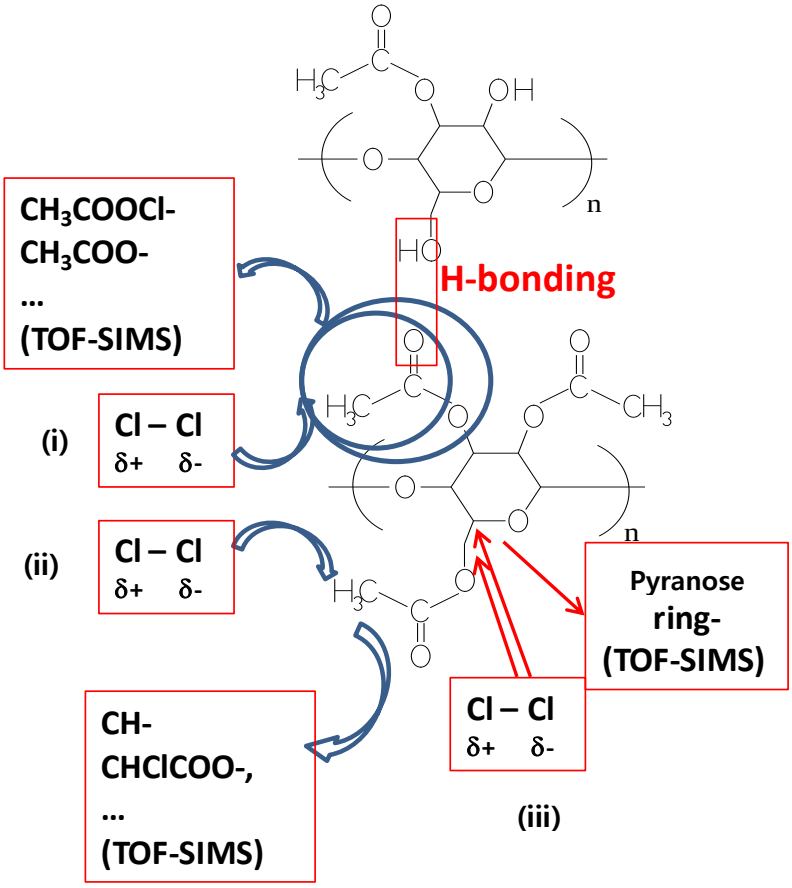

Figure 5.6 *Schematic proposal of possible reaction sites of chlorine with CTA/CA polymer*

Table 5.1 *Elements and fragments of the virgin and chlorinated CTA-based labmade FO membranes detected by ToF-SIMS*

(I)	Chlorinated species			
Cl-,	ClO_2-,	CO_2Cl-,	C_5H_8Cl-,	C_7H_8Cl-,

^{37}Cl-,	ClO_2H-,	ClO_3-,	C_4H_6OCl-,	$C_7H_8{}^{37}Cl$-,
ClO-,	Cl_2-,	CH_2Cl_2-,	C_5H_8OCl-,	$C_8H_{10}Cl$-,
^{37}ClO-,	HCl_2-,	C_3OCl-,	C_4H_6OCl-,	$C_6H_8O_2{}^{37}Cl$-,
$C_2{}^{37}Cl$-,	$Cl^{37}Cl$-,	C_3H_4OCl-,	C_6H_8Cl-,	$C_9H_{10}Cl$-,
C^2H_3Cl-,	C_2H_2OCl-,	C_2HO_2Cl-,	$C_6H_{10}Cl$-,	$C_{10}H_{12}O_2Cl$-,
COCl-,	C_3H_7Cl-,	$C_2H_3O_2Cl$-,	$C_4H_2O_2{}^{37}Cl$-,	$C_9H_{24}O_6Cl$-,
CHOCl-,	C_2H_3OCl-,	$C_2H_2O_2{}^{37}Cl$-,	$C_4H_8O_2Cl$-,	$C_{22}H_{46}O_8Cl$-.
CH_3OCl-,				

(II) Hydrocarbon species (C ≤ 2, most from acetate group)

H-,	C_2-,	OOH-,	CO_2-,	C_2H_4OO-,
C-,	CCH-,	C_2O-,	CHO_2-,	C_2HO_3-,
CH-,	C_2H_3-,	C_2HO-,	CHCOO-,	$C_2H_3O_3$-,
O-,	CH_3O-,	C_2H_2O-,	CH_2COO-,	C_2HO_4-,
OH-,	O_2-,	C_2H_3O-,	CH_3COO-,	CHO_5-

(III) Hydrocarbon species (C ≥ 3, originate pyranose ring)

C_3O-,	C_3HO_2-,	C_3HO_3-,	$C_6H_5O_2$-,	$C_4H_{11}O_6$-,
C_3-,	C_3H_2OO-,	$C_3H_4O_3$-,	$C_6H_6O_2$-,	$C_7H_9O_4$-,
C_3H_2-,	C_3H_3OO-,	$C_5H_3O_2$-,	$C_6H_7O_2$-,	$C_9H_9O_3$-,
C_3H_3-,	C_3H_4OO-,	$C_5H_5O_2$-,	$C_5H_5O_3$-,	$C_8H_{11}O_4$-,
C_3H_3O-,	C_3H_5OO-,	$C_5H_6O_2$-,	$C_5H_7O_3$-,	$C_9H_{11}O_4$-,
C_3H_5O-,	C_3H_7O2-,	$C_5H_8O_2$-,	$C_6H_5O_3$-,	$C_9H_{13}O_5$-,
C_3H_6O-,	C_5H_2O-,	$C_4H_5O_3$-,	$C_7H_9O_3$-,	$C_{17}H_{21}O_5$-.
C_4HO-,	C_5H_3O-,	$C_6H_3O_2$-,	$C_7H_{11}O_3$-,	
C_4H_3O-,	C_5H_7O-,	$C_6H_4O_2$-,		

Table 5.1 shows the detection of elements and fragments from polymers by ToF-SIMS. The more elements and fragments are detected, the weaker chemical bonds of polymers are. Apparently, this table exhibited the presence of chlorine-contain species in the structure of CTA-based labmade membrane after being exposed to the 2,000 ppm chlorine solution at pH 4. Fragments from ToF-SIMS were categorized into three groups, i.e., (I) chlorinated species, (II) hydrocarbon species C ≤ 2 (C number in the fragments not higher than 2, which are most from the acetate group), and (III)

hydrocarbon species C ≥ 3 (C number in the fragments not less than 3, which arise from the pyranose ring).

The total area of each species group above was normalized by the total area of these species obtained from the virgin membrane and shown in Table 5.2. Normalized areas of the group (I) increased with the increase of exposure time from 0 hour (virgin membrane) to 20 hours, indicating more effect of chlorine on the CTA-based membrane upon exposure time to chlorine solution at pH 4. At 1-hour exposure, hydrocarbon species of the group (II) (C ≤ 2 is 3.790) were detected more than sample 1-hour exposure of the group (III). This implied that chlorine firstly favored to react with acetate groups than pyranose groups. Then, the area of species C ≤ 2 decreased in 10 or 20-hour exposure while species C ≥ 3 tend to increased and reached the highest values at 20-hour exposure. The slope of species group (II) trended downward whereas the slope of species group (III) trended upward (Fig. 5.7). Thus, the hydrocarbon species C ≤ 2 of sample 10 and 20-hour exposure were less released because chlorine was likely binding to the pyranose ring at longer exposure time, and hydrocarbon species C ≥ 3 of sample 20-hour exposure were the most released (C ≥ 3 is 3.574) implied the reaction of chlorine with pyranose group increased with exposure time to the chlorine solution at pH 4. Normalized area of chlorinated species (group (i)) increased upon exposure time and consistent with the increase of Cl atomic percentage in XPS measurement (Fig. 5.1). The high correlation coefficient between Tof-SIMS and XPS data (0.922) in the Fig. 5.7 confirmed the confidence of these two measurements and strongly proved the hypothesis of chlorination mechanism of the CTA-based FO membranes.

Table 5.2 *Normalized area of fragments detected by ToF-SIMS of the virgin and chlorinated CTA-based labmade membranes upon various exposure time to the 2,000 ppm chlorine solution at pH 4*

Exposed time h	**XPS**	**TOF-SIMS**		
	Cl%	**Normalized area of chlorinated species**	**Normalized area of hydrocarbon species C ≤ 2**	**Normalized area of hydrocarbon species C ≥ 3**
0	0.000	1	1	1
1	0.716	9.184	3.790	2.686
10	0.952	21.609	2.843	2.546
20	1.023	26.717	3.052	3.574

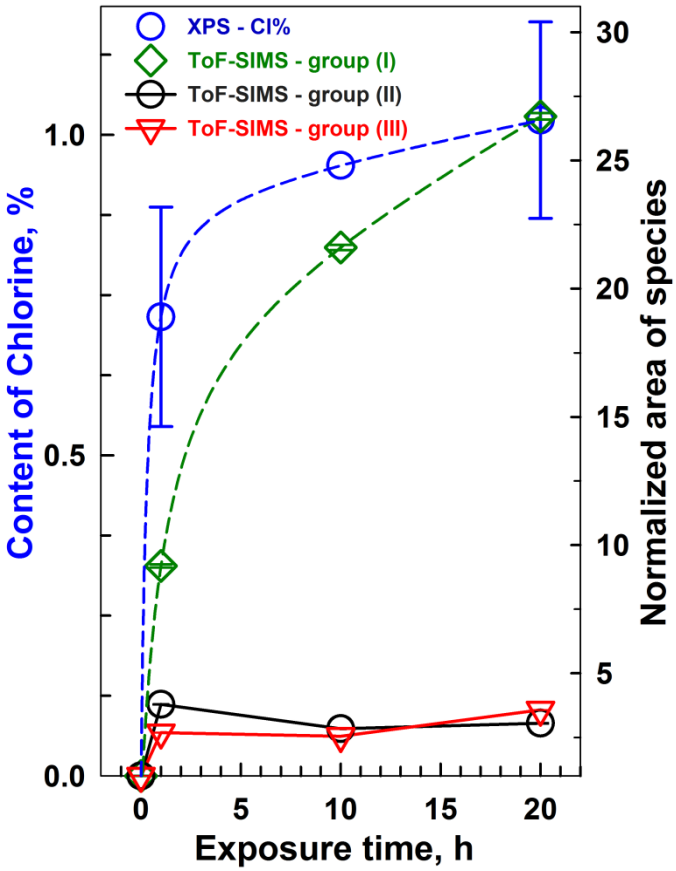

Figure 5.7 *Correlation of XPS data and ToF-SIMS data of the CTA-based labmade membranse upon various exposure times to the 2,000 ppm chlorine solutions at pH 4*

ToF-SIMS depth profiles of the virgin and chlorinated labmade membranes at various exposure times to the 2,000 ppm chlorine solutions at pH 4 were shown in Fig. 5.8. Being consistent with the XPS data and surface composition ToF-SIMS data, the intensity of Chlorine species increased upon increase of exposure time to chlorine solutions at pH 4. As hypothesized above, the chlorine reacted with the CTA/CA polymer of the membrane, weakened C-C or C-O bond resulting in high intensity of detected C and O-contain species of the membranes in depth profile ToF-SIMS measurement upon exposure time to chlorine solutions. Particularly, after 20-hour exposure, the membrane structure was likely damaged pronouncedly. As hypothesized in Table 5.2, after 20-hour exposure, the chlorine reacted with the pyranose ring. The collapse of pyranose structure might cause the noise of C and O depth profiles in Fig. 5.8. Moreover, as proposed in an elsewhere study, the CA was oxidized by chlorine and ultimately released CO_2 after pyranose opened [57]. This reduction of glucopyranose ring accounted for decrease intensity of C and O-contain species in ToF-SIMS measurement at 20-hour soaking compared to 1 or 10-hour soaking (Fig. 5.8d).

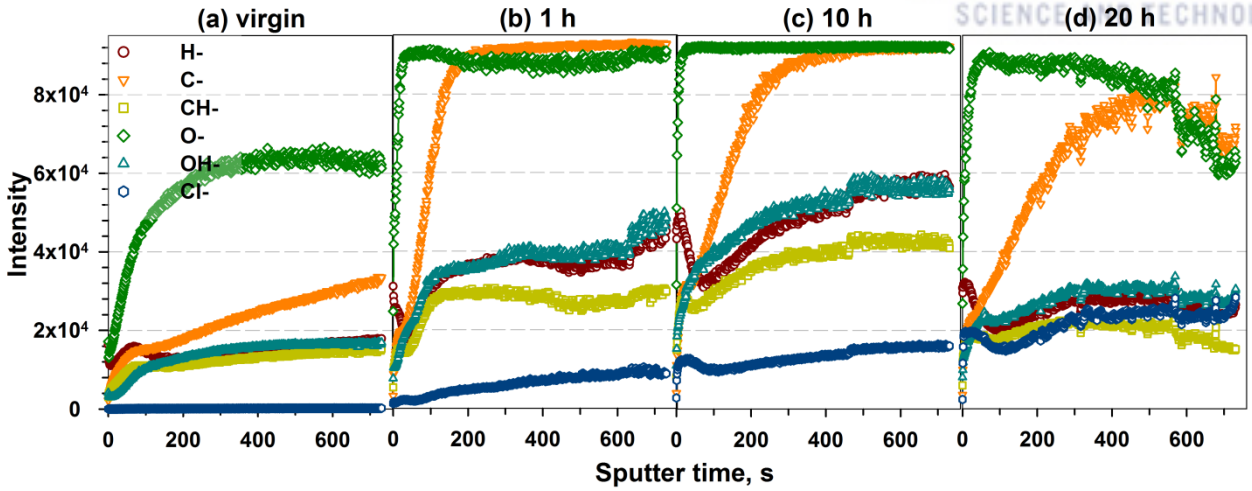

Figure 5.8 *ToF-SIMS depth profiles of elements and fragments of the virgin and chlorinated CTA-based labmade FO membranes upon various exposure time to the 2,000 ppm chlorine solutions at pH 4*

Solid-state NMR measurement with ^{13}C and ^{1}H of the virgin and chlorinated CA-based labmade FO membranes are shown in Fig. 5.9. The intensity of ^{13}C and ^{1}H of 1 and 10-hour soaking membranes increased compared to those of virgin one. However, the 20-hour soaking membrane showed the decrease of intensity. This decrease was consistent with the ToF-SIMS depth profile data to support the hypothesis that glucopyranose rings were oxidized and reduced after pyranose opened at 40,000 ppm.h (2,000 ppm for 20 hours). Figure 5.9 also exhibits that the ^{13}C chemical shift exhibited insignificantly change of C1, 2, 3, 4, 5 and 6 of glucopyranoside around 104, 73, 73, 72, 76 and 71 ppm [114-117]. The aliphatic C and acetyl (CH_3 and C=O) of the chlorinated samples slightly shifted to the upfield electric with low frequency and low concentration. ^{1}H of acetyl shows more clearly the chemical shift of the chlorinated samples to the upfield. After exposure to the chlorine solutions, chlorine reacted with the acetyl/acetate group resulting in breaking H-bond. The mobility of ^{1}H in acetyl end-group became strongly and showed the lower frequency in NMR spectra.

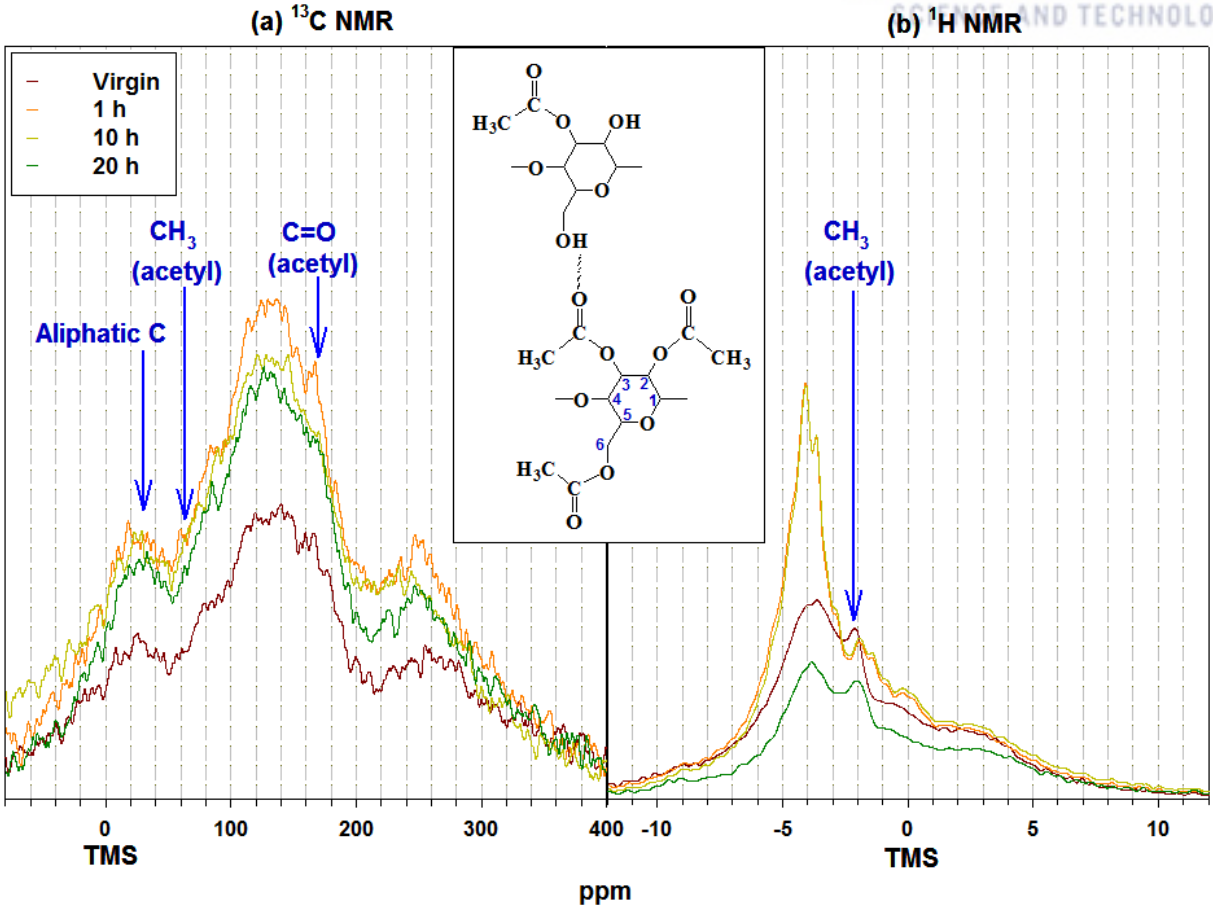

Figure 5.9 *^{13}C NMR (a) and ^{1}H (b) spectra of the virgin and chlorinated CTA-based labmade FO membranes to the 2,000 ppm chlorine solutions at pH 4*

5.2.2 Effect of chlorine concentration on CTA-based membrane

The CTA-based labmade FO membranes were tested with singular soaking tests in various chlorine concentrations and with a stepwise increase of chlorine concentration soaking tets. In the singular soaking test, the membranes were exposed to various chlorine concentrations 2,000, 5,000, 10,000, 15,000 and 17,000 ppm at pH 4 for 10 hours. Chlorine dosage in term of ppm.h is a combination effect of chlorine concentration and contacting time. The performance behaviors of chlorinated membranes were compared with the virgin one in Fig. 5.10a. In the stepwise increase of chlorine concentration, the membrane was first soaked in the lowest chlorine concentration of 2,000 ppm, afterward, tested in FO, and soaked in another higher chlorine concentration solution – 5,000 ppm, then tested again and repeated with 10,000 ppm. The performance behaviors of the successional soaking tests were shown in the Fig. 5.10b. After soaking in 2,000 ppm chlorine or 20,000 ppm.h chlorine for 10 hours, the water flux and RSF insignificantly increased. The water flux and RSF of the membranes increased about 10% and 7 times, respectively, in the singular test with 50,000 ppm.h

chlorine (5,000 ppm for 10 hours), and 50% and 10 times, respectively, in the stepwise test with 70,000 ppm.h chlorine (2,000 ppm for 10 hours and 5,000 ppm for another 10 hours). After chlorination, the labmade membrane increased water flux and RSF in all cases; however, in the singular test, the J_w and J_s slowly increased upon increase of chlorine dosage than the stepwise test. It interestingly notes that during 2-hour FO tests, the RSF increased in all cases; the water flux of singular tests started decreasing at high chlorine concentration of 150,000 ppm.h while this decrease of water flux could be observed from 70,000 ppm.h chlorine in the stepwise tests. This comparison suggests the hypothesis that the chlorinated membrane was more damaged during FO test, which accounts for the worse performance of the chlorinated membrane in stepwise test than singular test with low water flux and really high RSF at 170,000 ppm.h chlorine.

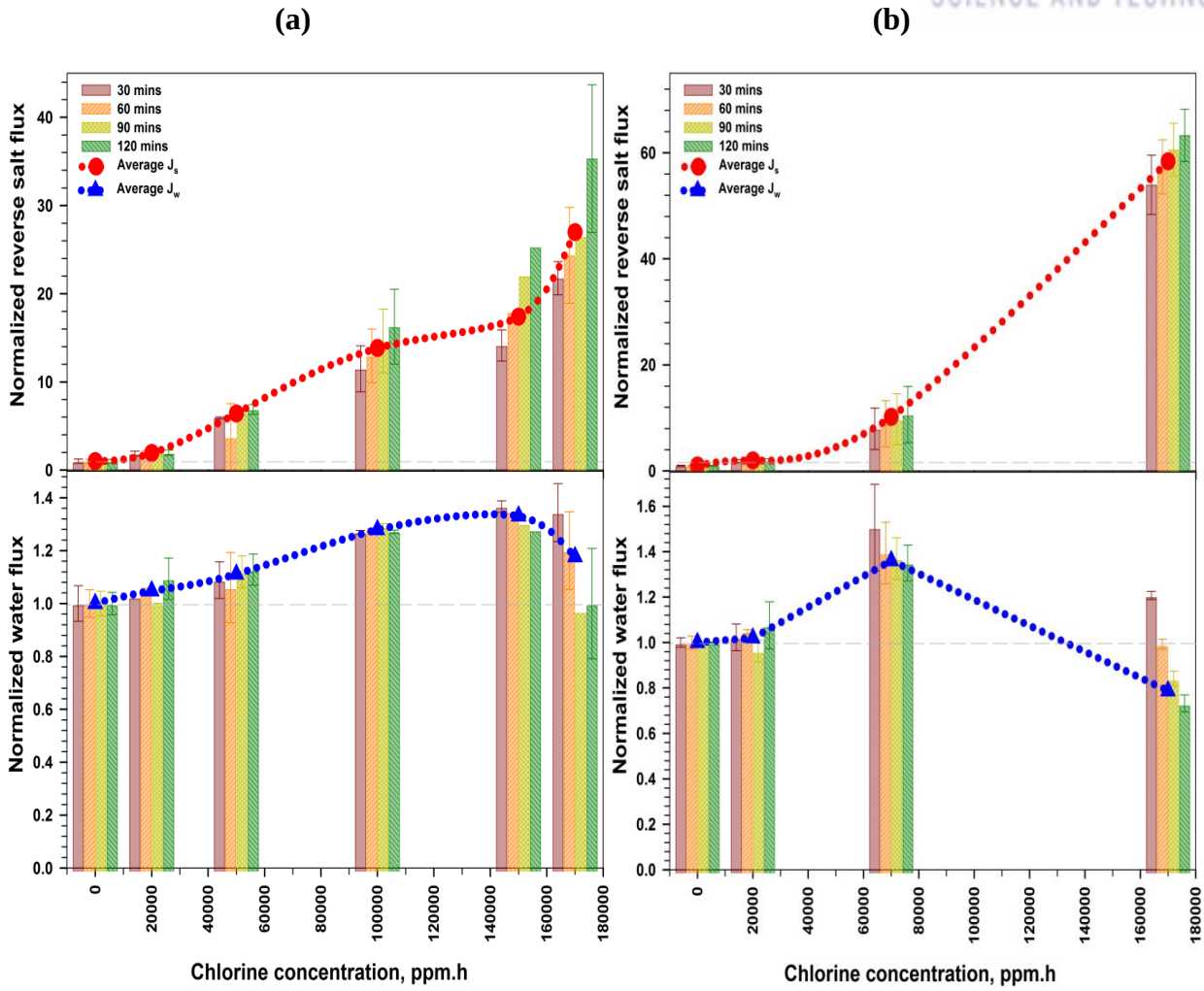

Figure 5.10 *Normalized performances of the labmade membranes in singular soaking tests in various chlorine concentrations at pH 4 (a) and in stepwise increase of chlorine concentration soaking tests at pH 4 (b). Operating conditions: NaCl 1M as DS, milli-Q as FS; 25°C 1.0 LPM; and active layer faces to FS*

5.2.3 Effect of pH of chlorine on chlorination of CTA-based membrane

Chlorination tests were conducted in acidic and alkaline pH based on a theory of chlorine speciation corresponding to pH of the solution. When the pH increases from 4 to 10, hypochlorous acid (HOCl) species decreases and hypochlorite ion (OCl^-) increase to become the dominant species (Fig. 5.11). The HOCl species have been known to be more oxidative compared with OCl^-, which have more oxidation of PA-based membrane at low pH. However, chlorine has been known to maximize oxidation of cellulose at pH 7 [118]. The effect of pH of chlorine solution on membrane performance after chlorination with 2,000 ppm at pH 4, 7 or 10 for 1 or 10-hour soaking was shown in Fig. 5.12. The water flux and RSF of the labmade membrane dramatically increased at pH 7

compared to pH 4 and 10. Especially, at 20,000 ppm.h chlorine (2,000 ppm for 10 hours) at pH 7, RSF of the labmade membrane increased almost 35 times.

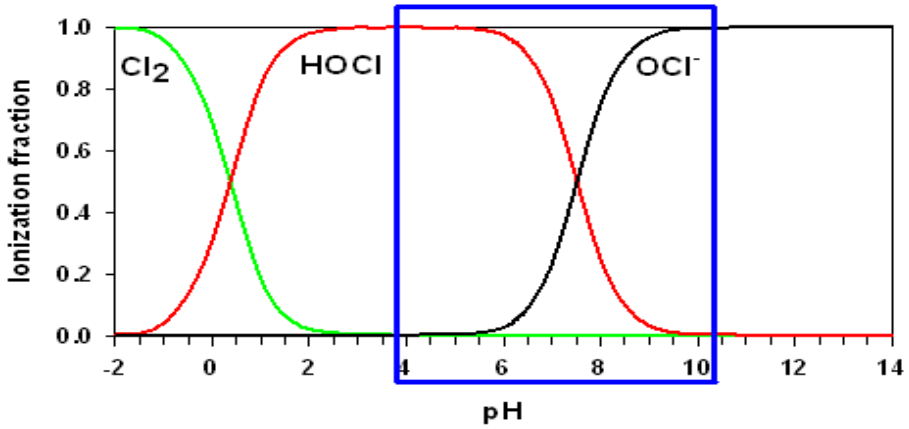

Figure 5.11. *Distribution diagram for chlorine species, 25℃, [Cl⁻] = $10^{-1.55}$ M (2,000 ppm), $C_{T,Cl}$ = [Cl_2] + [HOCl] + [OCl^-]*

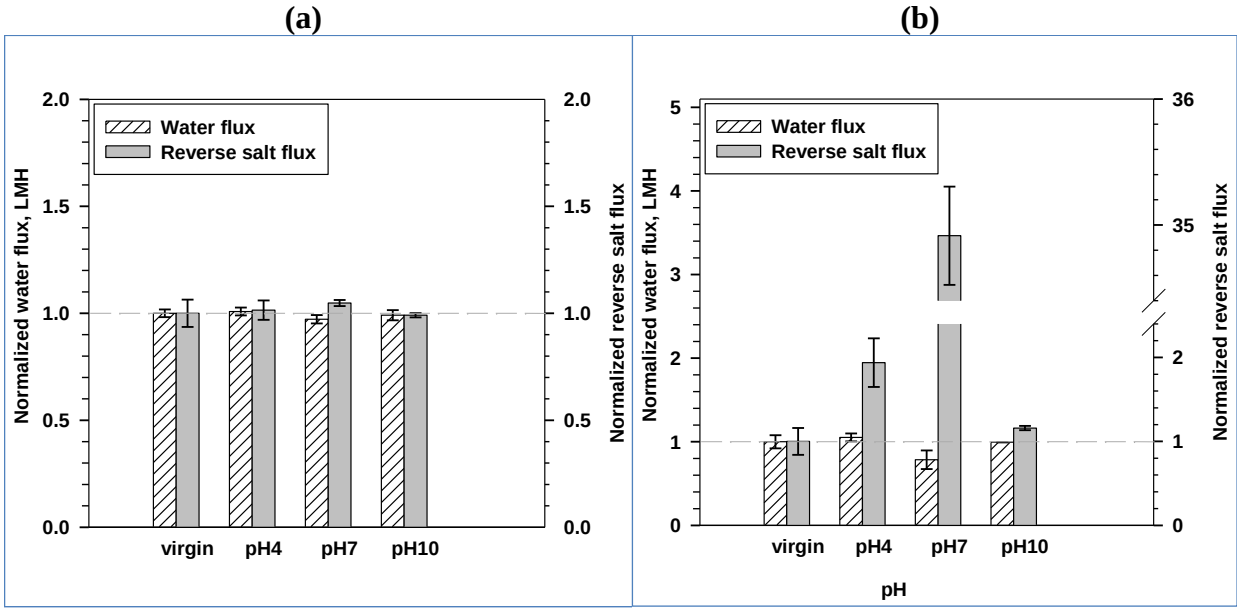

Figure 5.12. *Normalized performances of the labmade membranes with various pH values of the 2,000 ppm chlorine solutions with (a) 1-hour soaking and (b) 10-hour soaking. Operating conditions: NaCl 1M as DS, milli-Q as FS; 25°C 1.0 LPM; and active layer faces to FS*

5.2.4 Chlorination of CTA-based and TFC FO membranes in comparison with various membrane types

All membranes were tested at acidic and alkaline conditions of 2,000 ppm chlorine solution. The

increase of pH causes not only a change of chlorine species but also more negative charge of membrane surface as shown in Fig. 5.3. More negative charge of OCl^- species repulsively interacted with the negative charge of membrane surface, which resulted in less degradation of membrane due to chlorination at alkaline condition [59, 60]. This determination of chlorine speciation was consistent with XPS data in Table 5.3. The atomic contents of chlorine in both CTA/CA-based labmade and PA-based HTI3 membrane soaked in 2,000 ppm chlorine at pH 4 were approximately 2.7 and 3.5 times, respectively, higher than those at pH 10.

Table 5.3 *Compare XPS atomic percentage of chlorine in the CTA-based labmade and PA-based HTI3 membranes exposed to the 2,000 ppm chlorine solutions at pH 4 for 10 hours*

pH	Cl atomic percentage, %	
	Labmade	**HTI3**
pH4	0.95	14.99
pH10	0.35	4.24

Chlorination of the CTA-based (including labmade, HTI1 and HTI2) and TFC FO (HTI3) membranes were compared with the chlorination of m-phenylene diamine (MPD) PA-based membranes (NF90 and BW30) and piperazine PA-polyamide membrane (NF270) by soaking test in 2,000 ppm chlorine for 10 hours at pH 4 or pH 10. Chemical changes in ATR-FTIR spectra and performance changes in FO tests of these membranes were shown in Fig. 5.13 and Fig. 5.14, respectively. At both acidic and alkaline conditions, the spectra of CTA-based and piperazine PA-based membranes changed insignificantly. On the contrary, the deterioration of Amide II peak at ~1545 cm^{-1} and shifting of Amide I peak at ~1660 cm^{-1} of MPD PA-based membrane – HTI3, BW30 and NF90 – implied a deterioration of these membranes by chlorine. The change of spectra of these PA-based membranes at pH 4 (Fig. 5.13a) were more pronounced than at pH 10 (Fig. 5.13b). The chlorination of MPD PA-based RO membrane has been intensively studied [59-67], and piperazine PA-based membrane is tertiary amide that has an absence of amidic hydrogen and has been supposed to enhance chlorine tolerance of membranes [67].

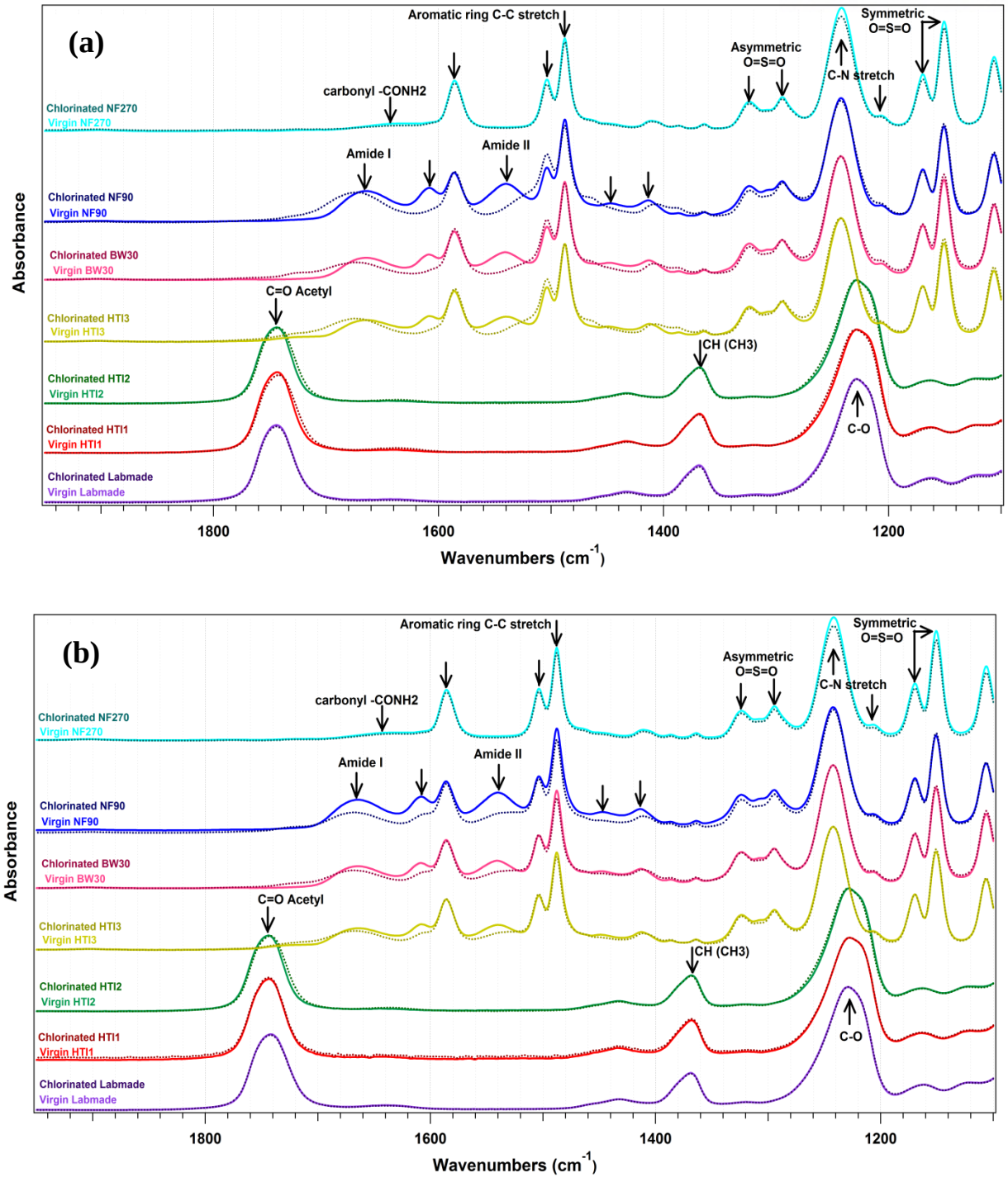

Figure 5.13 *ATR-FTIR spectra of various membranes before and after chlorination by 2,000 ppm chlorine solutions for 10 hours at pH 4 (a) and pH 10 (b)*

The water flux of all CTA-based membranes – HTI1, HTI2 and labmade – insignificantly changed after chlorinated at 2,000 ppm chlorine at pH 4 or pH 10 for 10-hour soaking. Meanwhile, the both types of MPD PA-based FO and RO membranes showed lower water flux after chlorinated at

pH 4 and higher flux at pH 10 compared with their virgin membranes. On the contrary, the piperazine PA-based membrane show increase water flux of both acidic and alkaline pH condition of chlorine solutions. The less increase of water flux of the CTA-based membranes could be explained by the higher chlorine resistance than the PA-based membranes. As shown in the Fig. 5.2 and 5.10, the membrane performance significantly changed from 40,000 ppm.h chlorine (2,000 ppm for 10-hour soaking). Table 5.3 clearly shows extremely higher chlorine bound in the PA-based HTI3 (14.99% at pH 4 and 4.24% at pH 10) compared with the CTA-based labmade membrane (0.95% at pH 4 and 0.35% at pH 10) when the membranes were soaked in 2,000 ppm chlorine for 10 hours. At pH 4, the polyamide was more adversely damaged by chlorine than other pH values. The H bonds of polymers chain might be fractured, then easily compacted and narrower the membrane pore size, resulting in the decrease of water flux and the increase of salt resistance (Fig. 5.13a). At pH 10, the PA-based membrane has negatively charged and swollen, creating more water pathway; therefore, increase water flux. Besides, the repulsive interaction of negatively charged PA-based membranes accounted for the high salt resistance in Fig. 5.14. Comparing with the commercial CTA-based membranes, the commercial PA-based membrane yielded worse performance after soaking in chlorine solution at acidic pH. Especially, low salt resistance was observed for commercial TFC HTI3 membrane after chlorinated at pH 4. This loss of selectivity of HTI3 might be due to the deterioration of coating layer that was introduced in the previous study [40]. The MPD PA-based membranes have been shown as high-water-flux and high salt resistance membranes in FO due to their thin thickness and high selective PA layer [40]. According to the current study, the MPD PA-based membranes need enhancing chlorine tolerance for FO application. Such a tertiary amide of piperazine PA-based like NF270 membrane seems to be a potential membrane for FO with high water flux and chlorine tolerance if it is prepared extremely thin on a thin and highly porous substrate like HTI3 membrane.

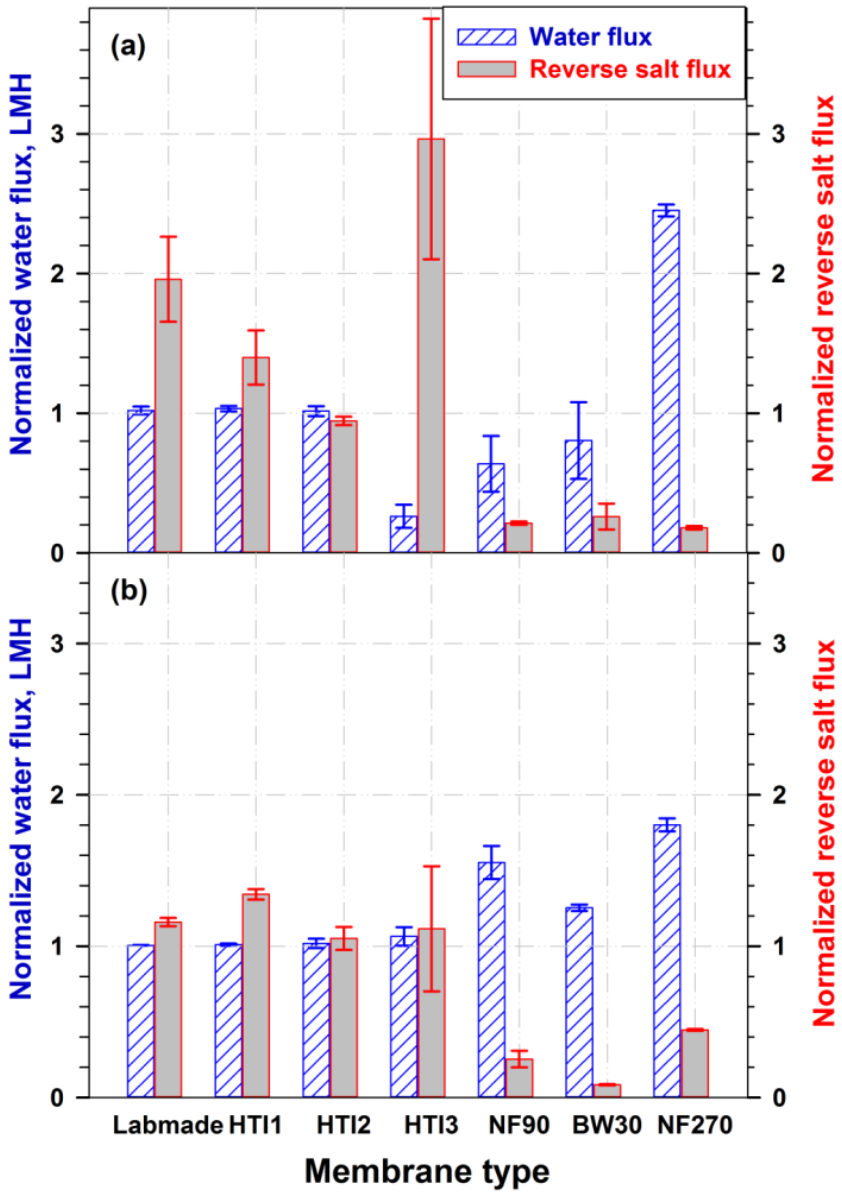

Figure 5.14 *Performance of various membranes before and after chlorination by 2,000 ppm chlorine for 10 hours at pH4 (a) and pH10 (b)*

5.3 Conclusion

This study studied on mechanism of the chlorination of CTA-based membrane in FO, also compared chlorination of CTA-based and TFC PA-based FO and RO membranes. Chlorination of integrally asymmetric CTA-based and TFC PA-based membranes was studied by investigating changes of membrane properties and performance after being soaked in chlorine solutions. Longer exposure time to chlorine or higher chlorine concentration caused more damaged CTA/CA-based membranes by chlorination resulting in increasing water flux and RSF of the membrane in FO. XPS and ToF-SIMS data confirmed chemically bound of

chlorine to the CTA-based membranes. ToF-SIMS data suggested that chlorine initially reacted with acetyl/acetate site of CTA/CA causing less H-bond in the polymer, which can be also seen in ^{1}H NMR spectra, then reacted with pyranose ring. After long exposure time or high chlorine dosage, from 40,000 ppm.h, the chlorine attack opened the pyranose rings, ultimately cleaved polymer chains, resulting in the decrease of C and O-contain fragment intensities in ToF-SIMS depth profiles and dramatically loss of salt resistance. Especially, the water flux of the CTA-based membrane was decreased lower than the virgin membrane at high chlorine concentration above 150,000 ppm.h at pH 4, and the membrane performance declined more adversely along filtration time. This performance failure was supposed to be as a result of a deterioration of the membrane at high chlorine dosage, at which the collapsed polymer structure reduced water channel but cleaved polymer chains keep losing salt resistance. The results also revealed that the CTA-based membrane was maximized oxidation by chlorine at pH 7.

Chlorination of PA-based membranes was more severe than that of the CTA-based membranes. Both membrane types were less affected by chlorine at alkaline pH than acidic pH. However, the water flux of the chlorinated CTA-based membranes changed insignificantly compared with the virgin one in both cased of pH conditions while the chlorine depressed the water flux of the MPD PA-based membranes at pH 4 but enhanced the water flux at pH 10. The piperazine PA-based membrane showed enhance of water flux and salt resistance after being soaking in chlorine solution at either pH 4 or 10. The TFC MPD PA-based membranes have currently been considered for FO with high water flux but need enhancing chlorine resistance according to this study. A TFC piperazine PA-based membrane prepared as the HTI3-like structure is expected to yield high performance in FO.

VI. CONCLUSIONS

With huge demand of application of osmotically-driven separation process in water/wastewater treatment, desalination and energy production, developing the desirable membrane for this process has been an emergent mission. This study contributed to the understanding the membrane structure of the desirable membranes for application of osmotically-driven separation process. Some conclusions were addressed regarding this contribution as following details.

The integrally asymmetric membranes, which were fabricated with CTA-based polymer on either a woven fabric or nonwoven fabric, were denser and smoother, causing lower water flux compared to the polyamide TFC membranes. However, the smoothness of the membranes conferred lower fouling propensity. The TFC membranes showed superior performance than the integrally asymmetric membranes under various test conditions, while the difference in performance between the two types of membranes became more pronounced during operation under alkaline conditions due to repulsive interactions within the negatively charged membrane and with solute anions.

In order to amplify the advantage of the integrally asymmetric membrane in terms of high resistance to fouling and chlorination, the CTA/CA-based forward osmosis membranes were successfully prepared by immersion precipitation using different casting compositions and preparation conditions, which were optimized to result in membranes with high water flux and low reverse salt flux. The optimized membrane was made by casting 6.3 wt.% CTA, 12.6 wt.% CA, 49.9 wt.% 1,4-dioxane, 17.2 wt.% acetone, 3.7 wt.% maleic acid, and 10.3 wt.% methanol to a thickness of 250 µm on a porous woven (WF1) support layer with subsequent evaporation for 30 seconds at 25 ^{o}C and annealing at 85 ^{o}C. The optimized membrane showed a more hydrophilic and smoother surface than the commercial integrally asymmetric FO membrane from HTI. Some suggestions were made for development of this integrally asymmetric membrane such as casting the membrane on the thin, porous (greather than 0.24 open space ratio) and post-treatment by heating in water not only allowed the release and removal of residual solvents and additives from the membranes but also improved performance of the membranes.

The polyamide-based TFC membranes have recently been considered for osmotically-driven separation process due to its advantage of high water flux. Study on the commercial TFC FO membrane revealed that the commercial TFC membrane (HTI3) from HTI still had low water flux compared to the TCK membranes from Toray Chemical Korea, but the RSF of HTI3 was very low. It is likely that the HTI3 was prepared from another monomer rather than trimesoyl chloride, or prepared with additives or a coating layer, which resulted in an increase of the O content in the polyamide layer, decrease of the negative charge, and improvement of fouling resistance. Meanwhile

the TCK-W membrane was still sensitive to fouling, yielding large decline of the water flux in desalination. That is one of the drawbacks of polyamide membranes, and challenges more study for improvement of the antifouling characteristic of polyamide membranes rather than CTA-based membranes. Some suggestions were made for desirable membranes for osmotically-driven separation process. Among the factors t_s, τ and ε, membrane thickness t_s was suggested to be the main factor contributing to low S values, associated with low concentration polarization effects and high water flux for FO membranes. The woven fabric type possesses more advantages than nonwoven fabric to obtain identical finger-like structures of the substrate, more fully cross-linked polyamide on the substrate, and narrower pore size. Thus, besides the requirement of a porous support layer for FO membranes, (i) ultra-thin substrate and small membrane thickness and (ii) woven type fabrics were important factors for the design of FO membranes. A preparation of FO membranes with both enhanced antifouling resistance and TCK membrane-like open and thin structure are required to develop FO membranes with desirable characteristics

Study on concentration polarization effect on performances of integrally asymmetric and TFC FO membranes revealed that when pure water was used as a FS, water flux in AL-DS was much higher than that in AL-FS due to the less dilutive ICP in the support layer of membranes; however, the presence of salts in FS depressed the water flux in AL-DS below the water flux in AL-FS due to severe effect of concentrative ECP. At the operation of membranes with higher initial water flux, the water flux depression was more obvious. When river water and seawater were used as FS and DS, respectively, the water flux of the membranes in AL-DS sharply declined and became lower than the water flux in AL-FS along short operation. AL-FS mode showed more stable and higher water flux; moreover, the membranes operated in AL-DS configuration were more easily fouled and showed lower water flux recovery after cleaning. This study suggests that the AL-FS configuration is preferable for application of PRO for optimal water flux and lower operating costs.

Although the application of both integrally asymmetric and TFC membranes in osmotically-driven separation process relies on the purpose such as considering fouling resistance or water flux, the effect of chlorination on both membranes need considering because chlorine is commonly used in pretreatment to control fouling as well as cleaning agent. Longer exposed time in chlorine caused more damaged CTA/CA-based membranes by chlorination, resulting in increasing water flux and RSF of the membranes in FO. ToF-SIMS data suggested that chlorine initially reacted with acetate site of CTA/CA causing less H-bonding in the polymer, then reacted with cellulosic ring. Ultimately, polymer chain was broken resulting in performance change at high chlorine concentration, approximately from 50,000 ppm.h. Chlorination upon chlorine concentration followed a similar trend with upon exposed time. However, the water flux was decreased lower than the virgin membrane as a result of a deterioration of the membrane at high concentration above 150,000 ppm.h, and the

membrane performance declined more adversely along filtration time. The CTA-based HTI membrane cast on nonwoven fabric (HTI2) showed slightly decline of water flux and RSF after chlorination while another type embedded (HTI1) or cast on woven fabric (labmade) showed significant increase of RSF. The woven-embedded polyamide FO membrane also showed profound effect by chlorine than other nonwoven-cast polyamide BW30 and NF90 membranes. The results also revealed that the CTA-based membrane was maximized oxidation by chlorine at pH 7. Chlorination of PA-based membranes was more severe than that of the CTA-based membranes. The TFC FO membrane was adversely affected by chlorine at acidic condition with about three-time increase of RSF and 70% reduction of water flux; however, its performance was insignificantly affected by alkaline chlorine solution. Both membrane types were less affected by chlorine at alkaline pH than acidic pH. However, the water flux of the chlorinated CTA-based membranes changed insignificantly compared with the virgin one in both cased of pH conditions while the chlorine depressed the water flux of the MPD PA-based membranes at pH 4 but enhanced the water flux at pH 10. The piperazine PA-based membrane showed enhance of water flux and salt resistance after being soaking in chlorine solution at either pH 4 or 10. The TFC MPD PA-based membranes have currently been considered for FO with high water flux but need enhancing chlorine resistance according to this study. A TFC piperazine PA-based membrane prepared as the HTI3-like structure is expected to yield high performance in FO.

REFERENCES

[1] W. W. O. (WWO), *http://www.theworldwater.org/water_facts.php*, 2010.

[2] J. O. Kessler and C. D. Moody, "Drinking water from sea water by forward osmosis," *Desalination,* vol. 18, pp. 297-306, 1976.

[3] W. L. Tang and H. Y. Ng, "Concentration of brine by forward osmosis: Performance and influence of membrane structure," *Desalination,* vol. 224, pp. 143-153, 2008.

[4] J. R. McCutcheon, R. L. McGinnis, and M. Elimelech, "A novel ammonia-carbon dioxide forward (direct) osmosis desalination process," *Desalination,* vol. 174, pp. 1-11, 2005.

[5] S. F. Zhao and L. D. Zou, "Effects of working temperature on separation performance, membrane scaling and cleaning in forward osmosis desalination," *Desalination,* vol. 278, pp. 157-164, 2011.

[6] Q. Saren, C. Q. Qiu, and C. Y. Y. Tang, "Synthesis and Characterization of Novel Forward Osmosis Membranes based on Layer-by-Layer Assembly," *Environmental Science & Technology,* vol. 45, pp. 5201-5208, 2011.

[7] M. Sairam, E. Sereewatthanawut, K. Li, A. Bismarck, and A. G. Livingston, "Method for the preparation of cellulose acetate flat sheet composite membranes for forward osmosis-Desalination using MgSO(4) draw solution," *Desalination,* vol. 273, pp. 299-307, 2011.

[8] T. Y. Cath, A. E. Childress, and M. Elimelech, "Forward osmosis: Principles, applications, and recent developments," *Journal of Membrane Science,* vol. 281, pp. 70-87, 2006.

[9] J. C.-T. Lin, D.-J. Lee, and C. Huang, "Membrane Fouling Mitigation: Membrane Cleaning," *Separation Science and Technology,* vol. 45, pp. 858-872, 2010.

[10] B. X. Mi and M. Elimelech, "Gypsum Scaling and Cleaning in Forward Osmosis: Measurements and Mechanisms," *Environmental Science & Technology,* vol. 44, pp. 2022-2028, 2010.

[11] M. Amirilargani, E. Saljoughi, T. Mohammadi, and M. R. Moghbeli, "Effects of Coagulation Bath Temperature and Polyvinylpyrrolidone Content on Flat Sheet Asymmetric Polyethersulfone Membranes," *Polymer Engineering and Science,* vol. 50, pp. 885-893, 2010.

[12] K. L. Lee, R. W. Baker, and H. K. Lonsdale, "Membranes for power generation by pressure-retarded osmosis," *Journal of Membrane Science,* vol. 8, pp. 141-171, 1981.

[13] S. Loeb and R. S. Norman, "Osmotic Power Plants," *Science,* vol. 189, pp. 654-655, 1975.

[14] B. E. Logan and M. Elimelech, "Membrane-based processes for sustainable power generation using water," *Nature,* vol. 488, pp. 313-319, 2012.

[15] J. R. McCutcheon and M. Elimelech, "Influence of concentrative and dilutive internal concentration polarization on flux behavior in forward osmosis," *Journal of Membrane Science,* vol. 284, pp. 237-247, 2006.

[16] G. T. Gray, J. R. McCutcheon, and M. Elimelech, "Internal concentration polarization in forward osmosis: role of membrane orientation," *Desalination,* vol. 197, pp. 1-8, 2006.

[17] C. Y. Y. Tang, Q. H. She, W. C. L. Lay, R. Wang, and A. G. Fane, "Coupled effects of internal concentration polarization and fouling on flux behavior of forward osmosis membranes during humic acid filtration," *Journal of Membrane Science,* vol. 354, pp. 123-133, 2010.

[18] W. A. Phillip, J. S. Yong, and M. Elimelech, "Reverse Draw Solute Permeation in Forward Osmosis: Modeling and Experiments," *Environmental Science & Technology,* vol. 44, pp. 5170-5176, 2010.

[19] N. T. Hancock and T. Y. Cath, "Solute Coupled Diffusion in Osmotically Driven Membrane Processes," *Environmental Science & Technology,* vol. 43, pp. 6769-6775, 2009.

[20] S. K. Yen, F. M. Haja, M. L. Su, K. Y. Wang, and T. S. Chung, "Study of draw solutes using 2-methylimidazole-based compounds in forward osmosis," *Journal of Membrane Science,* vol. 364, pp. 242-252, 2010.

[21] S. Phuntsho, H. K. Shon, S. Hong, S. Lee, and S. Vigneswaran, "A novel low energy fertilizer driven forward osmosis desalination for direct fertigation: Evaluating the performance of fertilizer draw solutions," *Journal of Membrane Science,* vol. 375, pp. 172-181, 2011.

[22] J. R. McCutcheon, R. L. McGinnis, and M. Elimelech, "Desalination by ammonia-carbon dioxide forward osmosis: Influence of draw and feed solution concentrations on process performance," *Journal of Membrane Science,* vol. 278, pp. 114-123, 2006.

[23] H. Y. Ng, W. L. Tang, and W. S. Wong, "Performance of forward (direct) osmosis process: Membrane structure and transport phenomenon," *Environmental Science & Technology,* vol. 40, pp. 2408-2413, 2006.

[24] J. C. Su and T. S. Chung, "Sublayer structure and reflection coefficient and their effects on concentration polarization and membrane performance in FO processes," *Journal of Membrane Science,* vol. 376, pp. 214-224, 2011.

[25] K. Y. Wang, R. C. Ong, and T. S. Chung, "Double-Skinned Forward Osmosis Membranes for Reducing Internal Concentration Polarization within the Porous Sublayer," *Industrial & Engineering Chemistry Research,* vol. 49, pp. 4824-4831, 2010.

[26] S. Zhang, K. Y. Wang, T. S. Chung, H. M. Chen, Y. C. Jean, and G. Amy, "Well-constructed cellulose acetate membranes for forward osmosis: Minimized internal concentration polarization with an ultra-thin selective layer," *Journal of Membrane Science,* vol. 360, pp. 522-535, 2010.

[27] J. Wei, C. Q. Qiu, C. Y. Y. Tang, R. Wang, and A. G. Fane, "Synthesis and characterization of flat-sheet thin film composite forward osmosis membranes," *Journal of Membrane Science,* vol. 372, pp. 292-302, 2011.

[28] X. Song, Z. Liu, and D. D. Sun, "Nano gives the answer: Breaking the bottleneck of internal concentration polarization with a nanofiber composite forward osmosis membrane for a high water production rate," *Advanced Materials,* vol. 23, pp. 3256-3260, 2011.

[29] N. Ma, J. Wei, S. Qi, Y. Zhao, Y. Gao, and C. Y. Tang, "Nanocomposite substrates for controlling internal concentration polarization in forward osmosis membranes," *Journal of Membrane Science,* vol. 441, pp. 54-62, 2013.

[30] J. G. Gai and X. L. Gong, "Zero internal concentration polarization FO membrane: Functionalized graphene," *Journal of Materials Chemistry A,* vol. 2, pp. 425-429, 2014.

[31] C. Qiu, L. Setiawan, R. Wang, C. Y. Tang, and A. G. Fane, "High performance flat sheet forward osmosis membrane with an NF-like selective layer on a woven fabric embedded substrate," *Desalination,* vol. 287, pp. 266-270, 2012.

[32] T. P. N. Nguyen, E.-T. Yun, I.-C. Kim, and Y.-N. Kwon, "Preparation of cellulose triacetate/cellulose acetate (CTA/CA)-based membranes for forward osmosis," *Journal of Membrane Science,* vol. 433, pp. 49-59, 2013.

[33] X. Liu and H. Y. Ng, "Double-blade casting technique for optimizing substrate membrane in thin-film composite forward osmosis membrane fabrication," *Journal of Membrane Science,* vol. 469, pp. 12-126, 2014.

[34] X. Li, K. Y. Wang, B. Helmer, and T.-S. Chung, "Thin-Film Composite Membranes and Formation Mechanism of Thin-Film Layers on Hydrophilic Cellulose Acetate Propionate Substrates for Forward Osmosis Processes," *Industrial & Engineering Chemistry Research,* vol. 51, pp. 10039-10050, 2012.

[35] N. Ma, J. Wei, R. Liao, and C. Y. Tang, "Zeolite-polyamide thin film nanocomposite membranes: Towards enhanced performance for forward osmosis," *Journal of Membrane Science,* vol. 405-406, pp. 149-157, 2012.

[36] D. Emadzadeh, W. J. Lau, T. Matsuura, A. F. Ismail, and M. Rahbari-Sisakht, "Synthesis and characterization of thin film nanocomposite forward osmosis membrane with hydrophilic nanocomposite support to reduce internal concentration polarization," *Journal of Membrane Science,* vol. 449, pp. 74-85, 2014.

[37] D. Emadzadeh, W. J. Lau, T. Matsuura, M. Rahbari-Sisakht, and A. F. Ismail, "A novel thin film composite forward osmosis membrane prepared from PSf-TiO2 nanocomposite substrate for water desalination," *Chemical Engineering Journal,* vol. 237, pp. 70-80, 2014.

[38] G. D. Mehta and S. Loeb, "Internal polarization in the porous substructure of a semipermeable membrane under pressure-retarded osmosis," *Journal of Membrane Science,* vol. 4, pp. 261-265, 1978.

[39] J. J. Qin, S. Chen, M. H. Oo, K. A. Kekre, E. R. Cornelissen, and C. J. Ruiken, "Experimental studies and modeling on concentration polarization in forward osmosis," *Water Science and Technology,* vol. 61, pp. 2897-2904, 2010.

[40] T. P. N. Nguyen, B.-M. Jun, J. H. Lee, and Y.-N. Kwon, "Comparison of integrally asymmetric and thin film composite structures for a desirable fashion of forward osmosis membranes," *Journal of Membrane Science,* vol. 495, pp. 457-470, 2015.

[41] G. D. Mehta and S. Loeb, "Performance of permasep B-9 and B-10 membranes in various osmotic regions and at high osmotic pressures," *Journal of Membrane Science,* vol. 4, pp. 335-349, 1978.

[42] M. A. Saad, "Biofouling prevention in RO polymeric membrane systems," *Desalination,* vol. 88, pp. 85-105, 1992.

[43] J. Yu, Y. Baek, H. Yoon, and J. Yoon, "New disinfectant to control biofouling of polyamide reverse osmosis membrane," *Journal of Membrane Science,* vol. 427, pp. 30-36, 2013.

[44] R. P. Schneider, L. M. Ferreira, P. Binder, E. M. Bejarano, K. P. Góes, E. Slongo*, et al.*, "Dynamics of organic carbon and of bacterial populations in a conventional pretreatment train of a reverse osmosis unit experiencing severe biofouling," *Journal of Membrane Science,* vol. 266, pp. 18-29, 2005.

[45] R. J. Xie, E. K. Tan, S. K. Lim, E. Haw, C. P. Chiew, A. Sivaraman*, et al.*, "Pre-treatment optimisation of SWRO membrane desalination under tropical conditions," *Desalination and Water Treatment,* vol. 3, pp. 183-192, 2009.

[46] W. G. Light, H. C. Chu, and C. N. Tran, "Reverse osmosis TFC magnum elements for chlorinated/dechlorinated feedwater processing," *Desalination,* vol. 64, pp. 411-421, 1987.

[47] X. Tang, S. H. Flint, R. J. Bennett, and J. D. Brooks, "The efficacy of different cleaners and sanitisers in cleaning biofilms on UF membranes used in the dairy industry," *Journal of Membrane Science,* vol. 352, pp. 71-75, 2010.

[48] E. Arkhangelsky, D. Kuzmenko, and V. Gitis, "Impact of chemical cleaning on properties and functioning of polyethersulfone membranes," *Journal of Membrane Science,* vol. 305, pp. 176-184, 2007.

[49] P. Wang, Z. Wang, Z. Wu, Q. Zhou, and D. Yang, "Effect of hypochlorite cleaning on the physiochemical characteristics of polyvinylidene fluoride membranes," *Chemical Engineering Journal,* vol. 162, pp. 1050-1056, 2010.

[50] V. Puspitasari, A. Granville, P. Le-Clech, and V. Chen, "Cleaning and ageing effect of sodium hypochlorite on polyvinylidene fluoride (PVDF) membrane," *Separation and Purification Technology,* vol. 72, pp. 301-308, 2010.

[51] S. Hajibabania, A. Antony, G. Leslie, and P. Le-Clech, "Relative impact of fouling and cleaning on PVDF membrane hydraulic performances," *Separation and Purification Technology,* vol. 90, pp. 204-212, 2012.

[52] A. Subramani and E. M. V. Hoek, "Biofilm formation, cleaning, re-formation on polyamide composite membranes," *Desalination,* vol. 257, pp. 73-79, 2010.

[53] B. X. Mi and M. Elimelech, "Organic fouling of forward osmosis membranes: Fouling reversibility and cleaning without chemical reagents," *Journal of Membrane Science,* vol. 348, pp. 337-345, 2010.

[54] S. Lee, C. Boo, M. Elimelech, and S. Hong, "Comparison of fouling behavior in forward osmosis (FO) and reverse osmosis (RO)," *Journal of Membrane Science,* vol. 365, pp. 34-39, 2010.

[55] W. C. L. Lay, T. H. Chong, C. Y. Tang, A. G. Fane, J. Zhang, and Y. Liu, "Fouling propensity of forward osmosis: Investigation of the slower flux decline phenomenon," in *Water Science and Technology* vol. 61, ed, 2010, pp. 927-936.

[56] K. D. Vos, I. Nusbaum, A. P. Hatcher, and F. O. Burris Jr, "Storage, disinfection, and life of cellulose acetate reverse osmosis membranes," *Desalination,* vol. 5, pp. 157-166, 1968.

[57] A. P. Murphy, "Deterioration of cellulose acetate by transition metal salts in aqueous chlorine," *Desalination,* vol. 85, pp. 45-52, 1991.

[58] E. Arkhangelsky, U. Goren, and V. Gitis, "Retention of organic matter by cellulose acetate membranes cleaned with hypochlorite," *Desalination,* vol. 223, pp. 97-105, 2008.

[59] Y. N. Kwon and J. O. Leckie, "Hypochlorite degradation of crosslinked polyamide membranes - II. Changes in hydrogen bonding behavior and performance," *Journal of Membrane Science,* vol. 282, pp. 456-464, 2006.

[60] Y. N. Kwon and J. O. Leckie, "Hypochlorite degradation of crosslinked polyamide membranes I. Changes in chemical/morphological properties," *Journal of Membrane Science,* vol. 283, pp. 21-26, 2006.

[61] G.-D. Kang, C.-J. Gao, W.-D. Chen, X.-M. Jie, Y.-M. Cao, and Q. Yuan, "Study on hypochlorite degradation of aromatic polyamide reverse osmosis membrane," *Journal of Membrane Science,* vol. 300, pp. 165-171, 2007.

[62] A. Antony, R. Fudianto, S. Cox, and G. Leslie, "Assessing the oxidative degradation of polyamide reverse osmosis membrane—Accelerated ageing with hypochlorite exposure," *Journal of Membrane Science,* vol. 347, pp. 159-164, 2010.

[63] A. Ettori, E. Gaudichet-Maurin, J.-C. Schrotter, P. Aimar, and C. Causserand, "Permeability and chemical analysis of aromatic polyamide based membranes exposed to sodium hypochlorite," *Journal of Membrane Science,* vol. 375, pp. 220-230, 2011.

[64] Y. N. Kwon, R. Joksimovic, I. C. Kim, and J. O. Leckie, "Effect of bromide on the chlorination of a polyamide membrane," *Desalination,* vol. 280, pp. 80-86, 2011.

[65] J. E. Gu, B. M. Jun, and Y. N. Kwon, "Effect of chlorination condition and permeability of chlorine species on the chlorination of a polyamide membrane," *Water Research,* 2012.

[66] B. C. Donose, S. Sukumar, M. Pidou, Y. Poussade, J. Keller, and W. Gernjak, "Effect of pH on the ageing of reverse osmosis membranes upon exposure to hypochlorite," *Desalination,* vol. 309, pp. 97-105, 2013.

[67] J. Glater, S.-k. Hong, and M. Elimelech, "The search for a chlorine-resistant reverse osmosis membrane," *Desalination,* vol. 95, pp. 325-345, 1994.

[68] M. Mulder, *Basic principles of membrane technology*, 2nd ed. Dordrecht ; Boston: Kluwer Academic, 1996.

[69] C. J. M. v. Rijn, "Chapter 1 Overview membrane technology," in *Membrane Science and Technology*. vol. Volume 10, C. J. M. v. Rijn, Ed., ed: Elsevier, 2004, pp. 1-23.

[70] C. J. M. v. Rijn, "Chapter 6 Polymeric membranes," in *Membrane Science and Technology*. vol. Volume 10, C. J. M. v. Rijn, Ed., ed: Elsevier, 2004, pp. 133-167.

[71] D. Purchas and K. Sutherland, *Handbook of Filter Media*: Elsevier Science, 2002.

[72] J. v. t. Hoff, "The Function of Osmotic Pressure in the Analogy between Solutions and Gases," *Proceedings of the Physical Society of London,* vol. 9, p. 307, 1887.

[73] S. U. Pickering, "The theory of osmotic pressure and its bearing on the nature of solutions," *Proceedings of the Physical Society of London,* vol. 10, pp. 354-366, 1888.

[74] R. H. Adie, "XLI. - On the osmotic pressures of salts in solution," *Journal of the Chemical Society, Transactions,* vol. 59, pp. 344-372, 1891.

[75] C. L. Speyers, "Osmotic pressure," *Journal of the American Chemical Society,* vol. 20, pp. 579-585, 1898.

[76] J. Van't Hoff, "The function of osmotic pressure in the analogy between solutions and gases," *Proceedings of the Physical Society of London,* vol. 9, pp. 307-334, 1886.

[77] M. H. V. Mulder, "Chapter 2 Polarization phenomena and membrane fouling," in *Membrane Science and Technology*. vol. Volume 2, D. N. Richard and S. A. Stern, Eds., ed: Elsevier, 1995, pp. 45-84.

[78] N. Y. Yip, A. Tiraferri, W. A. Phillip, J. D. Schiffman, and M. Elimelech, "High performance thin-film composite forward osmosis membrane," *Environmental Science and Technology,* vol. 44, pp. 3812-3818, 2010.

[79] S. Loeb, L. Titelman, E. Korngold, and J. Freiman, "Effect of porous support fabric on osmosis through a Loeb-Sourirajan type asymmetric membrane," *Journal of Membrane Science,* vol. 129, pp. 243-249, 1997.

[80] V. M. M. Lobo, "Mutual diffusion coefficients in aqueous electrolyte solutions " *Pure & Appl. Chern.,* vol. 65, pp. 2613-2640, 1993.

[81] H. K. Lonsdale, "Recent advances in reverse osmosis membranes," *Desalination,* vol. 13, pp. 317-332, 1973.

[82] A. Tiraferri, N. Y. Yip, W. A. Phillip, J. D. Schiffman, and M. Elimelech, "Relating performance of thin-film composite forward osmosis membranes to support layer formation and structure," *Journal of Membrane Science,* vol. 367, pp. 340-352, 2011.

[83] C. Y. Tang, Y.-N. Kwon, and J. O. Leckie, "Probing the nano- and micro-scales of reverse osmosis membranes—A comprehensive characterization of physiochemical properties of uncoated and coated membranes by XPS, TEM, ATR-FTIR, and streaming potential measurements," *Journal of Membrane Science,* vol. 287, pp. 146-156, 2007.

[84] M. Elimelech, W. H. Chen, and J. J. Waypa, "Measuring the zeta (electrokinetic) potential of reverse osmosis membranes by a streaming potential analyzer " *Desalination,* vol. 95, pp. 269-286, 1994.

[85] Y. H. Cho, J. Han, S. Han, M. D. Guiver, and H. B. Park, "Polyamide thin-film composite membranes based on carboxylated polysulfone microporous support membranes for forward osmosis," *Journal of Membrane Science,* vol. 445, pp. 220-227, 2013.

[86] R. W. Holloway, A. E. Childress, K. E. Dennett, and T. Y. Cath, "Forward osmosis for concentration of anaerobic digester centrate," *Water Research,* vol. 41, pp. 4005-4014, 2007.

[87] Y. Xu, X. Y. Peng, C. Y. Y. Tang, Q. S. A. Fu, and S. Z. Nie, "Effect of draw solution concentration and operating conditions on forward osmosis and pressure retarded osmosis performance in a spiral wound module," *Journal of Membrane Science,* vol. 348, pp. 298-309, 2010.

[88] C. Boo, M. Elimelech, and S. Hong, "Fouling control in a forward osmosis process integrating seawater desalination and wastewater reclamation," *Journal of Membrane Science,* vol. 444, pp. 148-156, 2013.

[89] B. S. Chanukya, S. Patil, and N. K. Rastogi, "Influence of concentration polarization on flux behavior in forward osmosis during desalination using ammonium bicarbonate," *Desalination,* vol. 312, pp. 39-44, 2013.

[90] D. Stillman, L. Krupp, and Y. H. La, "Mesh-reinforced thin film composite membranes for forward osmosis applications: The structure-performance relationship," *Journal of Membrane Science,* vol. 468, pp. 308-316, 2014.

[91] B. S. Chanukya, S. Patil, and N. K. Rastogi, "Influence of concentration polarization on flux behavior in forward osmosis during desalination using ammonium bicarbonate,"

Desalination, vol. 312, pp. 39-44, 2013.

[92] M. Xie, W. E. Price, L. D. Nghiem, and M. Elimelech, "Effects of feed and draw solution temperature and transmembrane temperature difference on the rejection of trace organic contaminants by forward osmosis," *Journal of Membrane Science,* vol. 438, pp. 57-64, 2013.

[93] K. Vasarhelyi, J. A. Ronner, M. H. V. Mulder, and C. A. Smolders, "DEVELOPMENT OF WET DRY REVERSIBLE REVERSE-OSMOSIS MEMBRANES WITH HIGH-PERFORMANCE FROM CELLULOSE-ACETATE AND CELLULOSE TRIACETATE BLENDS," *Desalination,* vol. 61, pp. 211-235, 1987.

[94] L. Kastelankunst, D. Sambrailo, and B. Kunst, "ON THE SKINNED CELLULOSE TRIACETATE MEMBRANES FORMATION," *Desalination,* vol. 83, pp. 331-342, 1991.

[95] A. M. Dave, S. S. Sahasrabudhe, B. V. Ankleshwaria, and M. H. Mehta, "ENHANCEMENT OF MEMBRANE PERFORMANCE WITH EMPLOYMENT OF CELLULOSE-ACETATE BLEND," *Journal of Membrane Science,* vol. 66, pp. 79-87, 1992.

[96] L. KastelanKunst, V. Dananic, B. Kunst, and K. Kosutic, "Preparation and porosity of cellulose triacetate reverse osmosis membranes," *Journal of Membrane Science,* vol. 109, pp. 223-230, 1996.

[97] I. Glavchev, R. N. Nikolov, and P. Valchev, "Determination of evaporation rates of mixed solvents with the formation of thin films for membranes," *Polymer Testing,* vol. 22, pp. 529-532, 2003.

[98] A. P. Duarte, M. T. Cidade, and J. C. Bordado, "Cellulose acetate reverse osmosis membranes: Optimization of the composition," *Journal of Applied Polymer Science,* vol. 100, pp. 4052-4058, 2006.

[99] S. Loeb and M. R. Bloch, "Countercurrent flow osmotic processes for production of solutions having a high osmotic pressure " *Desalination,* vol. 13, pp. 207-215, 1973.

[100] E. A. Grulke, "Solubility Parameter Values," in *Polymer Handbook*, J. Brandrup and E. H. Immergut, Eds., 3nd edition ed USA: Wiley, 1999, pp. VII/519-VII/559.

[101] B. A. Miller-Chou and J. L. Koenig, "A review of polymer dissolution," *Progress in Polymer Science,* vol. 28, pp. 1223-1270, 2003.

[102] A. Tiraferri, N. Y. Yip, W. A. Phillip, J. D. Schiffman, and M. Elimelech, "Relating performance of thin-film composite forward osmosis membranes to support layer formation and structure," *Journal of Membrane Science,* vol. 367, pp. 340-352, Feb 2011.

[103] H. Bokhorst, F. W. Altena, and C. A. Smolders, "Formation of asymmetric Cellulose-acetate membranes " *Desalination,* vol. 38, pp. 349-360, 1981.

[104] T. Mohammadi and E. Saljoughi, "Effect of production conditions on morphology and permeability of asymmetric cellulose acetate membranes," *Desalination,* vol. 243, pp. 1-7, 2009.

[105] N. Pereira, A. St John, R. W. Cattrall, J. M. Perera, and S. D. Kolev, "Influence of the composition of polymer inclusion membranes on their homogeneity and flexibility," *Desalination,* vol. 236, pp. 327-333, 2009.

[106] A. P. Duarte, J. C. Bordado, and M. T. Cidade, "Cellulose acetate reverse osmosis membranes: Optimization of preparation parameters," *Journal of Applied Polymer Science,* vol. 103, pp. 134-139, 2007.

[107] M. Elimelech, X. Zhu, A. E. Childress, and S. Hong, "Role of membrane surface morphology in colloidal fouling of cellulose acetate and composite aromatic polyamide reverse osmosis membranes," *Journal of Membrane Science,* vol. 127, pp. 101-109, 1997.

[108] S. Hong, I.-C. Kim, T. Tak, and Y.-N. Kwon, "Interfacially synthesized chlorine-resistant polyimide thin film composite (TFC) reverse osmosis (RO) membranes," *Desalination,* vol. 309, pp. 18-26, 2013.

[109] H. Choi, J. Park, T. Tak, and Y.-N. Kwon, "Surface modification of seawater reverse

osmosis (SWRO) membrane using methyl methacrylate–hydroxy poly(oxyethylene) methacrylate (MMA–HPOEM) comb-polymer and its performance," *Desalination,* vol. 291, pp. 1-7, 2012.

[110] Y.-N. Kwon, S. Hong, H. Choi, and T. Tak, "Surface modification of a polyamide reverse osmosis membrane for chlorine resistance improvement," *Journal of Membrane Science,* vol. 415–416, pp. 192-198, 2012.

[111] Y.-N. Kwon, K. Shih, C. Tang, and J. O. Leckie, "Adsorption of perfluorinated compounds on thin-film composite polyamide membranes," *Journal of Applied Polymer Science,* vol. 124, pp. 1042-1049, 2012.

[112] N. Fujiwara, K. Numata, A. Kumano, Y. Ogino, M. Nagai, and H. Iwahashi, "The effect of heavy metal ions on the oxidation of cellulose triacetate membranes," *Desalination,* vol. 96, pp. 431-439, 1994.

[113] M. Elimelech, W. H. Chen, and J. J. Waypa, "Measuring the zeta (electrokinetic) potential of reverse osmosis membranes by a streaming potential analyzer," *Desalination,* vol. 95, pp. 269-286, 1994/07/01 1994.

[114] H. Kono, S. Yunoki, T. Shikano, M. Fujiwara, T. Erata, and M. Takai, "CP/MAS 13C NMR Study of Cellulose and Cellulose Derivatives. 1. Complete Assignment of the CP/MAS 13C NMR Spectrum of the Native Cellulose," *Journal of the American Chemical Society,* vol. 124, pp. 7506-7511, 2002.

[115] H. Kono, H. Hashimoto, and Y. Shimizu, "NMR characterization of cellulose acetate: Chemical shift assignments, substituent effects, and chemical shift additivity," *Carbohydrate Polymers,* vol. 118, pp. 91-100, 2015.

[116] I. Nehls, B. Philipp, and W. Wagenknecht, "20 - 13C NMR spectroscopic studies on regioselective derivatization of cellulose," in *Cellulose and Cellulose Derivatives*, J. F. K. O. P. A. Williams, Ed., ed: Woodhead Publishing, 1995, pp. 153-160.

[117] B. Bose, S. Zhao, R. Stenutz, F. Cloran, P. B. Bondo, G. Bondo*, et al.*, "Three-Bond C—O—C—C Spin-Coupling Constants in Carbohydrates: Development of a Karplus Relationship," *Journal of the American Chemical Society,* vol. 120, pp. 11158-11173, 1998.

[118] V. A. Shenai and K. K. Sharma, "Studies in chemically modified celluloses. VIII. Hypochlorite oxidation of cellulose in the presence of cuprous hydroxide," *Journal of Applied Polymer Science,* vol. 20, pp. 377-383, 1976.

ACKNOWLEDGEMENTS

Time flies so fast when I think of the first day at UNIST in February of 2010 like just a few days ago, but still long enough when I think of the sleepless nights in the laboratory for checking experiments. It has been six years since I started my study at UNIST. It is definitely a meaningful and memorial 6-year course of my life. Looking back whole time I have spent at UNIST, I would like to express my sincere thanks to whom wamring my heart during cold winters at UNIST, cheering me up in my harsh time in research and supporting me pursuing Ph.D. degree.

First of all, I would like to thank my supervisor, professor Young-Nam Kwon (권영남교수님께 감사합니다). Thank you for your advice since the day I knew nothing about osmotically-driven separation process to this moment when I have just completed my dissertation about osmotically-driven separation process. I greatly appreciate your kind support and careness about my research and my life, your understating and tolerance of mistakes I have ever made.

I would like to thank professor Changha Lee for the opportunity of studying at UNIST he introduced when he visisted Vietnam. I would like to thank all UNIST instructors giving lectures to enrich my knowledge. I am especially grateful to professor Jaeweon Cho, Changha Lee, Nowon Kim and Dr. In-Chul Kim for serving as committee members on my defense day.

I would like to thank my labmates. The first labmate is Dr. Joung-Eun Gu. She was not only a senior helping me a lot at the beginning days in the laboratory at UNIST but also, a sister teaching me many things about Korean life. I would like to thank Byung-Moon Jun, who is my kind labmate helping each other in the lab, nice friend sharing stories about life and good academic partner discussing issues of our research. I would also like to thank other members of SMART Lab - Eun-Ho Kim, Sang-Woo Han, Eun-Tae Yun, Yu-Kyung Kim, Hyung-Kae Lee, Dr. Jayalakshmi Ayyavoo, Dr. Shashi Prabha Dubey and Van Vinh Nguyen - for all their help in research and for together time we had during lunches, dinner, coffee break and activities outside of campus.

I would also like to thank other friends in our department. Thanks to Dr. Hongshin Lee

who helped me in research, shared experience and encouraged me. Thanks to Hyung-Eun Kim, Hye-Jin Lee and Min Sik Kim for their help and their kindness during my study at UNIST.

Besides, I would like to thank my roommates, Ms. Thi Minh Thuy Nguyen, Thi Thu Ngoc Nguyen, Inseong Jo and Thi Bich Hong Tu for being kind to me all the time we shared the rooms in the dormitory. During my time at UNIST, I might bother their sleep many times because I frequently go back dormitory late night but never get complaints from them. I would like to thank other Vietnamese students at UNIST, of whose careness and sharing make me feel less homesick. Thanks to my closed friends in my homeland, Lieu Hai, Ha An, Thuy Vi, Ngoc Thao and Chi Le for all your careness.

I am especially grateful to my lovely boyfriend, Duc Tam Ho, for his endless love and careness to me. He helped me a lot during my research, also always beside to encourage me when I was in harsh time. He is the one I can always ask for help without explanation. He is also the best friend ever. Thank you so much.

And last but not least, I would like to say thanks to my family. I would like to express great thanks to my parents for their infinite love, their careness, their support and their encouragement. This dissertation is dedicated to my parents who cannot afford their dreams of further study when they were young. Thanks to my beloved sisters, my brother-in-laws, my nieces and my nephews for all your love and careness. You all make me never feel lonely and strong always so that I completed my research abroad.

Lời cảm ơn

(Acknowledgement in Vietnamese)

Lời cảm ơn này xin được viết riêng cho những người thân và những người bạn của tôi. Ngày hôm nay, ngồi hoàn thành cuốn luận văn sau sáu năm học tập nơi đất khách quê người, con xin cảm ơn Ba Má đã luôn dõi theo con, luôn yêu thương và lo lắng cho con. Cảm ơn các chị gái, các anh và các cháu đã luôn hỏi thăm động viên em/dì. Cảm ơn các bạn của tôi, Liễu Hải, Ân, Chi, Thảo và Vi, tụi mày luôn ở bên chia sẻ và động viên tao nhiều lắm. Cảm ơn người bạn thân Hồ Đức Tam, vừa là bạn trai, vừa là người anh trai luôn chăm sóc và nhường nhịn tôi, hiểu tôi hơn tôi. Đời tôi có lẽ đã rẽ một hướng khác nếu không có anh ở bên chia sẻ và giúp đỡ. Cảm ơn những người bạn, người chị, người anh, người em tại UNIST vì những sẻ chia cùng nhau trong những ngày tháng xa nhà.

___Ω___